Vidar Sørhus

Auxotonic Loading of the Cardiac Muscle: Experiments and Model Simulations

NTNU Trondheim
Norges teknisk-naturvitenskapelige universitet

Doktor ingeniøravhandling 2000:44
Institutt for datateknikk og informasjonsvitenskap

IDI-rapport 2000:4

Auxotonic Loading of the Cardiac Muscle: Experiments and Model Simulations

Vidar Sørhus

Norwegian University of Science and Technology

April, 2000

Auxotonic loading of the cardiac muscle: Experiments and model simulations
Vidar Sørhus

NTNU Trondheim
Norges teknisk-naturvitenskapelige universitet
Doktor ingeniøravhandling 2000:44
Institutt for datateknikk og informasjonsvitenskap
IDI-rapport 2000:4

ISBN 82-7984-067-2

ISSN 0802-6394

Abstract

For centuries, the heart has interested scientists. Its function has been studied in experimental setups and by different kinds of validation models. The doctoral study presented in this thesis has been devoted to the development of a mathematical model of the cardiac muscle function based on new experiments on isolated papillary muscles.

The goal was to develop a model with minimal complexity in which the model parameters were observable from measured variables. The cardiac muscle works under auxotonic loading conditions, i.e. simultaneous changes in stress and length, while most experiments have been performed under isotonic or isometric conditions or as quick load and length clamps. In order to study the isolated muscle under controlled auxotonic conditions and to perform experiments over a wide range of loading conditions on each individual muscle within a limited time span, we wanted to develop a new measurement and control system for the isolated papillary muscle.

We used digital technology to obtain maximal flexibility of the new control system. In addition to including the auxotonic control, i.e. proportional changes in length and stress, the new system made it possible to perform series of predefined contraction-relaxation sequences (twitches) with individual experimental settings including loading conditions, stimulation parameters, and acquisition parameters.

The auxotonic twitches at different auxotonic load demonstrated load-independent timing of contraction, i.e. the shape of the normalized developed stress was similar at different auxotonic load. This is different from conventional twitches with isometric-isotonic contraction sequence. In the relaxation phase, however, the timing was load dependent; time to half relaxation was highly correlated with peak stress.

The differences in load dependence between the contraction phase and the relaxation phase were further demonstrated with the use of two dimensionless expressions for mechanical dynamics, defined as the sum of normalized stress and normalized shortening. These expressions also allowed comparison of mechanical dynamics, i.e. changes in length or stress, in auxotonic twitches versus conventional twitch types.

The properties of the auxotonic twitches, which were demonstrated with the experiments, yielded a special attention towards the activation dynamics in the definition of a structure for the mathematical model. To obtain realistic auxotonic twitches, we defined one activity variable, representing the integrative effect of the length and velocity-dependent calcium-troponin C kinetics, activation of the thin filament, and cross-bridge kinetics. The activity was modeled as one model of activation and one model of inactivation. Three different approaches to separate activation and inactivation in time demonstrated realistic auxotonic behavior. A moderate increase in the model complexity was, however, needed to include specific features that are seen in isometric and afterloaded twitches.

Preface

This thesis has been submitted to the Norwegian University of Science and Technology (NTNU) in partial fulfillment of the requirements for the degree Doktor Ingeniør.

The doctoral project has been accomplished in a cooperation between Department of Physiology and Biomedical Engineering and Department of Computer and Information Science, NTNU, Trondheim, and Department of Human Physiology and Pathophysiology, University of Antwerp (RUCA), Antwerp. My supervisors have been professor Bjørn Angelsen and professor Stanislas Sys, while professor Jan Komorowski has been the administrative supervisor. The work has been supported by the Norwegian Research Council (NFR) grant # 107409/320.

Acknowledgements

During the work on this thesis, many people have been involved in guidance, discussions, solving practical problems, and motivating me. I would like to mention some of them here.

First, sincere thanks to professor Bjørn Angelsen, who introduced me to the field of medical cybernetics. In cooperation with professor Jan Komorowski, he initiated the project and involved me in it. His innovating nature and great knowledge in physics and mathematics has been an important help and source of inspiration. He also established the contact and opened up for the cooperation with professor Stanislas Sys at the University of Antwerp.

Based on the long and well-known experience in physiology and papillary muscle experiments in their group, professor Stanislas Sys taught me muscle physiology. He included me in his lab as one of his students and shared with me from his long scientific experience. His great hospitality and friendly nature have made him a highly regarded friend.

A good working environment including colleagues, supervisors, secretaries, and lab personnel has been an important factor for me to succeed with this project. During this project, I have been part of three different groups. First, I will thank the members of the Ultrasound Group (NTNU), led by professor Bjørn Angelsen and professor

Hans Torp. Special thanks to the (post-)doctoral students Steinar Bjærum, Andreas Heimdal, Sigve Hovda, Tonni Franke Johansen, Johan Kirkhorn, Stein Inge Rabben, Espen Remme, and Gunnar Taraldsen for making an inspiring scientific and social environment. I will also thank the members of the Dept. of Human Physiology and Pathophysiology (RUCA), led by professor Stanislas Sys and professor Dirk Brutsaert, for their hospitality and fruitful cooperation. Thanks to Marc Demolder for help with papillary muscle experiments and all sorts of practical issues. Thanks to the members of the Knowledge Systems Group (NTNU), led by professor Jan Komorowski, for guidance and support. Special thanks to my colleagues Staal Vinterbo and Alexander Øhrn for cooperation during the first part of the project.

As part of the cooperation with professor Stanislas Sys, Anders Natås did his diploma project in Antwerp. I will thank him for his contribution on the digital control system for the papillary muscle experiments. I will also thank him for our social events during our common stay in Antwerp.

During my doctoral work, two colleagues have played a special role. I have shared office with both of them during different phases of this work and they have became true friends. I will thank Frode Martinsen and Stein Inge Rabben for their friendship, discussions, and social contribution.

My thanks to my wife, Hilde, cannot be expressed with words. You have always encouraged me and believed in me, even when I did not. Your patience with my different "doctoral student moods" have been incredible. Hilde has also revised almost all the material I have written in English during these years.

The last year of this work, my son, Anders, has been my greatest source of inspiration. Thank you.

Vidar Sørhus

Trondheim, April 2000

Contents

Chapter 1

Introduction

This thesis can be divided into three parts. The first part contains four introductory chapters, including a general introduction to the doctoral project, followed by a brief description of the cardiac muscle structure and function, continued with a short review of auxotonic load on cardiac muscles, and finally a summary of the main conclusions and directions for further research.

The second part is the experimental part, and includes three self-contained papers that describe the experimental setup (paper A), analyses of the auxotonic behavior of the muscles in particular (paper B), and mechanical dynamics of contraction-relaxation sequences in general (paper C).

The third part contains the description of a mathematical model of cardiac muscle contraction-relaxation sequences. This part is written as one self-contained paper in the same format as the previous papers (paper D). The paper includes a description of the observed cardiac muscle features that our model arises from, a step by step description of the model development, model simulations, and a qualitative evaluation of the model against measurements.

1.1 Motivation

Cardiovascular diseases cause a major health care problem in the western world. According to Statistics Norway (http://www.ssb.no/emner/03/01/10/dodsorsak/), cardiovascular diseases were the primary cause of 44% of the total deaths in Norway in 1996. The most common cardiac diseases are related either 1) to altered load on the cardiac muscles due to pressure or volume overload or 2) to depressed oxygen delivery to the muscles due to narrowed or occluded coronary arteries. Belonging to the first group, are people with elevated blood pressure (hypertension), or valve diseases like narrowed valve opening (stenosis) or leakage through closed valves (regurgitation), who may develop hypertrophy, i.e. increased muscle mass either as increased wall surface or

as increased wall thickness. This is an intrinsic compensatory mechanism in the heart to make the heart able to adapt to new working conditions [35]. But if the load on the heart continues to increase, the compensatory mechanism will be insufficient and even lead to an additional load on the muscle fibers because of the altered chamber geometry.

The blood flow to the muscles, through the coronary arteries, reduces or abolishes in the presence of arteriosclerosis, i.e. development of fat plaque in the arterial wall, or embolus. This again may lead to reduced performance of a region of the ventricular wall and even necrosis of the muscle cells in the region (myocardial infarction).

The diagnosis and prognosis of the cardiovascular diseases are based on a number of variables, including an increasing number of measures according to the rapid development of new measurement techniques. In a situation with rapid increase in the amount of data, it is important to develop methods to extract the essential knowledge from the available data. This extraction includes quantification of diffuse measurements, classification of parameters, and model-based estimation of characteristic parameters from combinations of measures.

A prerequisite for extraction of information from different measurements is knowledge about the cardiovascular system through clinical studies and experimental research on all levels from molecules to the whole organ. For more than a century it has been an exponential increase in the amount of experiments on isolated myocytes, skinned muscle fibers, muscle preparations like isolated papillary muscles and trabecula, isolated hearts, and in situ models. These experiments have revealed a number of important phenomena about the cardiac muscle, including the Frank-Starling mechanism representing the beat-to-beat control of cardiac output [11], the contractile element and its force-velocity relation [1, 16], the sarcomere organization and the sliding filament theory [25–28], the isometric force-length relation [13], the excitation-contraction coupling and the length-dependent activation [2, 52], the cooperative effect [5], and the concept of load-dependent relaxation [8].

Despite the long history of research on the cardiac muscle, there are still open questions about the muscle function. It is a challenge to extrapolate the role and importance of experimental observations obtained in isolated experimental settings to the level of muscle function in the intact heart [48]. The experimental loading conditions for isolated papillary muscles have mainly been isometric (constant length) or isotonic (constant force) control or combinations of length and load clamps. Muscle behaviour under controlled auxotonic conditions has not been studied for the isolated papillary muscle.

Mathematical models can be used to represent physiological systems. This way it is possible to explain experimental and clinical observations. Mathematical models can also be used to estimate characteristic scalar parameters (i.e. the model parameters) from a set of measurements. This is done by fitting the model output to the measurements. A reliable estimate of the model parameters requires that the parameters are identifiable from the given measurements [3, 45], i.e. a unique set of parameters gives

the best fit of the model output to the measurements. The parameter identifiability depends on the model complexity, the relations between the parameters in the model, and the available measurements.

The history of cardiac muscle modeling is long and follows appearance of new experimental observations. Two major classes of muscle models were adopted from the models of skeletal muscle. The first class is based on the so-called Hill three-component model, consisting of a contractile element, a series-elastic element, and a parallel-elastic element. The force-velocity relation of the contractile element is described with Hill's equation [16]. The other class is based on the sliding filament theory (also called cross-bridge theory or Huxley-type models) [25, 27].

The main difference between skeletal and cardiac muscles are the differences in stimulation. In cardiac muscle, it is only single contraction-relaxation sequences (twitches), whereas the skeletal muscle can be stimulated to generate constant force (tetanus). A number of investigators have included time-varying activity in models based on skeletal muscle models [15, 36, 51, 53, 54]. To be able to represent detailed experimental observations on the excitation-contraction coupling of cardiac muscle, so-called compartment models have been proposed [21, 32, 40, 44]. In the compartment models, the concentrations of different configurations of calcium and the contractile proteins have been modeled. The complexity of these models, however, decreases the possibility to estimate parameters from the models, i.e. better representation of specific observations on the cost of reduced identifiability. On the other hand, very simple phenomenological models may fail to represent important muscle properties, i.e. increased idientifiability on the cost of reduced representation. Therefore, the trade-off between model complexity and accuracy is given by the purpose of the model.

1.2 Aims of the Study

This doctoral study has been part of a more general project where the main goal is to extract more information about the cardiac function from ultrasound measurements by using mathematical models and estimation techniques.

In this setting the aims of this doctoral study have been 1) to study twitches of isolated papillary muscles under a wide range of loading conditions, including auxotonic load and 2) to develop a mathematical model of cardiac muscle twitches based on the isolated papillary muscle experiments.

To be able to compare the dynamics of different twitch types with varying loading parameters on the same muscle with similar muscle performance, we wanted to develop a flexible digital measurement and control system for isolated papillary muscles.

In addition to conventional twitch types like isotonic, isometric, and afterloaded twitches with conventional (isotonic-isometric) and physiological (isometric-isotonic) relaxation sequences, we wanted to study the dynamics of twitches with controlled auxotonic loading conditions (simultaneous changes in length and stress). In partic-

ular, we wanted to study the mechanical dynamics, timing, and load dependence of contraction and relaxation in auxotonic twitches and compare it with conventional twitches obtained from the same muscles.

The mechanical dynamics of isolated papillary muscle twitches are complex and depend on a number of underlying processes. This may be described with very complex models that include the description of the underlying processes. We wanted to develop a mathematical model with minimal complexity in order to improve the identifiability of the model parameters.

1.3 Contributions

The main contributions of the doctoral project, as described in this thesis, can be summarized as follows:

- Development of a PC-based measurement and control system for isolated papillary muscle experiments. The system includes real-time control of isotonic, isometric, afterloaded, physiological, and auxotonic twitches. With this system, it is possible to perform series of twitches with individual settings for twitch type, loading, stimulation, and data acquisition.

- Implementation of a controlled auxotonic loading condition. In this condition, the controlled developed force is proportional to muscle shortening, as if the muscle is acting against an ideal spring. The auxotonic load (i.e. the spring constant) can be set on-line or defined in the experiment log, yielding series of auxotonic twitches with different auxotonic load.

- Analyses of the auxotonic twitch demonstrated a load-independent timing of contraction at different auxotonic load, which is different from afterloaded twitches with similar initial values and peak values of force and length. The timing of relaxation was, however, load dependent.

- Construction of two expressions of mechanical dynamics, defined as the sum of normalized stress and shortening. The results of these expressions demonstrated the differences in load dependence between contraction and relaxation in different twitch types. The mechanical dynamics, in terms of the defined expressions, represented nearly the same contraction patterns and a wide variation in relaxation pattern at different twitch types and load.

- Development of a simple mathematical model for simulation of contraction-relaxation sequences of cardiac muscle twitches, in particular auxotonic twitches at different auxotonic load. The model includes a lumped model of activity, separated into two models of activation and inactivation.

1.4 Summary of Papers

Paper A - Controlled Auxotonic Twitch in Papillary Muscle: A new Computer-Based Control Approach

This paper is the first of three papers about isolated papillary muscle experiments. In this paper, a new PC-based measurement and control system is described together with some preliminary experimental results. The new system was developed in order to increase the flexibility of the existing papillary muscle setup and to allow auxotonic control of the papillary muscle. We needed increased flexibility to allow experiments with a wide range of different settings on one single muscle within a reasonable time span. High flexibility was obtained by including 1) real-time feedback control of length and force, performed at a sample frequency of 5000 Hz on a DSP-board, 2) independent stimulation control, 3) measurement of muscle length and three segment lengths, 4) batch control of series of twitches with predefined settings for each twitch, and 5) on-line user-interaction with all relevant control parameters. Individual control algorithms were implemented for each twitch type, including the controlled auxotonic twitch. In the auxotonic twitch, the controlled force was proportional to the shortening, as if the muscle was acting against an ideal spring. The performance and the flexibility of the new system are demonstrated together with some early observations of the auxotonic twitch.

Paper B - Analysis of the Controlled Auxotonic Twitch in Isolated Cardiac Muscle

A study of the controlled auxotonic twitches obtained with the experimental setup described in paper A is presented in paper B. We wanted to study systematically the auxotonic behavior of the isolated cardiac muscle. In particular, we studied the dependence on auxotonic load and initial length of contraction and relaxation by means of timing of contraction and relaxation and positive and negative peak values of the derivative of stress. We found that in auxotonic twitches with initial length at l_{max} (i.e. length with maximal active isometric stress), the timing of contraction was independent of the auxotonic load. This yielded a common path of normalized developed stress during contraction. In the same twitches, timing of relaxation was highly correlated with peak developed stress. Twitch prolongation at increased initial length was more pronounced at lower loads, yielding a load-dependent timing of contraction at initial lengths different from l_{max}. The positive and negative peak values of derivative of stress further demonstrated the differences in load dependence between contraction and relaxation, and the difficulties connected to the use of these parameters as measures of muscle performance. Similar qualitative results were obtained when post extra-systolic potentiation was included as an inotropic intervention.

Paper C - Dimensionless Time Traces of Mechanical Dynamics in Papillary Muscle Twitches

The mechanical dynamics of cardiac muscles are expressed as changes in muscle length and force. In the controlled auxotonic twitch, presented in paper A and B, the developed stress and shortening are proportional, which means that the normalized developed stress and the normalized shortening from one auxotonic twitch are equal. In conventional twitches, the muscle undergoes sequences of isometric and isotonic loading conditions. We wanted to study the differences in mechanical dynamics in twitches with different loading conditions. Therefore, we represented the mechanical dynamics with two different expressions, defined as the sum of normalized stress and normalized shortening. In the first expression, we used normalized developed stress, and in the second expression, we used normalized instantaneous active stress as input. The resulting dimensionless time traces of mechanical dynamics demonstrated very similar shape of the contraction phase at the full range of loads from isotonic to isometric and in both auxotonic and afterloaded twitches. The same traces demonstrated wide variation during relaxation depending on load and twitch type. With the first expression, it was possible to obtain a rough estimate of peak isometric stress and peak isotonic shortening. Both expressions visualized qualitative differences in load dependence between the contraction and relaxation phases, which may have implications on the clinical interpretation of systolic versus diastolic function.

Paper D - Simulation Model of Auxotonic Contraction and Relaxation

Paper D contains the whole modeling part of the thesis. It is written as one self-contained paper with the same format as the previous papers. However, the content is more like in a regular thesis. Therefore, this paper contains a thorough description of the cardiac properties that the model development is based on, a detailed description of the modeling approach and the model development, together with the model simulations and discussion.

In this study we wanted to develop a mathematical model of contraction-relaxation sequences of the cardiac muscle under a wide range of loading conditions from isotonic to isometric. Especially, we wanted to incorporate auxotonic loading conditions. Furthermore, in order to strengthen the relation between the measured stress and length and the model parameters, we wanted to develop a model with minimal complexity. The model simulations of auxotonic twitches corresponded well to the experimental results. It was a trade-off between model complexity and a representative simulation of some features of isometric and afterloaded twitches. A moderate increase in the model complexity allowed more realistic simulation of the timing of isometric twitches at increasing length and the initial rapid stress decline after an abrupt change from isotonic to isometric relaxation in afterloaded twitches.

Chapter 2

Cardiac Muscle Structure and Function

The structure and function of the cardiac muscle are described in textbooks in anatomy, physiology, biophysics, and biomechanics. For the readers not familiar with the terminology of cardiac muscle physiology, this chapter will give a brief introduction to the basic terms. A more thorough description of some cardiac muscle properties is included in **paper D**.

2.1 Cardiac Muscle Structure

The cardiac muscle cells (myocytes) are organized in muscle fibers (myofiber) that are nested around the left and right ventricles with a fiber direction that varies from the outer layer (epicardium) through the ventricular wall (myocardium) to the inner layer (endocardium) [47](Figure 2.1). The inner wall of the ventricles are covered with trabecula, i.e. muscle fibers in various directions that form small leaflets yielding an irregular wall surface. The mitral valve and the tricuspid valve (Figure 2.1) in the ventricle inlets are connected to the myocardium through tendons and the papillary muscles. Both the trabecula and the papillary muscles have been popular preparates for isolated cardiac muscle experiments.

The cardiac muscle cells (Figure 2.2) are smaller and have a more irregular shape than the skeletal muscles, but the components of the muscle cells are the same. The main components of the myocyte (Figure 2.2) are the sarcomeres forming myofibrils (47% cell volume), the sarcoplasmic reticulum (SR, 3.5%), the mitochondria (36%), and the nuclei (2%) [29]. The myocyte is covered by the sarcolemma, representing a barrier between the extracellular (outside the cell) and intracellular (inside the cell) spaces. The surface of the sarcolemma is extended with about 50% by T-tubules

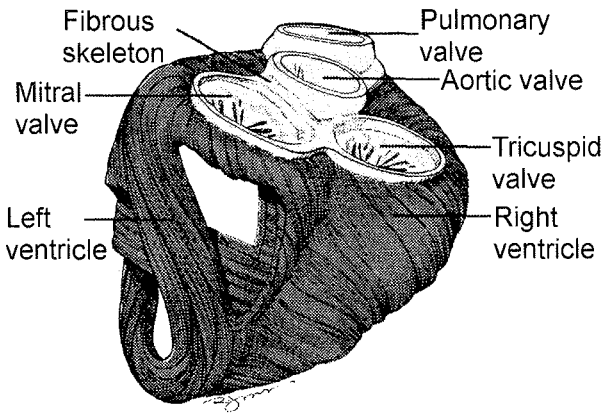

Figure 2.1: Schematic drawing of the muscle fiber structure in the heart. From Seeley et al. [46], with permission.

that are extending the sarcolemma into the central regions of the myocyte [29]. The mitochondria are responsible for most of the production of adenosine triphosphate (ATP). Sarcoplasmic reticulum is an internal storage buffer for calcium ions (Ca^{2+}).

The sarcomere is the basic contractile unit of the muscle, and is defined as the region between two Z-lines (Figure 2.2). Originating from the Z-lines, uniformly distributed thin filaments (ca. 1μm) are directed towards the next Z-line. Thick filaments (ca. 1.6μm) are distributed in parallel to the thin filaments and centrally located between two Z-lines. The different overlap regions between thick and thin filaments can be observed as a repeated pattern of dark and light regions, giving the name to cardiac and skeletal muscles as striated muscles. Force is generated through interaction between the thick and thin filaments and the muscle shortens when the filaments slide against each other.

The thick filament consists mainly of the protein myosin. The myosin molecule has a tail (ca. 1130 Å) which forms the backbone of the thick filament and two heads (ca. 620 Å) which form the cross-bridges between the thick and thin filaments (Figure 2.3). The thin filament consists of five different proteins. Two chains of actin monomers form the backbone of the thin filament. Tropomyosin molecules (ca. 400 Å) are located in the grooves between the two chains of actin monomers. The troponin complex, consisting of troponin C (TnC), troponin I, and troponin T, are connected to tropomyosin at approximately 400 Å intervals (Figure 2.3).

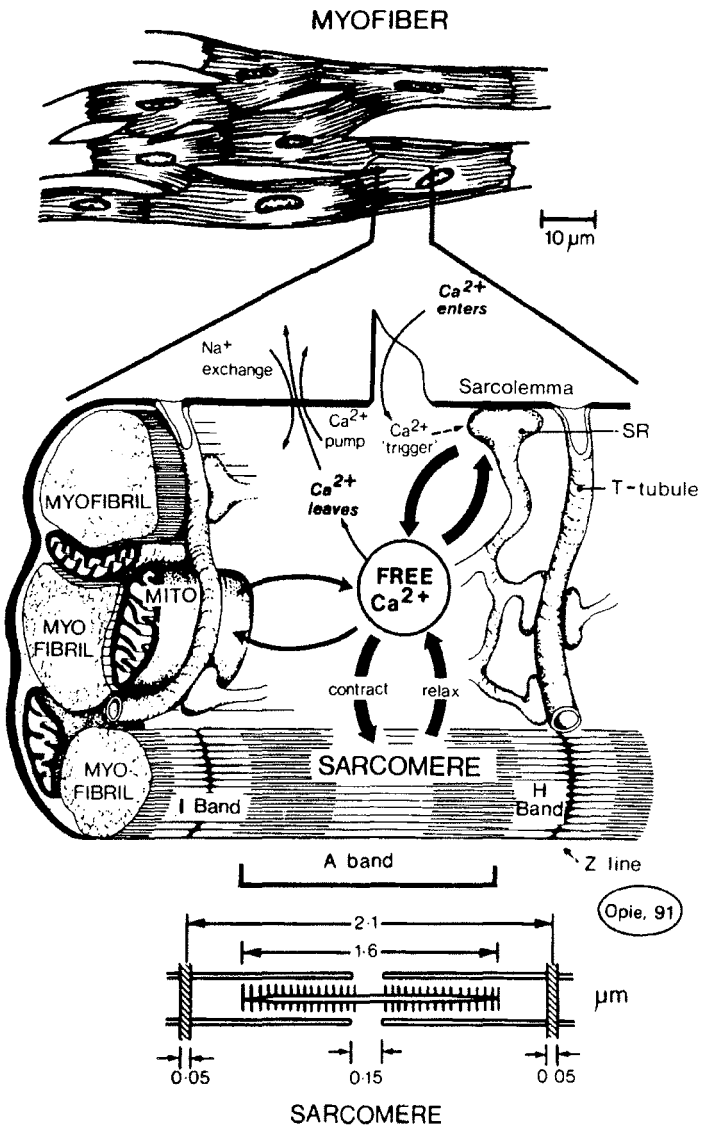

Figure 2.2: Schematic drawing of the structure and function of the cardiac muscle. From Opie [35], with permission.

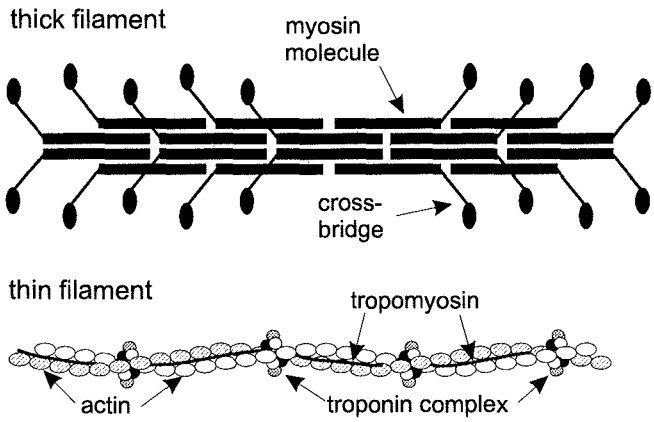

Figure 2.3: Schematic drawing of the structure of the thick and thin filaments. The thick filament contains mainly myosin molecules that are uniformly distributed in each direction from the center of the filament. The thin filament consists of two chains of actin monomers that are wound around each other. Two tropomyosin molecules lie in the grooves between the two actin chains on both sides. The troponin complexes consisting of troponin C, troponin I, and troponin T are distributed with approximately 400 Å intervals which is similar to the length of the tropomyosin molecule.

2.2 Cardiac Muscle Function

The key role of the myocyte is to contribute to the generation of ventricular pressure and volume flow out of the ventricle. On the level of myocytes or cardiac muscle fibers, the corresponding variables to pressure and volume are the force and length. According to Sys et al. [48], the determinants of instantaneous force can be described with Figure 2.4. Instantaneous force can be divided into passive and active force. Passive force is given by the force-length relation of extracellular and intracellular structures. Active force, represented by the cross-bridge interaction between myosin and actin, is given by the number of cross-bridges (CB) times the average force. The number of cross-bridges is regulated by the amount of activating calcium and the properties of the contractile proteins (CP) (see below). The instantaneous force is balanced against the external load and length, and modified by neurohumoral and cardiac endothelial control.

The underlying processes for the generation of active force may be divided into 1) excitation-contraction coupling, 2) cross-bridge cycling, and 3) ATP production. The excitation-contraction coupling includes the series of processes between the excitation of the cell by the action potential and the ability of the myosin heads to interact with

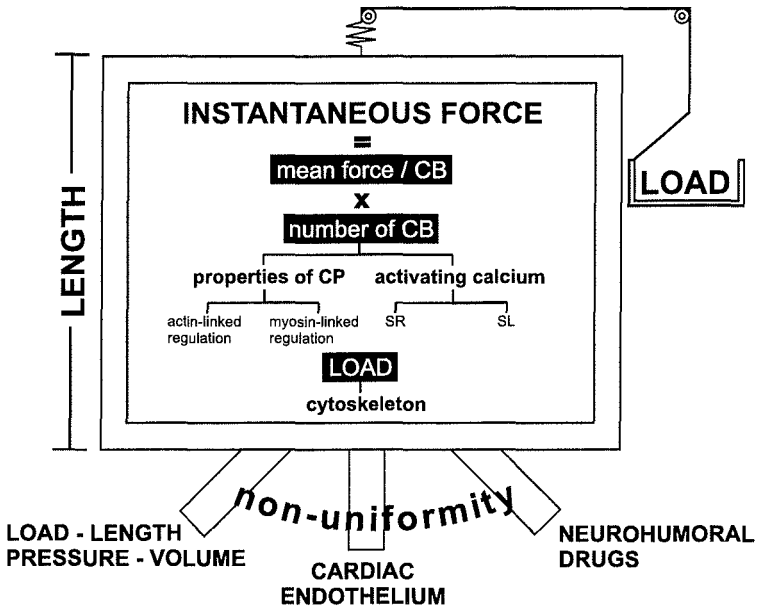

Figure 2.4: Schematic representation of the determinants of instantaneous force. CB - cross-bridge, CP - contractile proteins, i.e. myosin, actin, tropomyosin, and troponin complex, SR - sarcoplasmic reticulum, SL - sarcolemma. Reproduced with permission from Sys et al. [48].

actin. The action potential leads to a flux of Ca^{2+} into the cell, which in turn leads to a rapid release of Ca^{2+} from the sarcoplasmic reticulum [38, 52] (Figure 2.2). This yields a rapid increase in the level of intracellular Ca^{2+} (also called free calcium). In the absence of Ca^{2+}, the tropomyosin inhibit myosin-actin interaction by its position. When Ca^{2+} binds to TnC, this leads to a conformational change of the tropomyosin molecule, which in turn uncovers the binding sites on actin for the myosin heads [19]. This is called the calcium activation of the thin filament. The amount of activating calcium is therefore one important determinant of the instantaneous force.

A simplified cross-bridge cycle divided into four steps [29] is presented in Figure 2.5. Myosin and actin are dissociated in the initial resting state (state A). ATP is bound to the catalytic site of the myosin head (cross-bridge). ATP is then hydolyzed by the catalytic site of myosin (step 1). The hydrolytic products ADP and P_i remain bound to myosin, and chemical energy from the phosphate bond is stored in the cross-bridge, yielding an energized cross-bridge (state B). If the actin site is activated, it is now possible for the cross-bridge to attach to the actin site (step 2). The binding of the

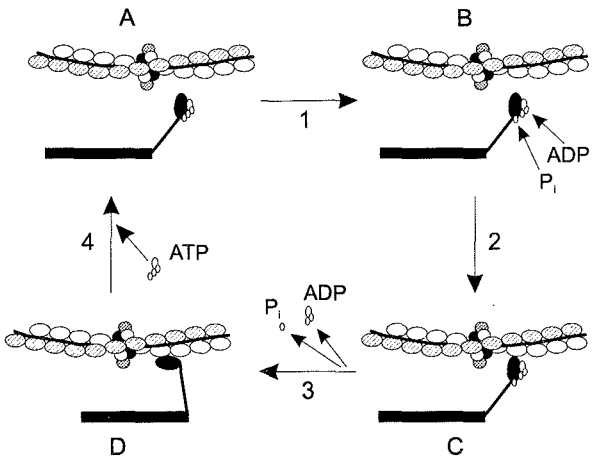

Figure 2.5: Schematic drawing of the cross-bridge cycle divided into four steps between four states. In state A, the muscle is relaxed and ATP is bound to the myosin head. Step 1 represents the ATP hydrolysis, which brings the cross-bridge into a relaxed, but energized state (B). Step 2 represents the attachment of myosin to actin, with the chemical energy still associated with the cross-bridge (state C or active complex). The chemical energy is transformed to mechanical work during step 3, when ADP and P_i (the products of ATP hydrolysis) are dissociated from the cross-bridge. This step brings the cross-bridge into the rigor state (D). Step 4 brings the muscle back to the relaxed state (A), which occurs when the cross-bridge dissociates from actin due to ATP binding to the myosin head.

cross-bridge to actin accelerates the dissociation of ADP and P_i from the cross-bridge (step 3). During this step, the chemical energy that is stored in the cross-bridge is transformed into mechanical work expressed as movement of the cross-bridge (state D). The cross-bridge dissociates from actin when ATP again binds to myosin (step 4).

As is clear from the cross-bridge cycle, the cross-bridges need ATP to perform work. ATP can be generated in two different ways, either as glycolysis or oxidative phosphorylation. Oxidative phosphorylation generates most of the ATP in normal hearts, but glycolysis becomes more important in the presence of ischemia. Mitochondria are specialized structures for oxidative phosphorylation [29, 35].

Chapter 3

Auxotonic Load

3.1 Definition

In this study, auxotonic loading is defined as simultaneous changes in stress and length. The phrase *controlled auxotonic twitch* means that the relation between the simultaneous changes in stress and length are controlled during a contraction-relaxation sequence (twitch).

3.2 Auxotonic Behavior in the Intact Heart

The cardiac cycle may be separated into different phases [8], for example, starting from electrical stimulation (i.e. the QRS-complex in the ECG diagram); isovolumetric contraction (IVC), ejection, isovolumetric relaxation (IVR), rapid filling (RFP), diastasis, and atrial contraction (AC). As a first approximation, the relation between the left ventricular (LV) pressure and the myocardial wall stress can be be described by LaPlace's law, given as:

$$p_{LV} = \frac{\sigma \cdot h}{r}$$

where p_{LV} is left ventricular pressure, σ is wall stress, h is wall thickness, and r is radius of curvature. This relation yields increased wall stress with increased radius, due to increased cavity volume, when pressure is constant. Given this relation it is clear that during the ejection and rapid filling phases, representing large volume changes and small pressure changes, there will be simultaneous changes in muscle fiber stress and shortening.

During IVC and IVR, both the mitral valve and the aortic valve are closed. There-

fore, the LV cavity volume is constant during these phases. A constant cavity volume, however, does not imply that the muscle fiber has a constant length (isometric) during the IVC and IVR phases. At least three different factors may contribute to auxotonic conditions on the level of muscle fibers. The possible role of torsion, changes in geometry, and non-uniformity will be described in the following.

3.2.1 Torsion

Streeter et al. [47] found that the muscle fiber angle (relative to the circumferential direction) varies across the myocardial wall from about 60° at the inner surface to about −60° at the outer surface. The variation in fiber orientation induces rotations of the apex region relative to the basis region of the ventricle. This rotation has been measured with magnetic resonance imaging (MRI) tagging, implanted markers, and optical devices [4, 12, 34, 41]. The counterclockwise rotation (viewed from the apex) during ejection is often called left ventricular twisting or torsion, and the back-rotation is often called untwisting. In normal hearts, Gibbons Kroeker et al. [12] measured an initial untwisting during IVC, followed by continuous twisting during ejection, yielding maximal rotation at approximately 15° close to end of ejection. A rapid untwisting is observed during IVR and early filling [12, 34].

The underlying mechanics of the observed rotation can be demonstrated with models of the left ventricle. With cylindrical and elliptical models, it has been found that left ventricular geometry, fiber architecture, compressibility, and active muscle performance have influence on the rotation dynamics [49]. Rademakers et al. [41] demonstrated that the speed and magnitude of untwisting during IVR and early filling were enhanced during inotropic intervention.

Both the timing and the magnitude of the apical rotation are altered in ischemic and hypertrophied hearts [30, 34].

3.2.2 Geometry

Although the ventricular chamber volume is constant during the IVC and IVR phases, the shape of the chamber may change during both phases. Changes in LV diameter and long axis have been measured, but not always with the same conclusions [17, 42, 43, 50]. Rankin et al. [42] found that the diameter decreased and the long axis lengthened during IVC and, while Tichonow [50] found the complete opposite. Rayhill et al. [43] reported isometric behavior of the intact papillary muscles during IVC and IVR. However, they also reported approximately 8% volume change during IVC, which implies that the chamber geometry changes relative to their ellipsoidal model for calculation of ventricular volume.

The changes in chamber geometry during IVC and IVR may be related to twisting [4] or non-uniformity (see below), but may also be related to other structural parameters than the variation in fiber orientation and to pressure differences between the left

and right ventricle [17].

Myocardial diseases, especially regional dysfunction may lead to more pronounced changes in isovolumetric chamber shape [43]. An ischemic region may be stretched by the contracting healthy region, yielding simultaneous shortening and lengthening of different parts of the myocardium.

3.2.3 Non-Uniformity

Differences in mechanical performance between different regions of the normally functioning ventricle have been demonstrated. Hittinger et al. [18] used ultrasound crystals to measure shortening of basal and apical segments. They found that the relative variance in shortening was especially pronounced during the isovolumetric phases. The physiological role of the non-uniformity on contraction and relaxation is reviewed by Brutsaert [6]. Non-uniform distributions of muscle fiber architecture, electrical activity, excitation-contraction coupling, and mechanical load may individually or together lead to auxotonic conditions locally, although the global condition is isovolumetric.

In diseased hearts, the auxotonic behavior are reported to be markedly altered [6, 30, 34, 43].

3.3 Auxotonic Load in Isolated Muscle Experiments

Sarcomere length of isolated muscle preparations can be measured with laser diffraction techniques [9, 31]. Segment lengths of isolated muscle preparations can be measured with glass microelectrodes, infused microspheres, tungsten pins, or derived from cross-sectional area [7, 22, 24, 39]. From such measurements it has been found that sarcomere or segment shortening occur also in twitches where the total muscle is isometric [7, 9, 23, 24, 31, 39]. The segment shortening in twitches with isometric muscle length has been attributed to increased compliance in the damaged end of the isolated muscle and to non-uniform muscle performance [7, 10, 20].

Despite the observed auxotonic behaviour on the sarcomere level of isometric contractions on the muscle level, very few attempts have been done to systematically study auxotonic properties on the level of isolated muscle. Paulus et al. [37] studied physiological loading of isolated papillary muscles, but that only included contraction, i.e. before the end of ejection. Leach et al. [33] used constant velocity experiments to study the concept of shortening deactivation, but also in this case they only studied the contraction phase. Another way to demonstrate auxotonic behavior is to control the muscles or sarcomeres to follow length trajectories that are extracted from intact heart measurements [14].

Chapter 4

Conclusions and Further Research

4.1 Conclusions

The goal of this study was to develop a mathematical model of the cardiac muscle function based on new experiments on isolated papillary muscles under a wide range of loading conditions.

The purpose of the study is important for the choice of an optimal modeling approach. In most cases, models of cardiac muscle function have been developed to represent experimental observations. Therefore, as the experiments are performed at lower and lower levels, the models also become more and more specific for the given experiments. A problem is then how to extrapolate the detailed findings to a higher level and under different loading conditions [48]. Another modeling direction is to describe the integrative effect of all the underlying processes with a phenomenological model. The problem with this approach is that the relation between the measured variables and the underlying mechanisms are reduced, which may reduce the possibility of the model to reproduce altered loading conditions or pathologies. In this study, we used experiments on isolated papillary muscle with a wide range of loading conditions to define the balance between detailed modeling of the dynamic processes and phenomenological representation of the integrative effect of the underlying processes.

Experiments on isolated papillary muscles are normally limited to isometric and isotonic control and quick load and length clamps. This is due to limitations of the control systems, but also due to the possibility of systematic analysis of muscle dynamics from such experiments. In the intact heart, the muscle fiber undergo auxotonic loading, i.e. simultaneous changes in stress and length, through all phases of the cardiac cycle. We wanted to study the isolated papillary muscle under controlled auxotonic conditions. This, however, required an extension of the existing experimental setup.

In order to incorporate auxotonic control and to compare muscle performance and dynamics under a wide range of loading conditions, we developed a flexible measurement and control system. This new system included real-time digital feedback control of length and force, stimulation control, individual control algorithms for different twitch types, and possibilities for on-line control or batch control of a series of predefined contraction-relaxation sequences with individual settings. The flexibility of the new measurement and control system made it possible to study the effects of altered loading conditions and other interventions on each individual muscle within a time span that allowed stable baseline muscle performance. Under auxotonic control, the developed force and shortening was proportional.

We studied the performance and dynamics of auxotonic twitches at different auxotonic load, i.e. different stress development-shortening ratio, and compared the results with conventional experiments from the same muscles under similar experimental conditions. In the auxotonic twitches, the stress development and shortening occur simultaneously, yielding continuous derivatives of stress and length. In afterloaded twitches, however, isotonic shortening follows isometric stress development, yielding discontinuous derivative of stress and length. The auxotonic twitches tended to develop more stress at similar shortening compared to afterloaded twitches. The initial conditions were the same in the two twitch types.

In contrast to afterloaded twitches, where contraction was prolonged at increasing afterload, the timing of auxotonic contraction was independent of load, when the initial length was at l_{max}. During relaxation, however, we found that stress decline was mainly dependent on the instantaneous stress, yielding high correlation between peak stress and time to half relaxation. These findings demonstrate fundamental differences in the properties of auxotonic contraction and relaxation.

The differences between load dependence of contraction and relaxation were further demonstrated when we plotted dimensionless time traces of mechanical dynamics by means of two expressions, defined as the sum of normalized stress and shortening. Differences in twitch type and loading conditions had little effect on the contraction pattern of these time traces of mechanical dynamics. But differences in load and twitch type yielded wide variations in the relaxation pattern of the same time traces. This implies that the loading conditions during contraction have little effect on the timing of contraction and the onset of relaxation, but may have serious implications on the mechanical dynamics and timing of relaxation.

The load dependence of contraction and relaxation and the timing and performance of auxotonic twitches were fundamental for our choice of model structure. We wanted a strong relation between the measured stress and length variables and the model variables in order to obtain identifiable model parameters. Therefore, we found it reasonable to incorporate the integrative effect of the calcium-troponin kinetics, the activation of the thin filament, and the cross-bridge kinetics in one variable, called activity. This activity variable was modeled as one model of activation and one model of inactivation. We investigated three different approaches to separate activation and inactivation according to our experimental findings on timing of contraction versus

timing of relaxation in auxotonic twitches. With all three approaches, the model simulated realistic series of auxotonic twitches. However, a moderate increase in the model complexity was needed to be able to reproduce realistic timing of isometric and afterloaded twitches and a rapid initial stress decline after the abrupt switch from isotonic lengthening to isometric stress decline in afterloaded twitches.

4.2 Directions for Further Research

The flexibility of the new digital measurement and control system enables a large potential for new features and applications. Different algorithms for the control of different twitch types allow easy implementation of new algorithms and definition of new twitch types, including e.g. length-trajectories, load-clamps, sequences of events in existing twitch types, and oscillations.

Increased bandwidth of the segment measurement system would improve the segment length control and the control of segment auxotonic twitches. Today there is a gap between the peak force of the isometric twitch versus peak force in the auxotonic twitch with the highest auxotonic load. Because the highest auxotonic load is limited by the bandwidth of the control system, the gap could be decreased with increased bandwidth.

In this study, we have analyzed a number of properties of the auxotonic twitch. Nevertheless, other analyses with alternative muscle preparations, interventions, and loading conditions, will be needed to uncover new features of the cardiac muscle. Based on the discussions in this study, a combined study of auxotonic twitches with simultaneous measurements of the intracellular Ca^{2+} transient may confirm our hypotheses or bring up new insight about the underlying processes.

The mathematical model presented in this thesis represents a general model structure with a number of possible adaptations. Three different models for separation of activation and inactivation were studied. These three models have different opportunities when it comes to possible extensions of the model, e.g. the first model approach enables extended modeling of the intracellular Ca^{2+} transient, while the third model approach enables smooth combination of individual models for different timing and loading.

References

1. Abbott BC and Mommaerts WFHM. A study of inotropic mechanisms in the papillary muscle preparation. *J. Gen. Physiol.* 42:533–551, 1959.

2. Allen DG and Kentish JC. The cellular basis of the length-tension relation in cardiac muscle. *J. Mol. Cell. Cardiol.* 17:821–40, 1985.

3. Angelsen BAJ, AAkhus S, Rabben SI, and Torp HG. Model-based estimation of vascular parameters: Evaluation of robustness and suitability of models. *Echocardiography* 11:409–23, 1994.

4. Beyar R, Yin FC, Hausknecht M, Weisfeldt ML, and Kass DA. Dependence of left ventricular twist-radial shortening relations on cardiac cycle phase. *Am. J. Physiol.* 257:H1119–26, 1989.

5. Bremel RD and Weber A. Cooperation within actin filament in vertebrate skeletal muscle. *Nat. New. Biol.* 238:97–101, 1972.

6. Brutsaert DL. Nonuniformity: A physiologic modulator of contraction and relaxation of the normal heart. *J. Am. Coll. Cardiol.* 9:341–8, 1987.

7. Brutsaert DL, Claes VA, Chuck LM, Housmans PR, Sys SU, and DeClerck NM. New technology in studying the origin of non-uniformity in cardiac muscle. In: Kitamura K and Abe H, eds., *New approaches in cardiac mechanics*, 31–45. Gordon and Breach, New York, USA, 1986.

8. Brutsaert DL and Sys SU. Relaxation and diastole of the heart. *Physiol. Rev.* 69:1228–315, 1989.

9. de Tombe PP and ter Keurs HE. Sarcomere dynamics in cat cardiac trabeculae. *Circ. Res.* 68:588–96, 1991.

10. Donald TC, Reeves DN, Reeves RC, Walker AA, and Hefner LL. Effect of damaged ends in papillary muscle preparations. *Am. J. Physiol.* 238:H14–23, 1980.

11. Frank O, Translated by Chapman CB, and Wasserman E. On the dynamics of cardiac muscle (Zur dynamik des herzmuskels). *Am. Heart. J.* 58:282–317, 1959.

12. Gibbons Kroeker CA, Ter Keurs HE, Knudtson ML, Tyberg JV, and Beyar R. An optical device to measure the dynamics of apex rotation of the left ventricle. *Am. J. Physiol.* 265:H1444–9, 1993.

13. Gordon AM, Huxley AF, and Julian FJ. The variation in isometric tension with sarcomere length in vertebrate muscle fibres. *J. Physiol.* 184:170–92, 1966.

14. Guccione JM, Le Prell GS, de Tombe PP, and Hunter WC. Measurements of active myocardial tension under a wide range of physiological loading conditions. *J. Biomech.* 30:189–92, 1997.

15. Guccione JM, Motabarzadeh I, and Zahalak GI. A distribution-moment model of deactivation in cardiac muscle. *J. Biomech.* 31:1069–73, 1998.

16. Hill AV. The heat of shortening and the dynamic constants of muscle. *Proc. R. Soc. Ser. B* 126:136–195, 1938.

17. Hittinger L and Crozatier B. Diameters and segment relations during the cardiac cycle in the canine left ventricle. *Basic. Res. Cardiol.* 83:501–9, 1988.

18. Hittinger L, Crozatier B, Belot JP, and Pierrot M. Regional ventricular segmental dynamics in normal conscious dogs. *Am. J. Physiol.* 253:H713–9, 1987.

19. Holmes KC. The actomyosin interaction and its control by tropomyosin. *Biophys. J.* 68:2S–7S, 1995.

20. Housmans PR, Chuck LH, Claes VA, and Brutsaert DL. Nonuniformity of contraction and relaxation of mammalian cardiac muscle. *Adv. Exp. Med. Biol.* 170:837–40, 1984.

21. Hunter PJ, McCulloch AD, and ter Keurs HE. Modelling the mechanical properties of cardiac muscle. *Prog. Biophys. Mol. Biol.* 69:289–331, 1998.

22. Huntsman LL, Day SR, and Stewart DK. Nonuniform contraction in the isolated cat papillary muscle. *Am. J. Physiol.* 233:H613–6, 1977.

23. Huntsman LL, Joseph DS, Oiye MY, and Nichols GL. Auxotonic contractions in cardiac muscle segments. *Am. J. Physiol.* 237:H131–8, 1979.

24. Huntsman LL, Rondinone JF, and Martyn DA. Force-length relations in cardiac muscle segments. *Am. J. Physiol.* 244:H701–7, 1983.

25. Huxley AF. Muscle structure and theories of contraction. *Prog. Biophys. Mol. Biol.* 7:255–318, 1957.

26. Huxley AF and Niedergerke R. Structural changes in muscle during contraction. *Nature* 173:971–973, 1954.

27. Huxley H. The double array of filaments in cross-striated muscle. *J. Biophysic. Biochem. Cytol.* 3:631–47, 1957.

28. Huxley H and Hanson J. Changes in the cross-striations of muscle during contraction and stretch and their structural interpretation. *Nature* 173:973–976, 1954.

29. Katz AM. *Physiology of the heart*. Raven Press, New York, 2nd edition, 1992.

30. Kroeker CA, Tyberg JV, and Beyar R. Effects of ischemia on left ventricular apex rotation. An experimental study in anesthetized dogs. *Circulation* 92:3539–48, 1995.

31. Krueger JW and Pollack GH. Myocardial sarcomere dynamics during isometric contraction. *J. Physiol.* 251:627–43, 1975.

32. Landesberg A and Sideman S. Mechanical regulation of cardiac muscle by coupling calcium kinetics with cross-bridge cycling: A dynamic model. *Am. J. Physiol.* 267:H779–95, 1994.

33. Leach JK, Brady AJ, Skipper BJ, and Millis DL. Effects of active shortening on tension development of rabbit papillary muscle. *Am. J. Physiol.* 238:H8–13, 1980.

34. Matter C, Nagel E, Stuber M, Boesiger P, and Hess OM. Assessment of systolic and diastolic LV function by MR myocardial tagging. *Basic. Res. Cardiol.* 91 Suppl 2:23–8, 1996.

35. Opie LH. *The heart: Physiology and metabolism*. Raven Press, New York, 2nd edition, 1991.

36. Panerai RB. A model of cardiac muscle mechanics and energetics. *J. Biomech.* 13:929–40, 1980.

37. Paulus WJ, Claes VA, and Brutsaert DL. Physiological loading of isolated feline cardiac muscle. The interaction between muscle contraction and vascular impedance in the production of pressure and flow waves. *Circ. Res.* 44:491–7, 1979.

38. Peskoff A and Langer GA. Calcium concentration and movement in the ventricular cardiac cell during an excitation-contraction cycle. *Biophys. J.* 74:153–74, 1998.

39. Peterson JN, Hunter WC, and Berman MR. Control of segment length or force in isolated papillary muscle: An adaptive approach. *Am. J. Physiol.* 256:H1726–34, 1989.

40. Peterson JN, Hunter WC, and Berman MR. Estimated time course of Ca2+ bound to troponin C during relaxation in isolated cardiac muscle. *Am. J. Physiol.* 260:H1013–24, 1991.

41. Rademakers FE, Buchalter MB, Rogers WJ, Zerhouni EA, Weisfeldt ML, Weiss JL, and Shapiro EP. Dissociation between left ventricular untwisting and filling. Accentuation by catecholamines. *Circulation* 85:1572–81, 1992.

42. Rankin JS, McHale PA, Arentzen CE, Ling D, Greenfield JCJ, and Anderson RW. The three-dimensional dynamic geometry of the left ventricle in the conscious dog. *Circ. Res.* 39:304–13, 1976.

43. Rayhill SC, Daughters GT, Castro LJ, Niczyporuk MA, Moon MR, Ingels NBJ, Stadius ML, Derby GC, Bolger AF, and Miller DC. Dynamics of normal and ischemic canine papillary muscles. *Circ. Res.* 74:1179–87, 1994.

44. Rice JJ, Winslow RL, and Hunter WC. Comparison of putative cooperative mechanisms in cardiac muscle: Length dependence and dynamic responses. *Am. J. Physiol.* 276:H1734–54, 1999.

45. Söderström T and Stoica P. *System identification*. Prentice Hall, Cambridge, UK, 1989.

46. Seeley RR, Stephens TD, and Tate P. *Anatomy and physiology*. Mosby Year Book, St. Louis, USA, 2nd edition, 1992.

47. Streeter DDJ, Spotnitz HM, Patel DP, Ross J, and Sonnenblick EH. Fiber orientation in the canine left ventricle during diastole and systole. *Circ. Res.* 24:339–347, 1969.

48. Sys SU, De Keulenaer GW, and Brutsaert DL. Physiopharmacological evaluation of myocardial performance: How to study modulation by cardiac endothelium and related humoral factors? *Cardiovasc. Res.* 39:136–47, 1998.

49. Taber LA, Yang M, and Podszus WW. Mechanics of ventricular torsion. *J. Biomech.* 29:745–52, 1996.

50. Tichonow KB. The geometry of the left ventricle in the isovolumic period. *Radiologe* 26:446–51, 1986.

51. Tözeren A. Continuum rheology of muscle contraction and its application to cardiac contractility. *Biophys. J.* 47:303–9, 1985.

52. Wier WG and Yue DT. Intracellular calcium transients underlying the short-term force- interval relationship in ferret ventricular myocardium. *J. Physiol.* 376:507–30, 1986.

53. Wong AY. Mechanics of cardiac muscle, based on Huxley's model: Mathematical stimulation of isometric contraction. *J. Biomech.* 4:529–40, 1971.

54. Wong AY. Mechanics of cardiac muscle, based on Huxley's model: Simulation of active state and force-velocity relation. *J. Biomech.* 5:107–17, 1972.

Paper A

Controlled Auxotonic Twitch in Papillary Muscle: A new Computer-Based Control Approach

Vidar Sørhus[1], Stanislas U. Sys[2], Anders Natås[1],
Marc J. Demolder[2], Bjørn A. J. Angelsen[1]

[1] Dept. of Physiology and Biomedical Engineering, NTNU, Trondheim, Norway
[2] Dept. of Human Physiology and Pathophysiology, UIA (RUCA), Antwerp, Belgium

Abstract

Based on new developments in digital technology, we developed a PC- and DSP-based measurement and control system for isolated papillary muscle experiments. High flexibility was obtained through a three level control. Length or force was controlled real-time with a sample frequency of 5000Hz. Muscle length and up to three segment lengths were measured simultaneously and each of these lengths could be chosen as feedback variable. Individual algorithms were implemented for different twitch types. Batches of twitches were organized in experiment protocols. The system included a new twitch type, namely a controlled auxotonic twitch. In this twitch, the muscle acted against a simulated ideal spring, giving a proportional change in developed force and shortening.

Keywords: real-time digital control; segment control; rabbit papillary muscle; cardiac muscle mechanics; non-isometric force development; first instable beat

1 Introduction

Experiments on papillary muscles have long been performed to gain knowledge about the physiology and mechanics of the cardiac muscle. The advantages of the papillary muscle are the uniform distribution of muscle fibers, uniform fiber directions, and the relatively small damage during dissection. Short term and long term response to mechanical and pharmacological interventions have been studied with different laboratory setups [2, 14, 19, 22, 23, 27]. To reduce the possible error due to the damaged ends of the papillary muscle, muscle segment length [14, 22] and sarcomere length [24] have been used as length measurement. Brutsaert and Sys [3, 28, 29] have developed a method to measure one or two central segments in addition to the damaged lower segment and the tendon end.

The muscles in traditional experimental setups have usually been controlled in either an isotonic state (constant force), an isometric state (constant length), or a sequential combination of the two states (afterloaded isotonic twitches) to represent the cardiac cycle. In addition, quick changes in load and length have been used to give information about cardiac muscle mechanics. Information from such experiments has been used to develop and evaluate models of the cardiac muscle [15, 18, 23, 31, 32]. However, on the fiber level in the intact heart, the cardiac cycle is not a sequence of strict isotonic and isometric states. In the ejection phase of the cardiac cycle, there are simultaneous and coupled changes in force and length. But also in the isovolumetric phases of contraction and relaxation there are changes in length at the muscle fiber level. This is mainly due to torsion or twisting [10, 25] and changes in left ventricular geometry [26]. It may also be caused by non-uniformity which is found in isolated muscles [3, 12, 14] and in intact hearts [11]. Huntsman et al. [14] have observed and analyzed such non-isometric traces of muscle segments (segment auxotonic) in muscle isometric twitches. Controlled auxotonic states, however, with simultaneous and coupled changes in both length and force throughout the entire twitch, have not been studied in the isolated papillary muscle.

Different control systems have been used for isolated papillary muscle experiments; e.g. analog feedback control of muscle length [23, 28] or adaptive calculation of an output trajectory from previous twitches [22]. These control approaches have some obvious limitations despite their advantages. In an analog feedback system, the configuration of different experiments must be done manually with knobs and buttons. This limits the flexibility and the possibility to do series of different experiments in one muscle during a limited time span. An adaptive control approach where the output trajectory for one twitch is calculated from previous twitches, needs some calculations before it converges. In addition, it needs several twitches at each output trajectory to get stabilized. Although the adaptive control approach gave very nice results for the time course of the twitch [22], it is not possible to study the first instable beat [16, 17, 21] with this approach. In each of these control approaches, it is difficult to include completely different experimental conditions like a controlled auxotonic twitch.

In order to analyze the isolated cardiac muscle under auxotonic conditions, to an-

alyze the differences between muscle and segment performance, and to analyze the muscle performance under a wide range of mechanical experiments on individual muscles under the same reference conditions, a new flexible control system is needed.

In recent years, there has been a rapid development of digital technology, resulting in a large number of digital control systems. Especially the development of the digital signal processor (DSP) has made it possible to implement real-time digital controls in a PC environment.

We wanted to utilize digital technology to develop a new measurement and control system for papillary muscle experiments. The first goal of the project was to introduce a new twitch type, namely a controlled auxotonic twitch with simultaneous and coupled changes in length and force as if the muscle was acting against an ideal spring. The second goal was to allow digital measurement and real-time feedback control of different lengths. We wanted to measure simultaneously both total muscle length and a number of segment lengths, and to use any of these measurements as feedback variable. The third goal was to increase the flexibility of the setup. We wanted to utilize the digital measurement and control system to develop a system to perform a wide range of experiments on each single muscle within a reasonable time span.

2 Methods

2.1 Muscle Preparation

The examples presented in this paper were all from rabbits weighing between 2.5 and 3 kg. The rabbit was anesthetized by cervical translocation and the heart was quickly excised. A papillary muscle was dissected from the right ventricle in a dissection bath with temperature controlled and oxygenated Krebs-Ringer solution (see below), containing 2,3-butanedione monoxime (BDM; 30mM) to inhibit actin-myosin cross-bridge cycling during dissection. The muscle was passively stretched with a preload of 6 mN/mm^2 of estimated cross-sectional area. Under a dissection microscope (WILD M3B from Leica) three tips of glass microelectrodes were inserted into the muscle perpendicular to the long axis. At the tip the diameters of the microelectrodes were less than 5 μm, and at the muscle surface the diameters were maximally 15 μm. Then the papillary muscle was installed vertically in a 3 ml bath. The Krebs-Ringer solution was circulating with a flow rate of approximately 10 ml/min and contained (in mM): NaCl 98, KCl 4.7, $MgSO_4.7H_2O$ 2.4, $NaHCO_3$ 25, $CaCl_2.2H_2O$ 1.25, glucose 4.5, Na-pyruvate 15 and Na-acetate 5, at 29°C bubbled with a gas mixture of 95 % oxygen and 5 % carbon dioxide. An electrical field between two platinum electrodes stimulated the papillary muscle at approximately 10 % above threshold.

2.2 Analog/Mechanical Setup

The papillary muscle setup was based on an analog/mechanical setup which is described in [2, 4]. The original system consisted of an electromagnetic force transducer with a bandwidth of approximately 500Hz, an optical displacement measurement transducer, and a control unit for isotonic, afterloaded, and isometric control and for stimulation control. The control unit had a static compliance of 0.25 μm/mN and negligible dynamic compliance during isometric control. The reference length and afterload values were adjusted manually. We replaced the control unit of the original setup with a PC with a DSP board and an interface unit between the PC and the transducers. With knowledge of the preload length of the muscle, instantaneous muscle length and relative shortening could be determined on-line.

The system also included a segment measurement system [3, 28] where three glass microelectrodes used to divide the muscle length into four muscle segments, were detected optically. A halogen lamp was mounted on one side of the muscle bath and a microscope with 4 or 10 times magnification was used to improve the resolution. A 1024 element CCD array with a scan rate of 1950 scans/s was mounted on the microscope. The lower edges of the shadows from the microelectrodes were detected and used to calculate segment lengths. The lengths of the lower segment and two central segments were measured directly, while the length of the tendon end could be found from the total muscle shortening and the three lower segments if the resting length of the muscle was known.

2.3 Digital Measurement and Control

The PC-based measurement and control system was divided into two hardware and software parts (Figure 1). The user interface and high level control was implemented on a 200MMX Pentium PC with Windows95. A Data Translation Fulcrum DT3801-G DSP board contained, in addition to the digital signal processor (TMS320C40, Texas Instruments), a 12-bit AD converter with up to 8 channels, a 16-bit DA converter, digital output, and a hardware timer. On this board, we implemented a control and acquisition application which was communicating with the user interface program on the host computer.

We developed an integrated control system where the overall control was divided into three different levels of control. On the highest level, was the *batch control* which controlled a user-defined sequence of twitches with individual settings. One of the settings in the experimental protocol was the twitch type. This setting enabled a specific *twitch control* which was the middle level of control. To make the overall system as flexible as possible and easy to extend with new control algorithms, we developed individual control algorithms for each twitch type. The lowest level of control was the *real-time feedback control.* The force transducer was used to control both force and lengths. For length control the measured (muscle or segment) length determined the output to the force transducer. For force control, the output to the force transducer was

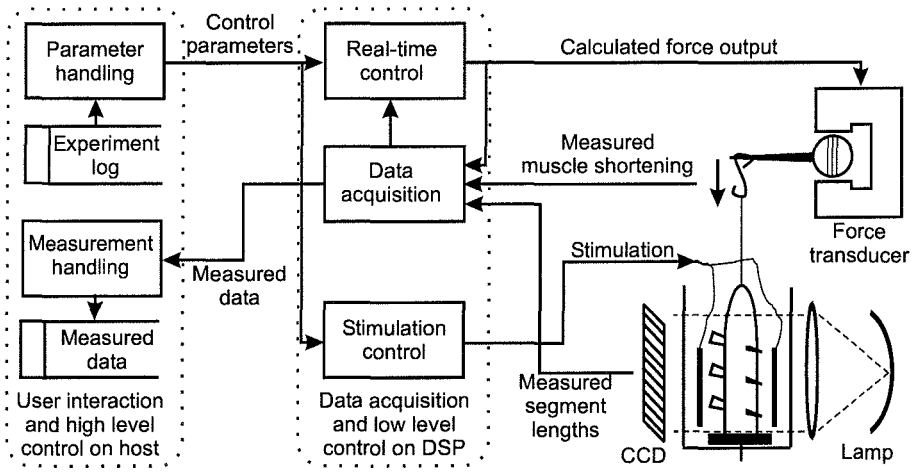

Figure 1: Main components and data flow in the system. An application for real-time control, data acquisition, and stimulation control was running on the DSP board. Total muscle shortening and muscle segment lengths were measured and sent via the DSP-board to the host computer through a measurement channel and optionally stored in a text-file (Measured data). An application for user interaction and high level control was running on the host computer. Control parameters set by the user or read from a text-file (Experiment log) were sent from the host computer to the DSP-board through a parameter channel.

the desired force. Control parameters were sent from the host computer application to the DSP board application while measurements were sent in the opposite direction (Figure 1).

2.3.1 Host-Program - High Level Control and User Interface

Visualization and storage of measured and calculated variables, on-line user interaction, and overall control of experiments were performed on the host computer. The program on this host computer was written in a standard programming language (Visual Basic 5.0). The host program had three main purposes. First, it downloaded the DSP-program to the DSP-board and established two communication channels between the host-program and the DSP, one for the control parameters and one for the measured data. Second, it handled the user-changeable parameters. Third, it visualized and saved on files the measured data that was sent from the DSP.

At the highest level of control, the system was designed to allow user interaction on all the relevant parameters in the system. Twitch parameters included twitch

type, reference length, preload, afterload, and muscle length. Stimulation parameters included stimulation frequency, stimulation pulse duration, and possibilities for paired stimulation. Furthermore, acquisition parameters included decimation factor, buffers to plot, and force scale factor. Finally, PID parameters included feedback variable, gain, derivation time constant, integral time constant, and filter constant.

It was possible to access the parameters in two different ways. First, parameter values were specified in an experiment log (text-file, Figure 2, lower panel), where each row contained one set of parameters. One of the parameters ("Iter", second last column) defined the number of twitches that should run with the same set of parameters before the protocol was switched to the next row. New parameter values were always sent to the DSP program immediately before the next stimulation. This time for parameter transfer was chosen to reduce the possibility for dangerous steps in the output to the muscle. Second, the parameters could also be changed on-line by user interaction with an options form. The on-line interaction was disabled when an experiment protocol was running.

Whenever a buffer of measured data was sent to the host computer, a special procedure for measurement organization started. The measured data could be presented in three different ways. Time-traces of measured muscle length and segment lengths and calculated force were plotted in a twitch plot. Initial and peak values of muscle length, segment lengths, and force were calculated for every twitch. These values could be plotted in either a trend plot or an XY plot, e.g. initial length vs. active force in order to determine l_{max} (the muscle length with the highest developed isometric force). The trend plot was used to watch the long-term performance of the muscle and to assure that the preparation was stable during experiment protocols. When an experiment protocol was running, it was possible to save the measured data to a text-file. The user could set a save option on each row in the experiment log-file.

2.3.2 DSP - Low Level Control and Acquisition

An individual application for feedback control and data acquisition was running on the DSP board (Figure 1). This application was programmed in the ANSI C language with a library for the SPOX operating system and the Data Translation DSP LAB software library. The application was communicating with the muscle setup through the I/O on the DSP-board and with the host computer through the internal bus. In addition to a control interrupt service routine for real-time feedback control (ControlISR), the DSP-program contained the following main components: a timer interrupt service routine for stimulation control, a procedure for receiving control parameters from the host program, and a procedure to send measured data to the host program.

Two levels of control were performed in the ControlISR, namely the *twitch control* and the *real-time feedback control*. We implemented control algorithms for five different twitch types (Figure 2 - Figure 5). 1) In preloaded isotonic twitches, force was constant and equal to preload (traces marked with "it" in Figure 2, panel A and B). 2) In isometric twitches, force was calculated with a PID-algorithm (see below) with a

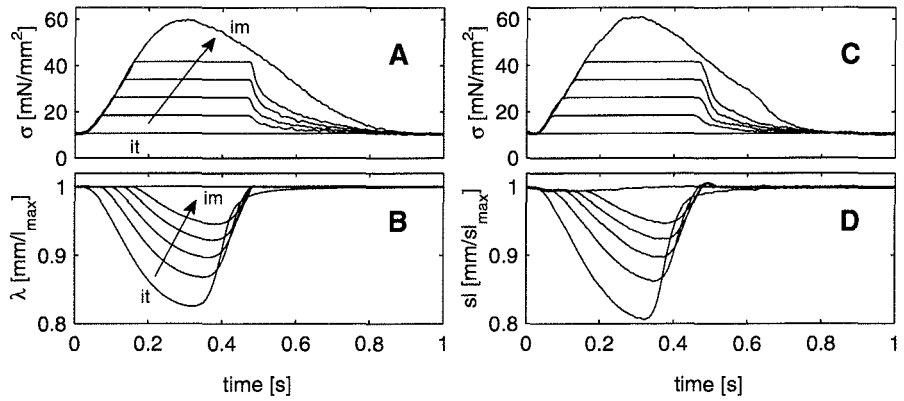

TwType	Feedback	MLRef	SRef	AL	PL	K	T	ΔT	PS	PST	Iter	Save
Isotonic	TotalLength				5.5		1667	5			8	0
											1	1
Afterloaded		-1		4							1	1
Isotonic											8	0
Afterloaded		-1		8							1	1
Isotonic											8	0
Afterloaded		-1		12							1	1
Isotonic											8	0
Afterloaded		-1		16							1	1
Isotonic											8	0
Isometric		-1									1	1
Afterloaded				10							1	0

Figure 2: *Upper panels*: Series of afterloaded isotonic twitches at increasing afterload (arrows) from preloaded isotonic (it) to isometric (im). Total length was controlled in one experiment (panel A and B) and segment length was controlled in another experiment (panel C and D) on the same muscle. Stress in panel A and C and relative length in panel B and D. *Lower panel*: Experiment log file for the series of afterloaded isotonic twitches in panel A and B. The columns contain, from left to right, twitch type (TwType), feedback variable (Feedback), muscle reference length (MLRef), segment reference length (SRef), afterload (AL [mN]), preload (PL [mN]), auxotonic constant (K), stimulation interval (T [ms]), stimulation pulse duration (ΔT [ms]), paired stimulation (PS [on/off]), paired stimulation interval (PST [ms]), number of twitches with the same parameters (Iter), and save measured data option (Save [on/off]). Empty cells mean that the stored values are used. -1 in the "MLRef" column means that the resting length from the previous twitch is used as reference length. Only the saved twitches (Save=1) are presented in panel A and B.

given total muscle or segment reference length (traces marked with "im" in Figure 2, panel A and B). 3) Afterloaded isotonic twitches (Figure 2), with isometric-isotonic contraction and isotonic-isometric relaxation sequences, were isometric at reference

length if the calculated force was less than preload + afterload. 4) For physiological twitches, with isometric-isotonic contraction and isometric-isotonic relaxation sequences [15, 28](Figure 5), the following sequence control was implemented. Initially, after stimulation the muscle was kept isometric at reference length until calculated force exceeded preload + afterload. Then, the force was kept constant at preload + afterload until shortening velocity became zero. The length at zero shortening velocity was used as reference length during isometric relaxation until calculated force reached the preload value. Then, the force was constant at preload for the remainder of the twitch (isotonic relaxation). 5) In auxotonic twitches (Figure 3), calculated force minus preload at initial length was proportional to shortening during the whole twitch.

The lowest level was the *real-time feedback control* with a sample frequency of 5000 Hz. When the AD converter had scanned through all four analog input channels (20kHz), it invoked the ControlISR. Then the control algorithm calculated a new control output and sent it to the force transducer through the DA converter. Force or length could be controlled in three different states. In the isotonic state, a constant force was sent to the force transducer. In the isometric state, a discrete version of the PID (proportional-integral-derivative) controller [20] with anti-windup and bumpless transfer was used. The parameters in the PID controller were set individually for muscle and segment length control. In the auxotonic state, the force output minus a reference force was proportional to the difference between length and reference length, with a user-defined proportionality factor.

3 Results

3.1 Performance of Digital Control

The reason why we wanted to develop a digital control system for the papillary muscle experiment was that we needed more flexibility, a new auxotonic twitch type, and the possibility to switch between control of muscle length and segment length. We will return to the advantages of the integrated control system in the discussion section.

In a digital feedback control, the signal has to be sampled, limiting the bandwidth of the system. Therefore, the design specifications for the control of isometric muscle length were different for the digital controller than for the analog controller. Values of static compliance (static deviation), dynamic compliance (ramp deviation), resolution, and noise level in the old and new control system are shown in Table 1. The numbers in the table are based on experiments on muscles with muscle length between 3 and 5.5 mm and segment length between 1.0 and 1.4 mm. Because the segment measurement system was the limiting part with respect to bandwidth and resolution, the performance was approximately the same with the digital and the replaced analog control system during segment control.

Table 1: System performance in replaced analog and new digital measurement and control system.

	Muscle analog control	Muscle digital control	Segment digital control (x4[a])	Segment digital control (x10[b])
static compliance	0.25 μm/mN	negligible	negligible	negligible
dynamic compliance	negligible	0.13 μm/mN	0.5 μm/mN	0.22 μm/mN
resolution	unlimited	1.22 μm	4.3 μm	1.6 μm
noise level		$\pm$1.22 μm	$\pm$4.3 μm	$\pm$1.6 μm

[a] Four times magnification on segment measurement microscope.
[b] Ten times magnification on segment measurement microscope.

3.2 Controlled Auxotonic Twitches

One major reason for the development of a digital control system was the introduction of the controlled auxotonic twitch. We developed an auxotonic twitch where the muscle acted against an ideal spring. Then, by changing the spring constant we obtained simultaneous and coupled changes in length and force with varying load. Ideally, the isotonic case was similar to a spring constant equal to zero, and the isometric case was similar to an infinitely large spring constant. Due to the bandwidth of the feedback control, we are not able to perform auxotonic twitches with unlimited spring constants. Developed force in auxotonic twitches exceeded 50 % of developed force in the isometric twitch, which means that the auxotonic twitches cover the physiological range of force development. Figure 3 shows the time traces of relative muscle length ($\lambda = l/l_{max}$) and stress (force per cross-sectional area) for a series of auxotonic twitches with increasing spring constant (a-d). Important to notice that this twitch type has continuous derivatives of length and stress throughout the twitch in contrast to afterloaded and physiological twitches. The controlled auxotonic twitch allowed a smooth transition from isotonic towards isometric loading conditions. Figure 4 shows how the auxotonic twitches represented a different pattern than both the afterloaded isotonic and the physiological twitches in the stress-length plot.

Although the main goal here is to present the auxotonic twitch, we also present two initial observations on 1) stress decline during relaxation in auxotonic twitches, and 2) stress development in auxotonic twitches compared with afterloaded and isometric twitches. We will return to these observations in the discussion section.

First, with the auxotonic twitch it is possible to study stress decline during non-isometric relaxation. In Figure 3, a series of auxotonic twitches is presented together with a phase plot of derivative of stress vs. stress (panel C). From this figure, we can see that the traces at different spring constants, and hence different lengths and velocities, follow the same trace as the isometric twitch during relaxation. This means that stress decline in auxotonic twitches is stress dependent.

Second, the amount of developed stress in the auxotonic and afterloaded isotonic twitches can only be compared when both twitch type experiments are obtained from

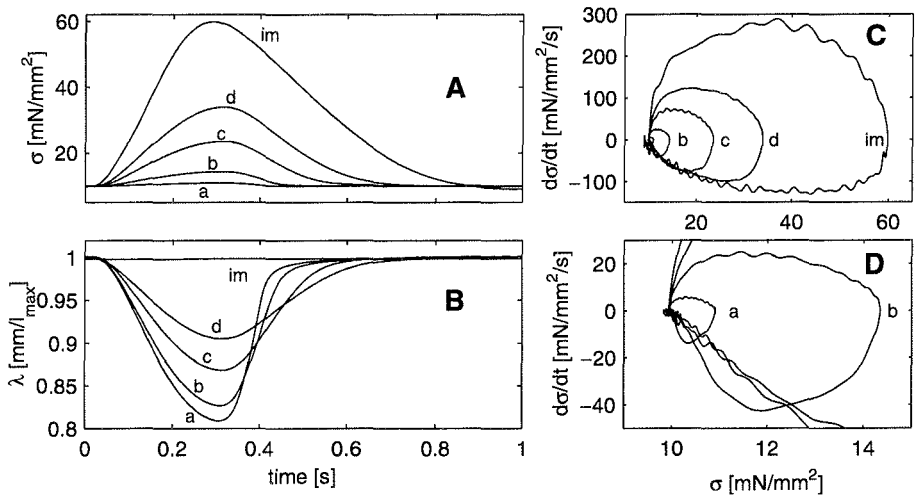

Figure 3: Series of auxotonic twitches at increasing spring constant (a-d) and one isometric twitch (im) with corresponding derivative of stress vs. stress. Stress traces in panel A, length traces in panel B, and derivative of stress vs. stress in panel C. Time direction is clockwise. Panel D shows derivative of stress vs. stress in auxotonic twitches close to isotonic from the same data as in panel C, except that it is zoomed out and the isometric twitch is removed.

the same muscle, and when muscle performance is unchanged between both experiments. Therefore, each experiment log included a preloaded isotonic and an isometric twitch to allow comparison of muscle performance (i.e. peak isotonic shortening and peak isometric stress). In all experiments we have done so far where we have comparable muscle performance, the auxotonic twitches develop more stress than the afterloaded isotonic twitches with the same peak shortening (alternatively, more shortening at the same developed stress). One example is presented in Figure 4, panel C and E. Furthermore, isometric twitches develop more stress than the auxotonic twitches at the same shortest length (panel D).

3.3 Standard Experiments and the Experiment Protocol

Time traces of muscle length and stress for a series of afterloaded isotonic twitches are presented in Figure 2, panel A and B respectively. Initial length was the same in all twitches, but the afterload varied from zero (preloaded isotonic twitch) until the afterload exceeded peak force (isometric twitch). A similar experiment with segment length control is presented in panel C and D (Figure 2). The experiments were organized in text files (Figure 2, lower panel). The first column in the experiment log was the twitch type. This could be set individually for each twitch so that we could get

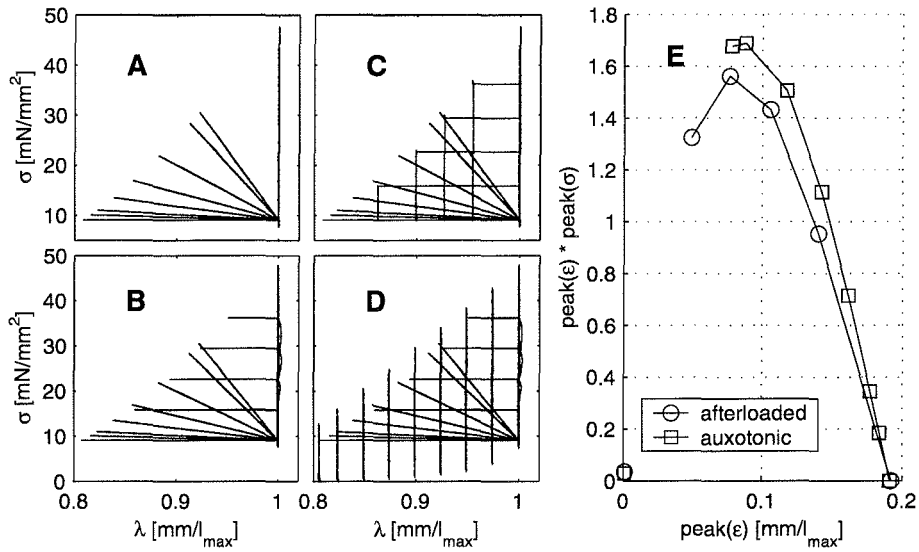

Figure 4: Series of auxotonic, afterloaded isotonic, physiological, and isometric twitches from consecutive experiments on one muscle in a stress-length plot. Auxotonic twitches in panel A, auxotonic and afterloaded isotonic twitches in panel B, auxotonic and physiological twitches in panel C, and auxotonic, afterloaded isotonic, and isometric twitches in panel D. Panel E shows differences in peak shortening (ε) times peak stress development in afterloaded isotonic versus auxotonic twitches. All measurements are from the same muscle.

the same conditions before each afterloaded isotonic twitch. In this example, we had eight (number of twitches in column "iter") isotonic twitches before each afterloaded isotonic twitch. The "save" column indicated whether the measured data was saved or not. This option combined with the "iter" parameter made it suitable to design compact experiment logs for complex experiments. "-1" in the "MLRef" column (total muscle reference length) or the "SRef" column (segment reference length) indicated that the resting length from the previous twitch was used as reference length. Another negative value in these columns meant that reference length was calculated from the resting length of the previous twitch (e.g. -0.95 gave a reference length equal to 95 % of the resting length in the previous twitch). An empty field in the experiment log indicated that the value of the respective parameter was not changed.

Like in afterloaded isotonic twitches, the physiological twitches were also sequences of isometric and isotonic states, but with a different sequence during relaxation (isometric-isotonic relaxation instead of isotonic-isometric relaxation). Two series of physiological twitches with varying afterload are presented in Figure 5. We performed two consecutive experiments with the same settings except that the feedback vari-

able was changed from total muscle (left panels) to segment length (right panels). The isometric-isotonic relaxation sequence gave a counterclockwise loop in the stress-length diagram (Figure 4, panel C), which was different from the afterloaded isotonic twitches (Figure 4, panel B).

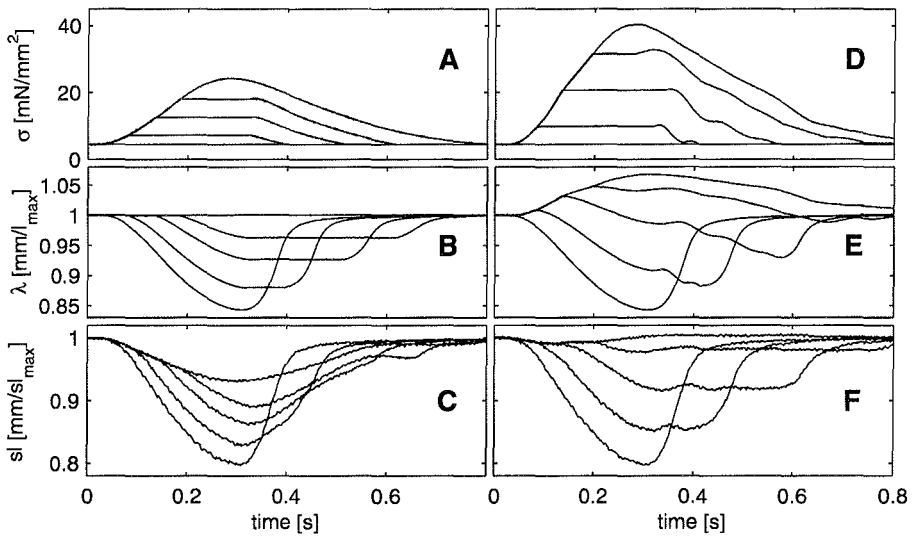

Figure 5: *Left panels*: Total muscle physiological twitches from preloaded isotonic to isometric with one simultaneous segment length measurement. Stress in panel A, controlled total muscle length in panel B, and segment length in panel C. *Right panels*: Segment physiological twitches from preloaded isotonic to isometric with simultaneous total length measurements. Stress in panel D, total muscle relative length in panel E, and controlled segment length in panel F.

3.4 Segment vs. Muscle Performance

As an example of segment non-uniformity, Figure 6 shows a series of muscle isometric twitches at different lengths together with simultaneous measurements of two segment lengths. One preloaded isotonic twitch was included as a reference twitch. In this figure, we can see that segment 1 (bottom segment) was lengthening (panel C) and segment 2 (central segment) was shortening (panel D) while muscle length was constant (panel B). In the new system, it was possible to use feedback control from total muscle length or from one of up to three muscle segments. All lengths were always measured, but obviously only one length at a time could be used as a feedback variable. The user could switch between different feedback variables at any time, or choose feedback variable in the experiment log (column 2 in Figure 2, lower panel).

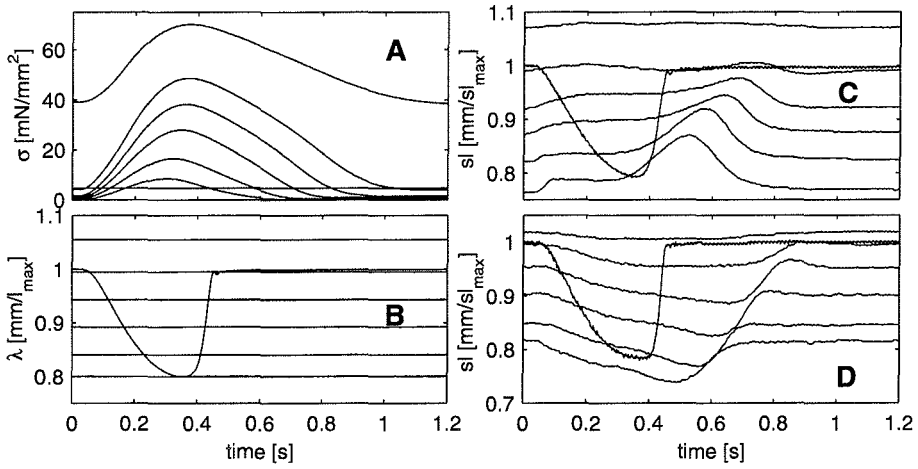

Figure 6: Series of total length isometric twitches at various lengths and one preloaded isotonic reference twitch with simultaneous segment length measurements. Stress in panel A, controlled total muscle length in panel B, segment 1 (bottom segment) length in panel C, and segment 2 (central segment) length in panel D.

The differences between muscle and segment performance can be analyzed from isometric length-tension diagrams. We performed three consecutive series of isometric twitches at different lengths for muscle length and two central segments (segment 2 and segment 3), respectively. Figure 7 presents passive and active stress vs. initial muscle length relative to l_{max} for the three series. The figure demonstrates significant differences both between segment and muscle and between the two central segments. There are differences in optimal length for stress development, in developed stress, and in passive stiffness. The latter is easier to see if we plot the passive stresses vs. initial length of the respective segment (Figure 7, right panel).

4 Discussion

4.1 Digital Control

To obtain the optimal flexibility in the control of the muscles we have divided the overall control system into *three different levels of control.* The highest level, the *batch control,* represents the control of user-defined parameters defining loading conditions, stimulation, twitch type, data acquisition, etc. One of the great advantages of a PC-based control is the possibility to change many variables, both directly by the user, but also indirectly in response to higher level changes and the measured data. Exper-

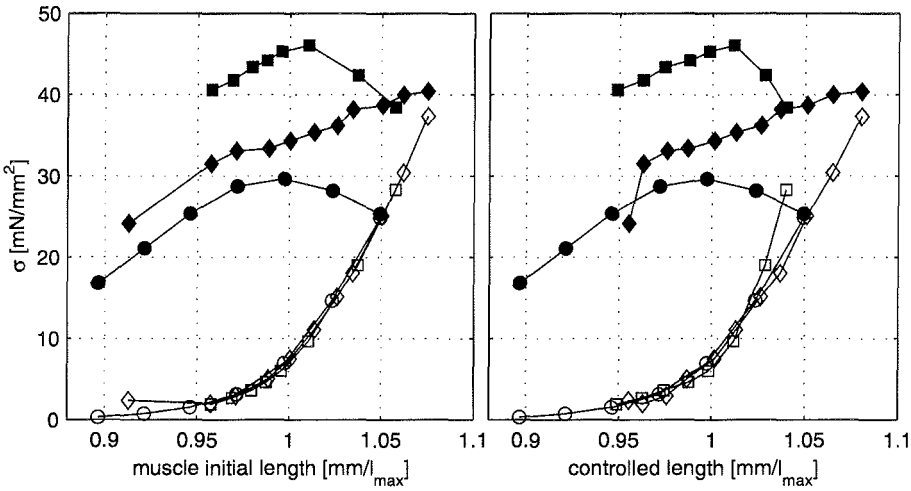

Figure 7: Active (closed symbols) and passive (open symbols) length-tension diagrams for muscle length control (circles) and segment length control of two central segments of the same muscle. S2 (squares) and S3 (diamonds) are lower central segment and upper central segment, respectively. Stress values are plotted against initial muscle length (left panel) and controlled muscle or segment length (right panel). All lengths are relative to muscle or segment length at muscle l_{max}.

iment protocols (Figure 2, lower panel) containing experiment variables for a series of twitches make it easy to perform and reproduce complex experiments automatically. On earlier analog systems, it has been difficult to perform experiments under a wide range of conditions on the same muscle, e.g. afterloaded isotonic and physiological twitches with different loading and feedback variables, and with the same history of stabilization twitches. Although it is possible to develop analog/mechanical systems for most relevant experiments, it is difficult to develop one analog/mechanical system where we can do all the experiments on the same muscle.

Many different experiments on one muscle within limited time also reduce the amount of animals needed, or in another way: More knowledge is available from the same number of animals. The example experiments shown in this paper take from one minute up to four minutes (36 beats per minute) to perform, and one experiment may be started immediately after another, reflecting the efficient use of muscles and animals.

The middle level of control, the *twitch control*, represents individual control of different twitch types. By this separation between control algorithms for different twitch types, we are able to optimize the algorithms for the specific conditions in a given twitch type. This allows two successive twitches in an experiment to be controlled

by two completely different control algorithms. Another strong property of this design is that it is very easy to include new control algorithms like the controlled auxotonic twitch.

The lowest level of control is the *real-time feedback control* of length and force. Two important questions may arise about this choice. The first is about the use of real-time feedback for control of papillary muscles in general and the second is about the utility of a digital version compared with an analog version of the real-time control.

Peterson et al. [22] discuss the limitations of a real-time feedback control approach. Their main arguments are the noise problem and the nonlinear and time varying behavior of the muscle. These are important arguments against a classical feedback control. The noise problem can only be reduced by improved measurement techniques, filtering, or resolution. Because low-pass filtering reduces the bandwidth of the feedback loop, the main focus should be set on the measurement techniques. To take care of the nonlinear and time varying behavior of the muscle, Peterson et al. [22] have described an adaptive approach where they calculate an output trajectory for the whole twitch based on previous twitches. However, such approach requires a number of twitches to converge and stabilize. Then it is difficult to know exactly if the metabolic state is the same in two different resulting twitches. Allen and Kentish [1] and Crozatier [7] have reviewed the short term and long term dependence of length on activation. With real-time feedback control, it may be more difficult to suppress noise, but it is possible to have the same history for different resulting beats. It is shown that a change in loading conditions of a given twitch affects the contraction and relaxation properties of subsequent twitches [16, 17, 21]. In our system, either the first instable beat or any other beat can be recorded and analyzed.

It may be argued that the performance of a digital real-time feedback control cannot improve the performance of analog feedback control due to the discretization. This is true for a conventional control of a given state variable under a limited working range and with a constant control situation. But when the dynamics of the controlled system is slow compared with the sample rate, the discretization will have little negative influence on the performance of the feedback control. In our system, however, the real-time feedback control is only one part of an integrated control system. The low-level control switches between different discrete control situations (constant force, constant length, or varying force and length). Furthermore, the system controls length from two different measurement systems. Finally, there are some advantages of digital control in general, e.g. saturation handling (anti-windup), smooth changes in control when control parameters changes (bumpless transfer), and handling of missing measurement values. We, therefore, also included this level of control in the digital system.

We compared the performance of the real-time feedback control in the analog and digital system for isometric control (Table 1). In the analog system, there was almost no dynamic compliance, but a small static compliance. With the digital control, there was a small dynamic compliance, but negligible static compliance. This difference is due to different control designs. The analog controller has a higher bandwidth, which made it possible to improve the response to fast changes. In the digital controller,

the bandwidth is limited by the discretization, and more focus has therefore been set on static compliance. The scan-rate and the numbers of elements of the CCD-array limited the bandwidth and resolution during segment isometric control. Hence, there were small differences in performance between digital and analog control of segment length. However, the performance of the feedback control, with respect to shortening in isometric twitches, is better for whole muscle control than for segment muscle (see results section). The reason for this is that both the resolution in time, quantification of length, and the signal to noise ratio are better for the total muscle length measurements than for the segment length measurements.

4.2 Controlled Auxotonic Twitch

According to the non-isometric behavior of intact muscle fibers throughout the cardiac cycle, experiments were considered with simultaneous and coupled changes in length and force, namely the controlled auxotonic twitch.

There are several candidate types of auxotonic twitches. First, instead of a constant reference length, one can use a time varying reference length. Then the task for the control system will be to follow this length trajectory with as small deviation as possible. Second, it is possible to control the velocity instead of the length, and for example try to keep the velocity constant or to follow a given velocity trajectory during contraction and/or during relaxation. Leach et al. [19] did this for parts of the contraction. This may result in muscle experiments that are comparable to constant flow measurements on isolated hearts [30]. A third candidate is to let the muscle act against an ideal spring. If the muscle is connected in series with an ideal spring, the active force development (total force minus initial preload) will always be proportional to the length change of the muscle. The proportionality factor is the spring constant. Then, by varying the spring constant from zero (isotonic) to infinity (isometric), it may be possible to fill the space between isotonic and isometric twitches.

So far, we have implemented a control algorithm for the latter type of auxotonic twitches. We chose this kind of auxotonic twitch for several reasons. First, this kind of auxotonic twitches has no discontinuities in length, velocity, stress, or $d\sigma/dt$. Second, the resulting stress-length traces were expected to follow a completely different path than for the afterloaded isotonic and the physiological twitches. This is demonstrated in Figure 4. These fan-like stress-length traces are comparable with the segment auxotonic measurements during whole muscle isometric contractions obtained by Huntsman et al. [14]. Third, we wanted twitches that were easy to interpret and to compare between different muscles and within one muscle at different loads. Finally, it represents a smooth transition from isotonic to isometric conditions.

Because the main purpose of this article is to present the auxotonic twitch and to demonstrate the new digital control system, an in-depth analysis of the auxotonic twitches is beyond the scope of the article. But we will discuss two observations about the twitch which seem to be characteristic.

First, by using phase-plots of derivative of force vs. force, Sys and Brutsaert [28] found that force decline was force dependent during isometric relaxation at the same length but with different loading history and timing. We found (Figure 3, panel C) that stress decline in auxotonic twitches at different spring constants, and hence different lengths and velocities, is also stress dependent as it is for isometric and physiological twitches [28]. This is true for auxotonic twitches with stress development exceeding 10 % of isometric stress development. If we zoom out the derivative of stress vs. stress and remove the isometric twitch, we can have a closer look at the auxotonic twitches that are close to preloaded isotonic (Figure 3, panel D). In auxotonic twitches close to isotonic (little stress development but high shortening), there is an overshoot in the stress decline compared to auxotonic twitches with higher stress development. This is consistent with the earlier finding by Sys and Brutsaert [28] that differences in isometric length slightly modulate the force-dependent rate of force decline.

The second observation compares the amount of developed stress in the auxotonic twitches to afterloaded isotonic twitches. In all experiments we have done so far where we have comparable muscle performance, the auxotonic twitches develop more stress than the afterloaded isotonic twitches with the same peak shortening, and isometric twitches develop more stress than the auxotonic twitches at the same shortest length (Figure 4). In addition to different timing of events, a major difference between the auxotonic and the afterloaded isotonic contraction phases is that in the afterloaded isotonic twitches the stress development and the shortening are divided into two sequential parts. In the isometric twitches, shortening occurs passively before the onset of the twitch. In the auxotonic twitches, however, active shortening occurs against a continuously increasing load, while in the afterloaded isotonic twitches there is active shortening against a constant high load. The differences in loading conditions through the contraction phase lead to a later peak shortening in afterloaded isotonic twitches which is also later than peak shortening in the preloaded isotonic twitch, hence at a time with a reduced "potential" for shortening. In a study on isolated canine hearts, Hunter [13] found a positive effect of ejection on pressure generation. Burkhoff et al. [6] connected this increased pressure generation in ejecting beats compared to isovolumetric beats to a prolonged time to end systole. The difference between our results on isolated muscles and Hunter's [13] results on isolated hearts may be due to the influence of ventricular geometry and ventriculo-arterial coupling on pressure and muscle fiber length.

4.3 Segment vs. Total Muscle Length

According to discussions about the effect of active shortening on muscle activity [9, 19] and the "so-called" cooperative effect [5, 15, 18], it has been important to avoid active shortening during isometric twitches. Due to damaged ends [8] and non-uniformity of muscle performance (Figure 6) [3, 12, 14], one of the goals with the new system was to include simultaneous measurement of both total length and segment lengths and also to allow control of any of the length measurements. This is an important feature

when we want to compare total muscle performance with performance of one or several muscle segments. The comparison will be much more reliable and valuable when the experiments are done on one individual muscle under the same conditions than if the experiments are done on different muscles or widely separated in time.

In addition to the differences between muscle and segment performance, there may be individual differences between different muscle segments. Our system allows measurement of up to three segment lengths, i.e. two central segments. As an example, we compared length-tension relations in isometric twitches with control muscle and two central segments, respectively (Figure 7). This example demonstrates both differences between muscle and segment and between central segments, and how this can be analyzed with the new system.

4.4 Conclusions

We have developed a digital measurement and control system for papillary muscle experiments including an algorithm for a controlled auxotonic twitch. With the new system, we are able to switch on-line between control of total muscle length or one of three different segment lengths. We are able to perform several different experiments under a wide range of loading conditions on one individual muscle within a limited period of time.

Acknowledgements: This research has been supported in part by the Norwegian Research Council (NFR) grant # 107409/320.

References

1. Allen DG and Kentish JC. The cellular basis of the length-tension relation in cardiac muscle. *J. Mol. Cell. Cardiol.* 17:821–40, 1985.

2. Brutsaert DL and Claes VA. Onset of mechanical activation of mammalian heart muscle in calcium- and strontium-containing solutions. *Circ. Res.* 35:345–57, 1974.

3. Brutsaert DL, Claes VA, Chuck LM, Housmans PR, Sys SU, and DeClerck NM. New technology in studying the origin of non-uniformity in cardiac muscle. In: Kitamura K and Abe H, eds., *New approaches in cardiac mechanics*, 31–45. Gordon and Breach, New York, USA, 1986.

4. Brutsaert DL, Meulemans AL, Sipido KR, and Sys SU. Effects of damaging the endocardial surface on the mechanical performance of isolated cardiac muscle. *Circ. Res.* 62:358–66, 1988.

5. Brutsaert DL and Sys SU. Relaxation and diastole of the heart. *Physiol. Rev.* 69:1228–315, 1989.

6. Burkhoff D, De Tombe PP, and Hunter WC. Impact of ejection on magnitude and time course of ventricular pressure-generating capacity. *Am. J. Physiol.* 265:H899–909, 1993.

7. Crozatier B. Stretch-induced modifications of myocardial performance: From ventricular function to cellular and molecular mechanisms. *Cardiovasc. Res.* 32:25–37, 1996.

8. Donald TC, Reeves DN, Reeves RC, Walker AA, and Hefner LL. Effect of damaged ends in papillary muscle preparations. *Am. J. Physiol.* 238:H14–23, 1980.

9. Ford LE. Mechanical manifestations of activation in cardiac muscle. *Circ. Res.* 68:621–37, 1991.

10. Gibbons Kroeker CA, Ter Keurs HE, Knudtson ML, Tyberg JV, and Beyar R. An optical device to measure the dynamics of apex rotation of the left ventricle. *Am. J. Physiol.* 265:H1444–9, 1993.

11. Hittinger L, Crozatier B, Belot JP, and Pierrot M. Regional ventricular segmental dynamics in normal conscious dogs. *Am. J. Physiol.* 253:H713–9, 1987.

12. Housmans PR, Chuck LH, Claes VA, and Brutsaert DL. Nonuniformity of contraction and relaxation of mammalian cardiac muscle. *Adv. Exp. Med. Biol.* 170:837–40, 1984.

13. Hunter WC. End-systolic pressure as a balance between opposing effects of ejection. *Circ. Res.* 64:265–75, 1989.

14. Huntsman LL, Joseph DS, Oiye MY, and Nichols GL. Auxotonic contractions in cardiac muscle segments. *Am. J. Physiol.* 237:H131–8, 1979.

15. Izakov VY, Katsnelson LB, Blyakhman FA, Markhasin VS, and Shklyar TF. Cooperative effects due to calcium binding by troponin and their consequences for contraction and relaxation of cardiac muscle under various conditions of mechanical loading. *Circ. Res.* 69:1171–84, 1991.

16. Jewell BR and Rovell JM. Influence of previous mechanical events on the contractility of isolated cat papillary muscle. *J. Physiol.* 235:715–40, 1973.

17. Kaufmann RL, Bayer RM, and Harnasch C. Autoregulation of contractility in the myocardial cell. Displacement as a controlling parameter. *Pflugers. Arch.* 332:96–116, 1972.

18. Landesberg A and Sideman S. Mechanical regulation of cardiac muscle by coupling calcium kinetics with cross-bridge cycling: A dynamic model. *Am. J. Physiol.* 267:H779–95, 1994.

19. Leach JK, Brady AJ, Skipper BJ, and Millis DL. Effects of active shortening on tension development of rabbit papillary muscle. *Am. J. Physiol.* 238:H8–13, 1980.

20. Olsson G and Piani G. *Computer Systems for Automation and Control.* Prentice Hall International, United Kingdom, 1992.

21. Parmley WW, Brutsaert DL, and Sonnenblick EH. Effects of altered loading on contractile events in isolated cat papillary muscle. *Circ. Res.* 24:521–32, 1969.

22. Peterson JN, Hunter WC, and Berman MR. Control of segment length or force in isolated papillary muscle: An adaptive approach. *Am. J. Physiol.* 256:H1726–34, 1989.

23. Pinto JG. A constitutive description of contracting papillary muscle and its implications to the dynamics of the intact heart. *J. Biomech. Eng.* 109:181–91, 1987.

24. Pollack GH and Huntsman LL. Sarcomere length-active force relations in living mammalian cardiac muscle. *Am. J. Physiol.* 227:383–9, 1974.

25. Rademakers FE, Buchalter MB, Rogers WJ, Zerhouni EA, Weisfeldt ML, Weiss JL, and Shapiro EP. Dissociation between left ventricular untwisting and filling. Accentuation by catecholamines. *Circulation* 85:1572–81, 1992.

26. Rayhill SC, Daughters GT, Castro LJ, Niczyporuk MA, Moon MR, Ingels NBJ, Stadius ML, Derby GC, Bolger AF, and Miller DC. Dynamics of normal and ischemic canine papillary muscles. *Circ. Res.* 74:1179–87, 1994.

27. Saeki Y, Totsuka T, Kato C, and Yanagisawa K. Length-tension relation of cat heart muscle studied by a segment- control method. *Heart Vessels* 2:208–12, 1986.

28. Sys SU and Brutsaert DL. Determinants of force decline during relaxation in isolated cardiac muscle. *Am. J. Physiol.* 257:H1490–7, 1989.

29. Sys SU and Brutsaert DL. Uniformity versus non-uniformity in isolated cardiac muscle. In: Sideman S and Beyar R, eds., *Imaging analysis and simulation of the cardiac system.*, 591–603. Freund Publ House, London, UK, 1990.

30. Wijkstra H and Boom HB. Left-ventricular dynamic model based on constant ejection flow periods. *IEEE Trans. Biomed. Eng.* 38:1204–12, 1991.

31. Wong AY. Mechanics of cardiac muscle, based on Huxley's model: Mathematical stimulation of isometric contraction. *J. Biomech.* 4:529–40, 1971.

32. Wong AY. Mechanics of cardiac muscle, based on Huxley's model: Simulation of active state and force-velocity relation. *J. Biomech.* 5:107–17, 1972.

Paper B

Analysis of the Controlled Auxotonic Twitch in Isolated Cardiac Muscle

Vidar Sørhus[1], Bjørn A. J. Angelsen[1], Stanislas U. Sys[2]

[1] Dept. of Physiology and Biomedical Engineering, NTNU, Trondheim, Norway
[2] Dept. of Human Physiology and Pathophysiology, UIA (RUCA), Antwerp, Belgium

Abstract

In the intact heart, there are simultaneous changes in stress and length throughout the cardiac cycle. In a recently developed digital control system for experiments on isolated papillary muscles from rabbit right ventricle, we included a controlled auxotonic twitch. This twitch allowed proportional changes in stress and length, as if the muscle was acting against an ideal spring. The auxotonic twitches had no discontinuities in length, velocity, stress, or derivative of stress and represented a smooth transition from isotonic to isometric loading. We wanted to use such twitches to analyze the dependence on auxotonic load and initial length of contraction and relaxation. Timing of contraction was independent of load when initial length was l_{max}. Timing of relaxation was highly correlated with peak stress. Twitch prolongation at increased initial length was more pronounced at lower loads. Similar results were obtained when post extra-systolic potentiation was included as an inotropic intervention. The relations between the load dependence of auxotonic contraction and relaxation, presented in this paper, may have implications for the in vivo left ventricular function analysis.

Keywords: rabbit papillary muscle; cardiac muscle mechanics; left ventricular function; load dependence; contraction-relaxation; activation-inactivation

1 Introduction

Our knowledge of the mechanics of the cardiac muscle is based on a long history of experiments on intact hearts, isolated muscles, and isolated myocytes. At the level of isolated muscle, the experiments have mainly been performed in isometric or isotonic conditions or as quick load or length clamps. Both the isotonic and the isometric conditions are extreme and non-physiological. However, concepts like calcium sensitivity [2], shortening deactivation [27], cooperative effects [36], and load-dependent relaxation [9, 38] have evolved from these kinds of experiments.

In the intact heart, there is a continuous change in muscle fiber length and stress throughout the cardiac cycle, i.e. muscle fiber conditions are auxotonic during isovolumetric contraction, ejection, isovolumetric relaxation, and filling. This is caused by a complex interaction between stress development and decline, shortening and lengthening, changes in LV geometry, twisting, and non-uniformity [4, 13, 18, 35].

In previous attempts to mimic in vivo conditions by dynamic loading conditions in the isolated papillary muscle, e.g. Paulus et al. [34], the experiments only had dynamic loading during the contraction, i.e. till the end of the ejection phase. Therefore, we still know little about the dynamics of the whole cardiac cycle. Until now, the perfect integration of the muscle-pump has never been realized.

To examine the mechanics of the isolated cardiac muscle during simultaneous and coupled changes in stress and length, we developed a digital control system for papillary muscle experiments that included a controlled auxotonic twitch [37]. In this twitch, the muscle acted against an virtual ideal spring. The new digital control system has made it possible to perform series of different experiments like isotonic, isometric, afterloaded, physiological (isometric-isotonic relaxation sequence), and controlled auxotonic twitches on the same muscle. Experiments could be designed on-line with stabilization twitches, twitch types, loading conditions, stimulation properties, segment or muscle length control, and storing options. The isotonic and isometric twitches are also the extreme cases of the auxotonic twitch; the auxotonic twitches with different auxotonic loads represent a smooth transition between isotonic and isometric twitches.

Because most features of muscle contraction and relaxation have been derived from twitches with no simultaneous changes in length and stress, there are open questions about the dynamics and load dependence of auxotonic twitches.

The purpose of this present study has therefore been to evaluate the behavior of the contraction and relaxation phases in the controlled auxotonic twitches. The contraction and relaxation phases in the auxotonic twitches will be compared with isometric, afterloaded isotonic, and physiological twitches from the same muscle under equal experimental conditions and with the same muscle performance. In particular we analyzed 1) the timing of contraction and relaxation in auxotonic twitches at different auxotonic loads, 2) the load dependence of timing of length and stress changes during contraction and relaxation, and 3) the dependence on initial length and stimulation of contraction and relaxation.

2 Methods

2.1 Muscle Preparation

Rabbits (n=13, weight 2.5-3kg) were anesthetized by cervical translocation and the heart was quickly excised. A papillary muscle was dissected from the right ventricle in a dissection bath with temperature controlled and oxygenated Krebs-Ringer solution (see below), containing 2,3-butanedione monoxime (BDM; 30mM) to inhibit actin-myosin cross-bridge cycling during dissection. The muscle was passively stretched with a preload of 6 mN/mm^2 of estimated cross-sectional area. Under a dissection microscope (WILD M3B from Leica), three tips of glass microelectrodes were inserted into the muscle perpendicular to the long axis. At the tip, the diameters of the microelectrodes were less than 5 μm, and at the muscle surface the diameters were maximally 15 μm. Then the papillary muscle was installed vertically in a 3 ml bath. The Krebs-Ringer solution was circulating with a flow rate of approximately 10 ml/min and contained (in mM): NaCl 98, KCl 4.7, $MgSO_4.7H_2O$ 2.4, $NaHCO_3$ 25, $CaCl_2.2H_2O$ 1.25, glucose 4.5, Na-pyruvate 15 and Na-acetate 5, at 29°C bubbled with a gas mixture of 95 % oxygen and 5 % carbon dioxide. The average muscle characteristics of the 13 muscles used in this analysis is presented in Table 1.

Table 1: Muscle characteristics. Average values of 13 muscles.

Measure	mean ± SD	
muscle length (l_{max})	4.3±1.1	mm
cross-sectional area at l_{max}	0.84±0.41	mm^2
peak isotonic shortening	16.1±3.2	$\%l_{max}$
resting stress at l_{max}	7.3±2.7	mN/mm^2
peak total isometric stress at l_{max}	41±22	mN/mm^2

2.2 Experimental Setup

The papillary muscle setup was based on an analog/mechanical setup, described in Brutsaert and Claes [6] and Brutsaert et al. [8]. The original system consisted of a force transducer, an optical displacement measurement transducer, a papillary muscle bath with a clip for the lower muscle end, two platinum electrodes for electrical stimulation, and a control unit for isotonic and isometric control and for stimulation. The system also included a segment measurement system based on detection of position of microelectrodes with a CCD-array [7, 38].

The control unit of the original setup was replaced with a PC with a digital signal processor (DSP) board and an interface unit between the PC and the transducers, as described in Sørhus et al. [37] (Figure 1). An individual application for low-level feedback control and data acquisition was running on the DSP board at a sample rate

of 5000 samples per second. This application included different algorithms for different twitch types. Another application running on the host computer handled visualization and storage of measured and calculated variables, on-line user interaction, and overall control of experiments.

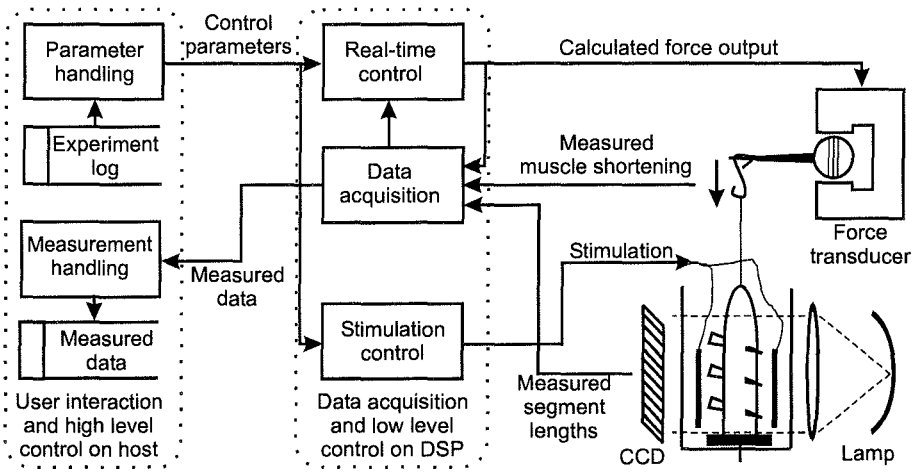

Figure 1: Main components and data flow in the system. An application for real-time control, data acquisition, and stimulation control was running on the DSP board. Total muscle shortening and muscle segment lengths were measured and sent via the DSP-board to the host computer through a measurement channel and optionally stored in a text-file (Measured data). An application for user interaction and high level control was running on the host computer. Control parameters set by the user or read from a text-file (Experiment log) were sent from the host computer to the DSP-board through a parameter channel.

The system included a controlled auxotonic twitch where the muscle was acting against an ideal spring:

$$\sigma(t) \quad = \quad k_a(l_{max} - l(t)) + \sigma_r(l_{max})$$

where σ, l, and $\sigma_r(l_{max})$ denote total stress, measured length, and resting stress at l_{max}, i.e. the length with maximal isometric active stress development, respectively. The stiffness of the spring was given by the user-defined spring constant, k_a times 80 (mN/mm) [times 125 (mN/mm) for segment control], representing a smooth transition from isotonic ($k_a = 0$) to isometric ($k_a \to \infty$).

2.3 Experiment Protocol

We measured resting diameter of all muscles at l_{max}. We have used stress (force per resting cross sectional area) and relative length ($\lambda = l/l_{max}$) in all analyses unless otherwise stated.

Three different experiment protocols were followed in order to perform quantitative analyses of the auxotonic twitches. First, we performed consecutive experiments with auxotonic twitches at different spring constants, afterloaded twitches, both with conventional and physiological relaxation sequences, with different afterloads, and isometric twitches at different reference lengths in 13 muscles. All the auxotonic and afterloaded twitches were performed with reference length at l_{max}. Second, we performed auxotonic twitches with different spring constants and with different reference lengths together with isometric twitches at different reference lengths in six of the muscles. Third, we performed the first protocol with post extra-systolic potentiation (PESP) in the last stabilization twitch before the measured twitch in seven muscles. In three of these seven muscles we also performed the second protocol with PESP. Finally, on some muscles we performed the same experiments with segment control. This was done to confirm the results from the muscle length controlled experiments, but was not included in the quantitative analysis.

2.4 Data Analysis

The analyses and visualization of the measured data were performed with Matlab (The MathWorks Inc.). This included calculation of stress and relative length from force and length measurements, calculation of the first derivatives of stress and length, calculation of normalized developed stress, and calculation of time to half contraction (THC), time to peak contraction (TPC), and time to half relaxation (THR). In auxotonic twitches THC, TPC, and THR were the same in both shortening and developed stress. We used relative length traces to calculate THC, TPC, and THR in the auxotonic twitches. We calculated THC, TPC, and THR from the stress traces in all isometric twitches. THC and THR cannot be calculated in afterloaded and physiological twitches because length and stress changes occurred sequentially during contraction and relaxation, but TPC was calculated from relative length as time to peak shortening.

The statistical analyses were performed with Excel (Microsoft Corp.). To be able to compare the values of THC, TPC, and THR from different muscles, we normalized the timing values to TPC of the preloaded isotonic reference twitch with initial length at l_{max} (TPC(it,l_{max})).

3 Results

3.1 The Controlled Auxotonic Twitch

A series of muscle length controlled auxotonic twitches with different spring constants is presented in Figure 2, together with one isometric and one preloaded isotonic twitch. For a given spring constant, the shortening and the developed stress traces were proportional. Peak shortening decreased and peak developed stress increased at increasing spring constants. Markers of time to half contraction (THC), time to peak contraction (TPC), and time to half relaxation (THR), are included in the stress plot (upper panel). Figure 3 shows a similar series of central segment auxotonic twitches from the same muscle. The gap between the auxotonic twitch with the highest spring constant and the isometric twitch was caused by the bandwidth of the measurement system; the bandwidth was lower for segment length measurements than for muscle length measurements.

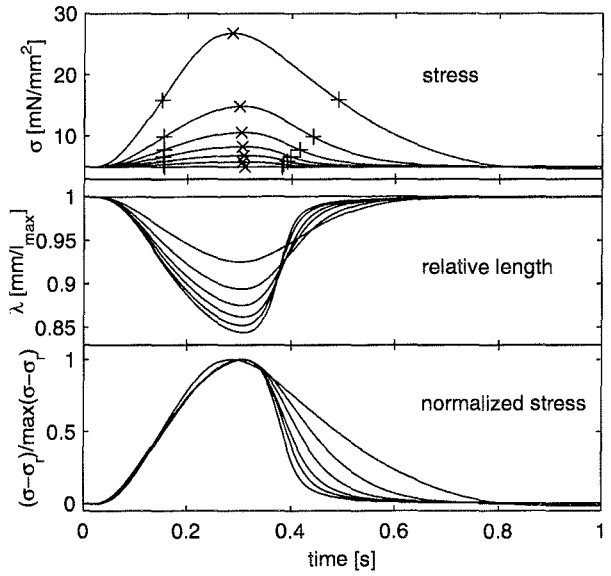

Figure 2: Series of muscle length auxotonic twitches with varying auxotonic constants with preloaded isotonic and isometric reference twitches. Stress in upper panel, controlled muscle length in middle panel, and normalized stress in lower panel. Markers in stress plot represent (from left to right) THC (+), TPC (x), and THR (+). Notice that eight preloaded isotonic stabilization twitches were included before each measured twitch.

Compared to afterloaded twitches with conventional or physiological relaxation (Figure 4), the auxotonic twitches were different in several ways. The auxotonic

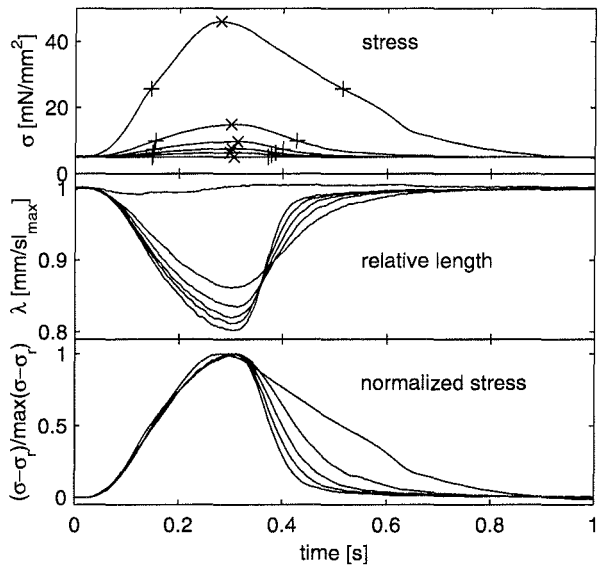

Figure 3: Series of central segment length auxotonic twitches with varying auxotonic constants with preloaded isotonic and isometric reference twitches. Stress in upper panel, controlled central segment length in middle panel, and normalized stress in lower panel. Markers represent (from left to right) THC (+), TPC (x), and THR (+).

twitches displayed no discontinuities in length, velocity, stress, or derivative of stress. In the afterloaded twitches either length or total stress was always constant, while in the auxotonic twitches both length and total stress were changing. This resulted in a different loading history, i.e. different paths in the stress-length plot (Figure 4). In the afterloaded twitches the muscle shortened against a constant afterload whereas in the auxotonic twitches the muscle shortened against an increasing load given by the spring constant. The auxotonic twitches allowed a smooth transition from the isotonic twitch toward the isometric twitch.

3.2 Normalized Auxotonic Twitches

Because of the proportionality between stress and strain in the auxotonic twitches, all the dynamics of the twitch are included in the stress trace as well as in the length trace. Therefore, the timing of contraction and relaxation at different spring constants can be demonstrated by normalizing either the stress traces or the length traces (Figure 2, lower panel). In a series of auxotonic twitches with different spring constants the normalized stress traces (or shortening traces) were following the same trajectory during

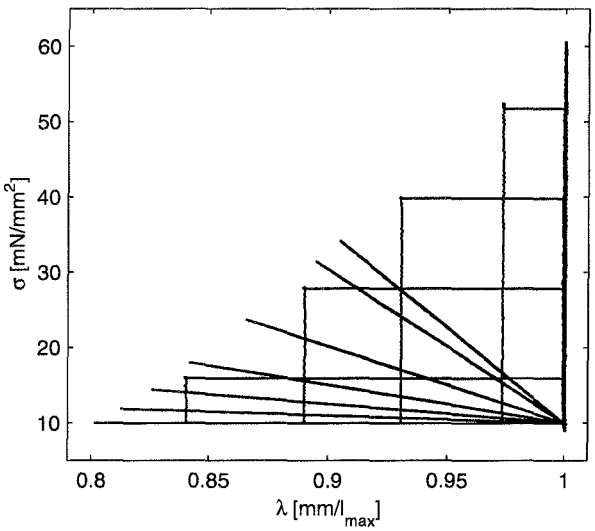

Figure 4: Series of auxotonic and physiological twitches from consecutive experiments on one muscle in a stress-length plot.

contraction, but were following individual trajectories during relaxation. At high loads the relative lengthening/relative stress decline was slower than at lower loads. The same result was found for central segment auxotonic twitches (Figure 3, lower panel). Because of the separated shortening and stress development in afterloaded twitches, it was not possible to do a similar scaling of length or stress traces from afterloaded twitches.

3.3 Timing of Auxotonic Contraction and Relaxation

THC, TPC, and THR were the same for shortening and stress in auxotonic twitches. One example of THC, TPC, and THR in auxotonic twitches at different spring constants and isometric twitches at different lengths, and TPC in afterloaded twitches at different afterloads is presented in Figure 5.

We calculated regression lines for the normalized timing values, similar to the regression lines in Figure 5. For the afterloaded twitches, where TPC increased with increasing afterload until the afterload exceeded a certain level, we used the twitches with afterloads less than this level to calculate the regression line for TPC. The resulting average slopes of 13 muscles are summarized in Table 2. The slopes of auxotonic TPC were significantly different from afterloaded TPC (paired t-test; $P<0.0001$), but not significantly different from zero. The slopes of auxotonic and isometric THC were not significantly different from zero either. However, both auxotonic and isometric

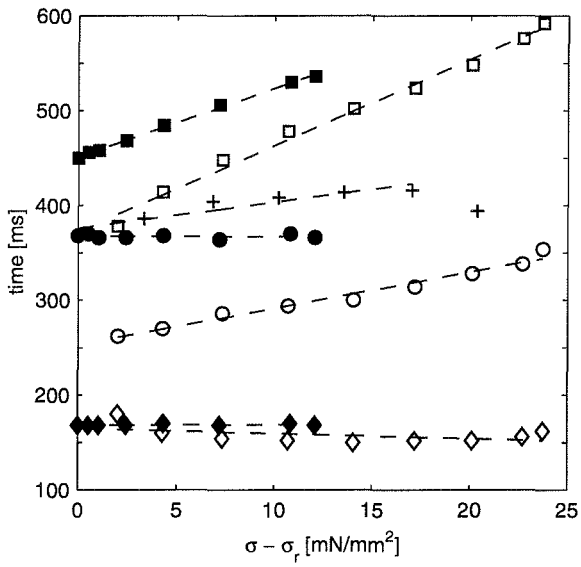

Figure 5: THC (diamonds), TPC (circles), and THR (squares) in isometric twitches (open symbols) at increasing muscle length (from left to right) and auxotonic twitches (filled symbols) at increasing spring constant, in addition to TPC of afterloaded twitches (crosses) at increasing afterload, are plotted against peak developed stress. Regression lines are also plotted. See text for details.

THR were highly correlated with relative developed stress [$R^2 = 0.995 \pm 0.003$ (mean $\pm$ SD) and $R^2 = 0.988 \pm 0.009$, respectively].

Table 2: Average slopes of regression lines (mean $\pm$ SD) together with the results of a paired t-test between the regression slopes and the zero slope.

	auxotonic	isometric	afterloaded
THC	-0.0008±0.0248, P=0.91	0.0293±0.0585, P=0.11	
TPC	0.0262±0.0576, P=0.13	0.2654±0.0732, P<0.0001	0.2179±0.1003, P<0.0001
THR	0.5291±0.1466, P<0.0001	0.6694±0.1259, P<0.0001	

3.4 Influence of Initial Length on Twitch Duration

In order to describe the influence of initial length on timing in auxotonic twitches, we performed auxotonic experiments with initial lengths different from l_{max} on six

muscles, i.e. at 95% l_{max} and at 102.5% l_{max}. We used resting stress at the new reference length. This was done automatically in the experiment log by including an isometric twitch at the actual reference length in the beginning of the experiment, measuring resting stress in this twitch, and then using this stress as preload in the respective auxotonic twitches. This gave the following relation between stress and length in auxotonic conditions:

$$\sigma(t) \quad = \quad k_a(l_{ref} - l(t)) + \sigma_r(l_{ref})$$

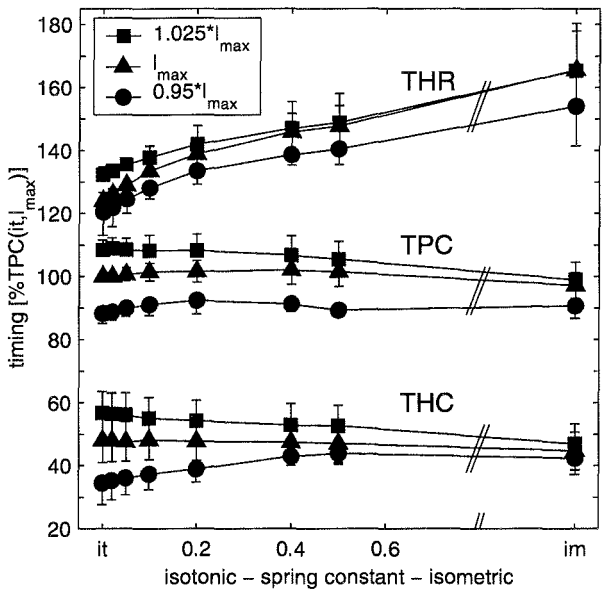

Figure 6: THC, TPC, and THR, normalized to TPC of the preloaded isotonic (it) reference twitch, from isotonic twitches (far left), auxotonic twitches with increasing k_a (from left to right), and isometric twitches (far right) with initial length at l_{max} (triangles), at 95% l_{max} (circles), and at 102.5% l_{max} (squares). Mean ± SD of six muscles.

Average ± SD values of THC, TPC, and THR normalized to TPC(it,l_{max}) are plotted against increasing spring constants in Figure 6. With $k_a = 0.5$, developed stress was 52±6.4% of isometric developed stress. There were significant prolongation of THC (paired t-test; P<0.001), TPC (P<0.001), and THR (P<0.025) when initial length increased from 95% l_{max} to 102.5% l_{max}. For THC and TPC the prolongation with increased initial length was more prominent at low auxotonic load compared to isometric (P<0.0025 for k_a<0.4) (Figure 7). This implies that the timing of auxotonic contraction was dependent on auxotonic load when initial length was different from l_{max}.

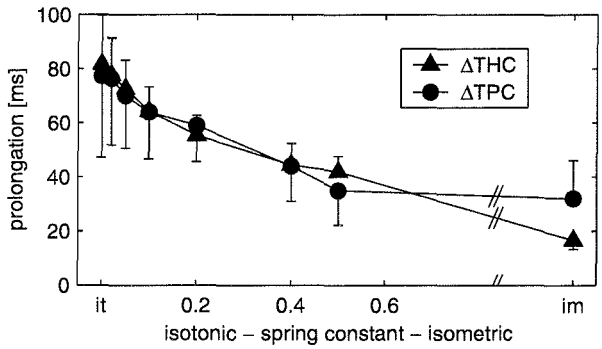

Figure 7: Average ± SD prolongation of THC (triangles) and TPC (circles) after a change in initial length from 95% to 102.5% l_{max} in auxotonic twitches versus k_a. The prolongation was significantly larger for k_a<0.4 than for isometric (paired t-test; P<0.0025).

3.5 Auxotonic Twitches after PESP

In seven muscles, we performed series of auxotonic twitches with post extra-systolic potentiation (PESP), i.e. an extra stimulus in the isotonic stabilization twitch preceding the auxotonic twitch. Two consecutive experiments with PESP and normal stimulation are presented together in Figure 8. We found that the PESP did not affect the dependence of twitch duration on auxotonic load (Figure 9).

In three of the seven muscles, we also performed series of auxotonic twitches at shorter (95% l_{max}) and longer (102.5% l_{max}) initial lengths, but still with PESP in the preceding stabilization twitch. This limited number of muscles yielded a similar dependence of timing on initial length (Figure 10) as was the case with normal stimulation (Figure 7). However, the average prolongation was less with PESP.

3.6 Peak Derivative of Stress

Another approach to load dependence of contraction and relaxation dynamics is to calculate positive and negative peak values of time derivative of stress (dF/dt). This is related to the clinical measure dP/dt which is often used as an index of contractility.

This measure can be normalized in several ways. We calculated absolute $\dot{\sigma}_t$ $[mN/mm^2/s]$ and $\dot{\sigma}_t$ normalized to instantaneous total stress ($\sigma_t(t)$), and normalized to peak developed stress ($max\{\sigma_t - \sigma_r\}$). Figure 11 presents the average values of 13 muscles versus auxotonic load.

Notice that this analysis again reflects the different dependence on load of timing of contraction and relaxation. None of the measures demonstrated similar dependence on load in both contraction and relaxation. Peak positive $\dot{\sigma}_t/max\{\sigma_t - \sigma_r\}$ was indepen-

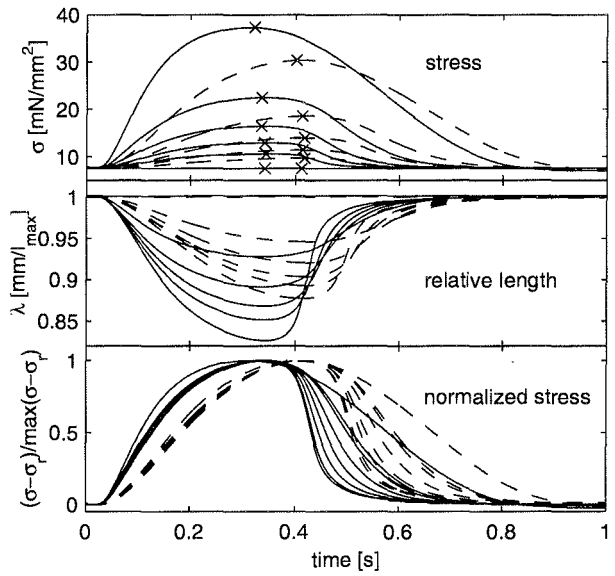

Figure 8: Stress (upper panel), relative length (middle panel), and normalized stress (lower panel) from one series of auxotonic twitches after PESP (solid) and one series with normal stimulation (dashed). Markers of TPC are included in the stress plot.

dent of auxotonic load (5.20 ± 0.68 s^{-1} for all k_a), as one can see from the normalized developed stress (Figure 2, lower panel). But the peak negative values of the same measure was load dependent. Both the peak positive and peak negative values of $\dot{\sigma}_t$ were load dependent, but peak negative values of $\dot{\sigma}_t/\sigma_t$ were little affected by auxotonic load except at very small loads, i.e. for a wide range of k_a values, the rate of stress decline $\dot{\sigma}_t$ was proportional to the instantaneous stress σ_t. This demonstrated the concept of load-dependent stress decline.

4 Discussion

We have found that timing of auxotonic contraction was independent on auxotonic load as long as the initial length was equal to l_{max} in contrast to afterloaded contractions where twitches prolonged at increasing afterload. However, timing of auxotonic contraction was dependent on both initial length and auxotonic load when initial length was different from l_{max}. Timing of auxotonic relaxation was similar to isometric relaxation, highly correlated with peak developed stress. Post extra-systolic potentiation in the preceding twitch gave similar results.

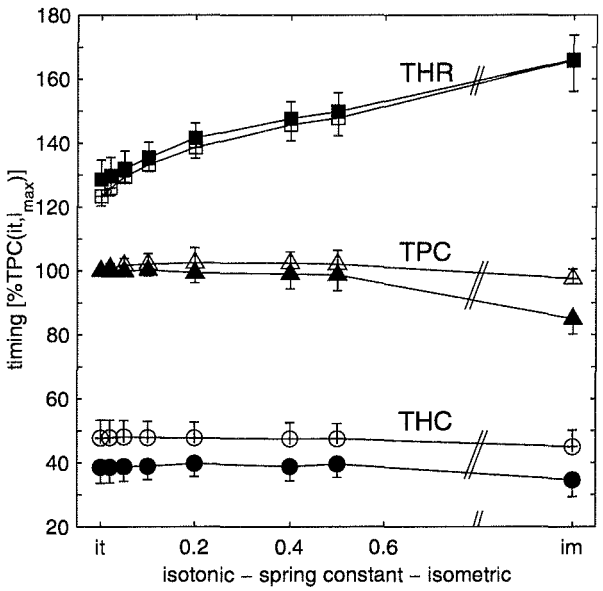

Figure 9: Average ± SD values of normalized THC (circles), TPC (triangles), and THR (squares) with PESP (closed symbols) and normal stimulation (open symbols) versus k_a.

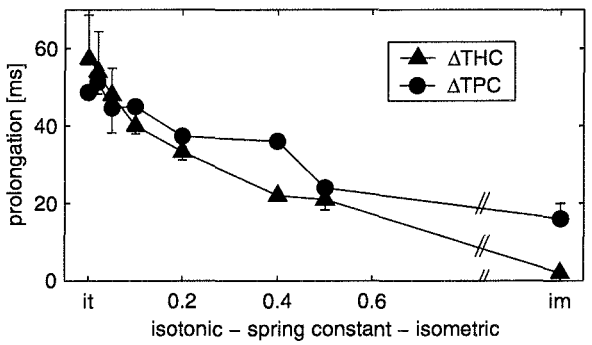

Figure 10: Average ± SD prolongation of THC (triangles) and TPC (circles) after a change in initial length from 95% l_{max} to 102.5% l_{max} in auxotonic twitches after PESP versus k_a.

Length and stress changes both originate from the same basic process, namely the cross-bridge cycle. This process is not fully understood, especially under non-isometric

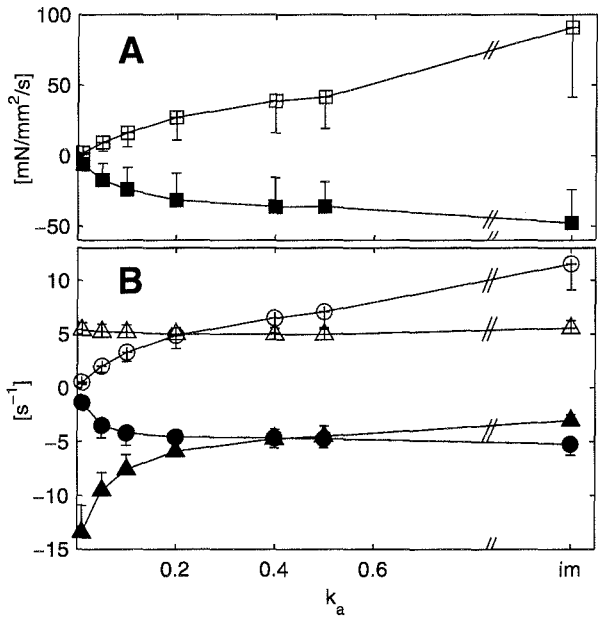

Figure 11: Positive and negative peak values (mean ± SD) from contraction (open symbols) and relaxation (closed symbols) respectively of $\dot{\sigma}_t$ (squares), $\dot{\sigma}_t/\sigma_t$ (circles) and $\dot{\sigma}_t/max\{\sigma_t - \sigma_r\}$ (triangles) versus k_a.

conditions. Therefore, it is difficult to explain the load-independent auxotonic contraction at l_{max} without speculating. Therefore, we will focus on two questions: Why is afterloaded contraction prolonged at increasing afterload? And, what makes the timing of auxotonic contraction load dependent when initial length is different from l_{max}? Additionally, we will discuss the finding that PESP does not affect load dependence of auxotonic twitch duration nor the differences between contraction and relaxation. But before we discuss the presented results, we will recall what factors influence the dynamics of contraction and relaxation in cardiac muscle twitches. Because our experiments are performed on isolated muscles with the same series of stabilization twitches (i.e. eight isotonic twitches with resting length at l_{max}) we will only include factors with direct effect on the dynamics inside a single twitch.

4.1 Contraction and Relaxation Parameters

The mechanical dynamics of cardiac muscle twitches is given by the attachment and detachment of force-generating cross-bridges. Depending on the load, the amount of activating Ca^{2+}, and the properties of the contractile machinery, this is expressed as changes in muscle length and force. The different factors mentioned here are extensively

reviewed by Brutsaert and Sys [9], especially their role during relaxation. Instantaneous force is given by the number of force generating cross-bridges and the mean force of each cross-bridge. In an isometric twitch, peak force is reached when the rate of detachment of cross-bridges exceeds the rate of attachment of new cross-bridges. We call this the balance between activation and inactivation. Peak shortening in an isotonic twitch also occurs when the rate of detachment of cross-bridges exceeds the rate of attachment of new cross-bridges. This is because the muscle shortens when the force developed by the cross-bridges exceeds the load on the cross-bridges and that the shortening is zero at peak shortening.

4.1.1 Load

The load on the cross-bridges results from both internal and external loads. External load is the load imposed on the muscle, here by the experimental setup. A force is required to stretch the muscle to lengths longer than the so-called slack length (i.e. $l \approx 0.85 \cdot l_{max}$). This yields an exponential passive stress-length relation at these lengths [31]. During isotonic shortening, active stress must increase to balance the reduction in passive stress, and hence the local steepness of the passive stress-length relation will influence on the mechanical dynamics of the twitch.

Geometrical limitations from the structure of the sarcomere and the surrounding connective tissue yield internal restoring forces that oppose shortening at lengths shorter than slack length [17, 33]. Together with the passive stress-length relation, the restoring forces influence the relation between changes in the number of cross-bridges and the external mechanical responses.

4.1.2 Ca^{2+} Availability

Ca^{2+} must bind to troponin C (TnC) to activate the thin filament and allow cross-bridge attachment. The level of intracellular Ca^{2+} is therefore an important activation variable. The intracellular Ca^{2+} has a very rapid initial rise and the peak occurs well before peak stress in isometric twitches. The initial rise is followed by an exponential decline. It is also known that the intracellular Ca^{2+} transient is prolonged in isotonic twitches compared with isometric twitches and that a subsequent increase follows active shortening in afterloaded twitches [3, 21, 25]. Changes in the intracellular Ca^{2+} transient may influence on the mechanical activity of the muscle and a prolonged and elevated transient around peak force or peak shortening may therefore also prolong activation and/or delay inactivation.

When the level of intracellular Ca^{2+} is very low (during relaxation) the force is dependent on the life cycle of the cross-bridges and the number of cross-bridges, yielding the concept of load-dependent relaxation [9].

Post extra-systolic potentiation is the positive inotropic effect of the first beat following an extra-systole [10, 23]. This is related to an increase in the intracellular Ca^{2+} transient. The augmented availability for calcium will enhance the activation,

reflected in an increased rate of stress development.

4.1.3 Contractile Machinery

Ca^{2+} binding to TnC leads to a conformation change on the thin filament. Tropomyosin moves from an inhibitory position to a position that makes it possible for myosin to bind with actin [20]. The series of processes from Ca^{2+} binding to TnC to force-binding cross-bridges may be influenced by length, velocity, and the number of cross-bridges. Hofmann and Fuchs [19] demonstrated that cross-bridges can keep the thin filament activated in the absence of activating Ca^{2+}. The rate of isometric stress development is enhanced by cooperative mechanisms [2, 36], which may be modeled as a lower dissociation rate of Ca^{2+} from TnC complexes that are linked to force-bearing cross-bridges [26]. The concept of shortening deactivation may be explained by an absence or reduction of this latter cooperative mechanism [21].

A lot of research has been directed towards the length dependence of isometric stress development [1, 2, 11, 12, 14, 15, 16, 28, 29, 32, 39]. At least three factors may play a role on timing of both contraction and relaxation and the balance between activation and inactivation: calcium sensitivity, filament spacing, and cooperativity. The degree of filament overlap alone does not account for the steep ascending limb in the active stress-length relation of the cardiac muscle. Length-dependent calcium sensitivity has been proposed to be responsible for this effect [2]. Some investigators, indeed, have found that the calcium sensitivity of the cardiac isoform of TnC is more length dependent than the skeletal isoform [1, 15, 16] while others however did not find a significant difference [28, 32]. An alternative explanation is that reduced interfilament spacing according to increased length increases the probability of cross-bridge attachment [12, 29, 39]. Cooperativity may enhance the calcium sensitivity further [11, 19]. However, the resulting shift in the stress-pCa relation with length may explain the prolongation of isometric twitches at increasing lengths. The increased sensitivity for calcium will postpone the balance between activation and inactivation.

4.2 Timing of Afterloaded Contraction

TPC in afterloaded twitches was prolonged compared to TPC in auxotonic twitches (Figure 5). The increasing TPC with increasing afterload in afterloaded twitches may lead to the conclusion that it is the peak stress that determines the prolongation of TPC. Our results indicate that peak stress is not the whole story. The afterloaded and the auxotonic twitches had the same initial conditions and approximately the same peak shortening and peak stress development (Figure 4). The only difference is the loading history which therefore seems to be more important. In the afterloaded twitch, peak stress is developed during an (early) isometric phase. Cooperative mechanisms, including a lower dissociation rate of Ca^{2+} from TnC complexes [26], yields an enhanced activation in afterloaded twitches during the isometric phase compared with the same phase of the auxotonic twitches.

In afterloaded twitches, like in isometric and isotonic twitches, TPC will occur when the number of detachment of cross-bridges exceeds the attachment of new cross-bridges. Starting from the same isometric condition when the afterloaded twitch switches from isometric to isotonic, the increased number of cross-bridges in the afterloaded twitch will only account for the reduction of passive stress due to the passive stress-length relation. Therefore, more Ca^{2+} must dissociate from TnC, and with the same dissociation rate this will take longer time and prolong TPC compared to the isometric twitch. This is consistent with the measured increased and prolonged intracellular Ca^{2+} transient after a switch from isometric to isotonic conditions [3, 21, 25]. The isometric ($k_a \rightarrow \infty$) and isotonic ($k_a = 0$) conditions are extreme cases of the auxotonic condition, and afterloaded contraction switches between the two extreme conditions. This may be the explanation why the timing of auxotonic contraction is more similar to isometric and isotonic than to afterloaded contractions.

4.3 Effects of Initial Length on Timing of Contraction

Our result confirmed previous findings that TPC and THR of isometric twitches increase at increasing length [3, 22] with most pronounced increase in THR (Figure 5). To compare the timing of auxotonic twitches with timing of isometric twitches, we performed series of auxotonic twitches with reference length different from l_{max}. Several effects may contribute to the resulting load dependence of auxotonic contraction at lengths different from l_{max}. We will first discuss the factors that are expressed in both isometric and auxotonic twitches and then some factors that may explain the more pronounced prolongation of timing at low auxotonic loads (Figure 7).

4.3.1 Isometric Twitches

We have already discussed the length dependence of isometric stress development. Enhanced activation due to increased calcium sensitivity, cooperativity, and reduced filament spacing throughout the whole contraction phase may explain the prolongation of the whole contraction phase in isometric twitches at increasing length. Stress decline during relaxation has been found to be mainly dependent on the stress level and only modified by length [38]. Therefore, THR-TPC will increase with increasing peak stress, i.e. until the isometric length exceeds l_{max} (Figure 6).

4.3.2 Isotonic and Auxotonic Twitches

Although most research on the length dependence of activation has been related to isometric contractions, it is reasonable to assume that the described factors will also be present during non-isometric contractions [9]. We found that the dependence on length of timing of non-isometric contractions were more pronounced than for isometric contractions (Figure 7). At least two more factors may have an additional effect on the timing of auxotonic twitches. First, the exponential shape of the passive stress-length

relation yields that passive stress must be replaced by active stress during shortening. This effect is more pronounced when the passive stress-length relation is steeper, i.e. shortening in twitches that start from longer lengths will have an apparently slower initial phase, although the rate of cross-bridge cycling is the same. Second, internal restoring forces [17, 33] may lead to a slower and abbreviated late phase of contraction. Together, these two factors with their effects on the early and late part of the contraction, respectively, may therefore explain the small difference in prolongation between THC and TPC (Figure 7).

4.4 Effects of Post Extra-Systolic Potentiation

We used PESP (see Cooper [10] for review) as an inotropic intervention in our protocol. Although PESP markedly altered the duration of the twitches (Figure 12), the timing of the auxotonic twitches after PESP was qualitatively similar to the auxotonic twitches with normal stimulation (Figure 9 and Figure 10). Together with the finding that relaxation seems to be least modified by PESP, this may support the idea that PESP mainly augments the calcium transient and does not alter the properties of the contractile machinery [10, 24, 40]. According to our discussion about the balance between activation and inactivation and the calcium sensitivity, an elevated intracellular Ca^{2+} transient should imply a delayed balance between activation and inactivation. The increased activation due to more activating calcium in the early phase of the twitch will however lead to earlier appearance of saturating effects like internal restoring forces and maximal activation of the thin filament. This may therefore explain the abbreviated TPC after PESP.

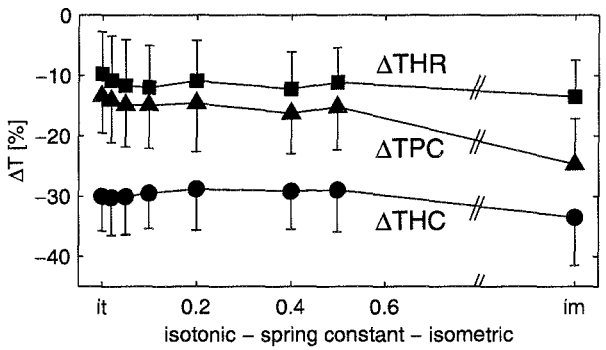

Figure 12: Average ± SD relative change in timing ($\Delta T = 100 \cdot (T_{PESP} - T_N)/T_N$) from normal stimulation to PESP for THC (circles), TPC (triangles), and THR (squares) in auxotonic twitches versus k_a.

4.5 Contraction - Relaxation

Whereas we found a load-independent TPC in auxotonic twitches, THR varied with different spring constants. This makes a distinct functional difference between contraction and relaxation. This was further underscored by the calculations of derivative of stress development and decline. It is previously found that isometric stress decline is stress dependent [38] during isometric relaxation. Since TPC is the same for different spring constants (i.e. different peak stress) and THR is highly correlated with peak developed stress, stress decline in auxotonic relaxation must also be stress dependent. The plot of peak negative $\dot{\sigma}_t/\sigma_t$ in Figure 11 shows that this is true for different auxotonic loads except small loads. Two possible explanations of the high correlation between peak developed stress and THR are 1) that activation is remained because more calcium is bound to TnC due to cross-bridge dependent dissociation rates (as noticed above) [26] or 2) that TnC is kept activated by the cross-bridges themselves [19, 36].

The differences between the load dependence of contraction and relaxation in the auxotonic twitch may have implications on the evaluation of the in vivo left ventricular function. The normalized developed stress during auxotonic contraction (Figure 2) demonstrated a load-independent timing of contraction, but still an inversely related distribution of stress development and shortening. This way, the loading conditions during contraction play an important role for the duration of relaxation. Therefore, evaluation of systolic and diastolic function should not be performed separately without considering the importance of the loading conditions on the coupling between contraction and relaxation.

dP/dt with different kinds of normalization have been used to describe the cardiac dynamics, and also as an index of contractility [5, 30, pp. 279-280]. $\dot{\sigma}_t$ is the counterpart of dP/dt on the muscle level. We found that the value of this measure with different normalization factors was altered after PESP. But because of the load dependence of these measures, it is only possible to evaluate relative changes in contractility after an intervention. This, however, requires that the loading conditions are the same. The only load-independent measure for the auxotonic twitches was the positive peak value of $\dot{\sigma}_t/max\{\sigma_t - \sigma_r\}$. The average peak value of all muscles and all auxotonic loads (including isometric) increased from 5.20 ± 0.68 s^{-1} with normal stimulation to 6.90 ± 0.79 s^{-1} after PESP. In the intact heart, however, where the loading conditions are more complex, also this measure may be load dependent. In an conventional afterloaded twitch, this measure will be very dependent on the afterload, especially when the peak value is reached in the isometric phase.

4.6 Normalized Auxotonic Twitches

The normalized auxotonic twitch (Figure 2, lower panel) demonstrated a synchronized contraction phase. One may argue that this result would be an obvious consequence of the control algorithm where we have proportionality between shortening and developed

stress. We will demonstrate mathematically that the observed synchroneity is not a consequence of the control algorithm.

The control algorithm gives the following relation between developed stress and shortening in a twitch i with spring constant $k_{a,i}$:

$$\Delta\sigma_i(t) = \sigma_i(t) - \sigma_r = k_{a,i}\Delta l_i(t)$$

The developed stress in two twitches i and j can be written:

$$\begin{aligned} \Delta\sigma_i(t) &= f(t) \cdot max\{\Delta\sigma_i\} \\ \Delta\sigma_j(t) &= g(t) \cdot max\{\Delta\sigma_j\} \end{aligned}$$

,where $f(t)$ and $g(t)$ are functions with values between 0 and 1. The control algorithm implies:

$$\begin{aligned} k_{a,i} \cdot \Delta l_i(t) &= f(t) \cdot max\{k_{a,i} \cdot \Delta l_i\} \\ k_{a,j} \cdot \Delta l_j(t) &= g(t) \cdot max\{k_{a,j} \cdot \Delta l_j\} \\ &\Downarrow \\ \Delta l_i(t) &= f(t) \cdot max\{\Delta l_i\} \\ \Delta l_j(t) &= g(t) \cdot max\{\Delta l_j\} \end{aligned}$$

If the control algorithm would imply that $f(t) = g(t)$ in the contraction phase (i.e. synchroneity) then the same algorithm should also imply that $f(t) = g(t)$ in the relaxation phase, which is not the case. Therefore, the control algorithm does not imply synchroneity.

4.7 Conclusions

The controlled auxotonic twitch demonstrated fundamental differences between contraction and relaxation. The timing of contraction was independent on auxotonic load when initial length was at l_{max}, both with normal stimulation and after post extrasystolic potentiation. At initial length different from l_{max}, the timing of contraction was dependent of auxotonic load, resulting in a prolonged contraction at increasing initial length, which was more pronounced at lower auxotonic load. Timing of relaxation was highly correlated with peak developed stress, both in isometric twitches at increasing length and auxotonic twitches at increasing spring constant. The relations between the load dependence of contraction and relaxation, presented in this paper, may have implications for the in vivo left ventricular function analysis.

Acknowledgements: We thank professor Dirk L. Brutsaert for his comments and contributions to our discussions. This research has been supported in part by the Norwegian Research Council (NFR) grant # 107409/320.

References

1. Akella AB, Su H, Sonnenblick EH, Rao VG, and Gulati J. The cardiac troponin C isoform and the length dependence of Ca2+ sensitivity of tension in myocardium. *J. Mol. Cell. Cardiol.* 29:381–9, 1997.

2. Allen DG and Kentish JC. The cellular basis of the length-tension relation in cardiac muscle. *J. Mol. Cell. Cardiol.* 17:821–40, 1985.

3. Allen DG and Kurihara S. The effects of muscle length on intracellular calcium transients in mammalian cardiac muscle. *J. Physiol.* 327:79–94, 1982.

4. Beyar R, Yin FC, Hausknecht M, Weisfeldt ML, and Kass DA. Dependence of left ventricular twist-radial shortening relations on cardiac cycle phase. *Am. J. Physiol.* 257:H1119–26, 1989.

5. Braunwald E. Assessment of cardiac function. In: Braunwald E, ed., *Heart Disease: A Textbook of Cardiovascular Medicine*, volume 1, 419–443. W. B. Saunders Company, Philadelphia, USA, 4th edition, 1992.

6. Brutsaert DL and Claes VA. Onset of mechanical activation of mammalian heart muscle in calcium- and strontium-containing solutions. *Circ. Res.* 35:345–57, 1974.

7. Brutsaert DL, Claes VA, Chuck LM, Housmans PR, Sys SU, and DeClerck NM. New technology in studying the origin of non-uniformity in cardiac muscle. In: Kitamura K and Abe H, eds., *New approaches in cardiac mechanics*, 31–45. Gordon and Breach, New York, USA, 1986.

8. Brutsaert DL, Meulemans AL, Sipido KR, and Sys SU. Effects of damaging the endocardial surface on the mechanical performance of isolated cardiac muscle. *Circ. Res.* 62:358–66, 1988.

9. Brutsaert DL and Sys SU. Relaxation and diastole of the heart. *Physiol. Rev.* 69:1228–315, 1989.

10. Cooper MW. Postextrasystolic potentiation. Do we really know what it means and how to use it? *Circulation* 88:2962–71, 1993.

11. Fitzsimons DP and Moss RL. Strong binding of myosin modulates length-dependent Ca2+ activation of rat ventricular myocytes. *Circ. Res.* 83:602–7, 1998.

12. Fuchs F and Wang YP. Sarcomere length versus interfilament spacing as determinants of cardiac myofilament Ca2+ sensitivity and Ca2+ binding. *J. Mol. Cell. Cardiol.* 28:1375–83, 1996.

13. Gibbons Kroeker CA, Ter Keurs HE, Knudtson ML, Tyberg JV, and Beyar R. An optical device to measure the dynamics of apex rotation of the left ventricle. *Am. J. Physiol.* 265:H1444–9, 1993.

14. Gordon AM, Huxley AF, and Julian FJ. The variation in isometric tension with sarcomere length in vertebrate muscle fibres. *J. Physiol.* 184:170–92, 1966.

15. Gulati J. Molecular biology of the length-tension relation in cardiac muscle. *Adv. Exp. Med. Biol.* 332:593–602, 1993.

16. Gulati J, Sonnenblick E, and Babu A. The role of troponin C in the length dependence of Ca(2+)-sensitive force of mammalian skeletal and cardiac muscles [published erratum appears in J. Physiol. 1991 Dec;444:778]. *J. Physiol.* 441:305–24, 1991.

17. Helmes M, Trombitas K, and Granzier H. Titin develops restoring force in rat cardiac myocytes. *Circ. Res.* 79:619–26, 1996.

18. Hittinger L, Crozatier B, Belot JP, and Pierrot M. Regional ventricular segmental dynamics in normal conscious dogs. *Am. J. Physiol.* 253:H713–9, 1987.

19. Hofmann PA and Fuchs F. Evidence for a force-dependent component of calcium binding to cardiac troponin C. *Am. J. Physiol.* 253:C541–6, 1987.

20. Holmes KC. The actomyosin interaction and its control by tropomyosin. *Biophys. J.* 68:2S–7S, 1995.

21. Housmans PR, Lee NK, and Blinks JR. Active shortening retards the decline of the intracellular calcium transient in mammalian heart muscle. *Science* 221:159–61, 1983.

22. Janssen PM and Hunter WC. Force, not sarcomere length, correlates with prolongation of isosarcometric contraction. *Am. J. Physiol.* 269:H676–85, 1995.

23. Katz AM. *Physiology of the heart.* Raven Press, New York, 2nd edition, 1992.

24. Kirby MS, McCall E, Orchard CH, and Boyett MR. The role of Na(+)-Ca(2+) exchange in paired pulse potentiation of ferret ventricular muscle. *J. Physiol.* 472:415–42, 1993.

25. Lab MJ, Allen DG, and Orchard CH. The effects of shortening on myoplasmic calcium concentration and on the action potential in mammalian ventricular muscle. *Circ. Res.* 55:825–9, 1984.

26. Landesberg A and Sideman S. Mechanical regulation of cardiac muscle by coupling calcium kinetics with cross-bridge cycling: A dynamic model. *Am. J. Physiol.* 267:H779–95, 1994.

27. Leach JK, Brady AJ, Skipper BJ, and Millis DL. Effects of active shortening on tension development of rabbit papillary muscle. *Am. J. Physiol.* 238:H8–13, 1980.

28. McDonald KS, Field LJ, Parmacek MS, Soonpaa M, Leiden JM, and Moss RL. Length dependence of Ca2+ sensitivity of tension in mouse cardiac myocytes expressing skeletal troponin C. *J. Physiol.* 483:131–9, 1995.

29. McDonald KS and Moss RL. Osmotic compression of single cardiac myocytes eliminates the reduction in Ca2+ sensitivity of tension at short sarcomere length. *Circ. Res.* 77:199–205, 1995.

30. Milnor WR. *Hemodynamics*. Williams & Wilkins, Baltimore, USA, 2nd edition, 1989.

31. Mirsky I and Parmley WW. Assessment of passive elastic stiffness for isolated heart muscle and the intact heart. *Circ. Res.* 33:233–43, 1973.

32. Moss RL, Nwoye LO, and Greaser ML. Substitution of cardiac troponin C into rabbit muscle does not alter the length dependence of Ca2+ sensitivity of tension. *J. Physiol.* 440:273–89, 1991.

33. Niggli E and Lederer WJ. Restoring forces in cardiac myocytes. Insight from relaxations induced by photolysis of caged ATP. *Biophys. J.* 59:1123–35, 1991.

34. Paulus WJ, Claes VA, and Brutsaert DL. Physiological loading of isolated feline cardiac muscle. The interaction between muscle contraction and vascular impedance in the production of pressure and flow waves. *Circ. Res.* 44:491–7, 1979.

35. Rademakers FE, Buchalter MB, Rogers WJ, Zerhouni EA, Weisfeldt ML, Weiss JL, and Shapiro EP. Dissociation between left ventricular untwisting and filling. Accentuation by catecholamines. *Circulation* 85:1572–81, 1992.

36. Rice JJ, Winslow RL, and Hunter WC. Comparison of putative cooperative mechanisms in cardiac muscle: Length dependence and dynamic responses. *Am. J. Physiol.* 276:H1734–54, 1999.

37. Sørhus V, Sys SU, Natås A, Demolder MJ, and Angelsen BAJ. Controlled auxotonic twitch in papillary muscle: A new computer-based control approach. *Submitted* 2000.

38. Sys SU and Brutsaert DL. Determinants of force decline during relaxation in isolated cardiac muscle. *Am. J. Physiol.* 257:H1490–7, 1989.

39. Wang YP and Fuchs F. Osmotic compression of skinned cardiac and skeletal muscle bundles: Effects on force generation, Ca2+ sensitivity and Ca2+ binding. *J. Mol. Cell. Cardiol.* 27:1235–44, 1995.

40. Wier WG and Yue DT. Intracellular calcium transients underlying the short-term force- interval relationship in ferret ventricular myocardium. *J. Physiol.* 376:507–30, 1986.

Paper C

Dimensionless Time Traces of Mechanical Dynamics in Papillary Muscle Twitches

Vidar Sørhus[1], Marc J. Demolder[2], Stein I. Rabben[1], Bjørn A. J. Angelsen[1], and Stanislas U. Sys[2]

[1] Dept. of Physiology and Biomedical Engineering, NTNU, Trondheim, Norway

[2] Dept. of Human Physiology and Pathophysiology, UIA (RUCA), Antwerp, Belgium

Abstract

The mechanical dynamics of cardiac muscles are expressed as changes in muscle length and force. In isolated muscle, the length and force dynamics have been studied separately. Under auxotonic loading conditions, however, there are simultaneous changes in length and force. We wanted to study the differences in mechanical dynamics in twitches with different loading conditions. We represented the mechanical dynamics with two different expressions, defined as the sum of normalized stress and shortening. The first used normalized developed stress and the second used normalized instantaneous active stress as input. The resulting dimensionless time traces of mechanical dynamics demonstrated very similar shape of the contraction phase at the full range of loads from isotonic to isometric and in both auxotonic and afterloaded twitches. The same traces demonstrated wide variation during relaxation depending on load and twitch type. With the first expression, it was possible to obtain a rough estimate of peak isometric stress and peak isotonic shortening from two or more intermediate twitches. Both expressions visualized qualitative differences in load dependence between the contraction and relaxation phases, which may have implications on the clinical interpretation of systolic versus diastolic function.

Keywords: load dependence; cardiac muscle; auxotonic; contraction-relaxation; systolic function; diastolic function

1 Introduction

Mechanical dynamics in cardiac muscles can be defined as changes in muscle length and force. The changes in length and force result from interactions between force-generating units (cross-bridges) in the muscle and the loading conditions applied on the muscle. Shortening occurs when the force generated by the cross-bridges exceeds the load on the cross-bridges. Instantaneous force is given by the number of cross-bridges and the mean force on each cross-bridge, which in turn depend on loading conditions, calcium handling, and properties of the contractile proteins [9].

The mechanical dynamics of the fully activated (tetanized) muscle have been studied from quick release (and quick stretch) experiments, constant velocity experiments, and sinusoidal perturbation [10, 13, 19, 20, 23]. These experiments have been used to obtain information about the cross-bridge dynamics. The cross-bridge dynamics have been represented by the force-velocity relation with the related Hill equation and force recovery time constants [14, 20, 23].

In traditional experimental setups for isolated papillary muscles, the muscle twitches (single contraction-relaxation sequences) have been controlled in either isometric (constant length) or isotonic (constant total force) conditions or sequential combinations of isometric and isotonic loading conditions [9, 26, 28]. In muscle twitches, the sarcomeres are not fully activated. In such twitches we observe an initial transient rise in activation which is continued with a relaxation phase. This means that the mechanical dynamics result from a combination of activation dynamics and cross-bridge dynamics. It is not well-known whether the cross-bridge dynamics is the same under sub-maximal activation as it is under maximal activation and thereby separable from the activation dynamics.

The mechanical dynamics of muscle twitches have been quantified with indices like (positive and negative) peak dF/dt and peak shortening and peak lengthening velocity [4, 24]. These indices are related to intact heart measures like peak positive and negative dP/dt and maximal velocities of ejection and filling flow [3, 4]. The slope of the last part of the isovolumetric pressure decline has been used as an index of impaired relaxation or diastolic function [22].

In the intact heart, there are coupled and simultaneous changes in both length and stress during all phases of the cardiac cycle [7, 12, 15, 17, 29, 30]. Changes in length and stress are coupled both through the loading conditions and their common origin, namely the cross-bridge cycling. Therefore, mechanical dynamics are expressed as changes in both stress and length, more or less simultaneously. Single measures of mechanical dynamics based on either stress or shortening may therefore be dependent on the loading conditions and insufficient to describe the true mechanical dynamics. To be able to study isolated muscles with simultaneous changes in length and stress, we included auxotonic loading in an experimental setup for isolated papillary muscles [33].

The purpose of this study was to compare the mechanical dynamics of isolated papillary muscles under different loading conditions. We therefore constructed two different expressions of the mechanical dynamics, defined as the sum of normalized stress and shortening. Based on these expressions we wanted to 1) visualize the qualitative differences in mechanical dynamics between twitches with different loading conditions, 2) derive quantitative parameters of the muscle performance, and 3) discuss the influence of the loading conditions on cardiac muscle modeling.

2 Methods

2.1 Muscle Preparation

Rabbits (n=9) were anesthetized by cervical translocation and the heart was quickly excised. A papillary muscle was dissected from the right ventricle in a dissection bath with temperature controlled and oxygenated Krebs-Ringer solution (see below), containing 2,3-butanedione monoxime (BDM; 30mM) to inhibit actin-myosin cross-bridge cycling during dissection. The muscle was passively stretched with a preload of 6 mN/mm^2 of estimated cross-sectional area. Under a dissection microscope (WILD M3B from Leica) three tips of glass microelectrodes were inserted into the muscle perpendicular to the long axis. At the tip, the diameters of the microelectrodes were less than 5 μm, and at the muscle surface the diameters were maximally 15 μm. Then the papillary muscle was installed vertically in a 3 ml bath. The Krebs-Ringer solution was circulating with a flow rate of approximately 10 ml/min and contained (in mM): NaCl 98, KCl 4.7, $MgSO_4.7H_2O$ 2.4, $NaHCO_3$ 25, $CaCl_2.2H_2O$ 1.25, glucose 4.5, Na-pyruvate 15 and Na-acetate 5, at 29°C bubbled with a gas mixture of 95 % oxygen and 5 % carbon dioxide. An electrical field between two platinum electrodes stimulated the papillary muscle at approximately 10 % above threshold.

2.2 Experimental Setup

The papillary muscle setup was based on an analog/mechanical setup, described in Brutsaert and Claes [6] and Brutsaert et al. [8]. The original system consisted of a force transducer, an optical displacement measurement transducer, a papillary muscle bath with a clip for the lower muscle end, two platinum electrodes for electrical stimulation, and a control unit for isotonic and isometric control and stimulation. The system also included a segment measurement system based on detection of position of microelectrodes with a CCD-array [7, 34].

The control unit of the original setup was replaced with a PC with a DSP board and an interface unit between the PC and the transducers, as described in Sørhus et al. [33] (Figure 1). An individual application for low-level feedback control and data acquisition was running on the DSP board at a sample rate of 5000 samples per second. This application included different algorithms for different twitch types.

Another application for visualization and storage of measured and calculated variables, on-line user interaction, and overall control of experiments was running on the host computer.

The system included a controlled auxotonic twitch where the muscle was acting against an virtual ideal spring:

$$\sigma_t(t) \quad = \quad k_a(l_{max} - l(t)) + \sigma_r(l_{max})$$

where σ_t, l, and $\sigma_r(l_{max})$ denote total stress, measured length, and resting stress at the length with maximal isometric active stress development, respectively. The stiffness of the virtual spring was given by the user-defined spring constant, k_a (mN/mm), representing a smooth transition from isotonic ($k_a = 0$) to isometric ($k_a \to \infty$).

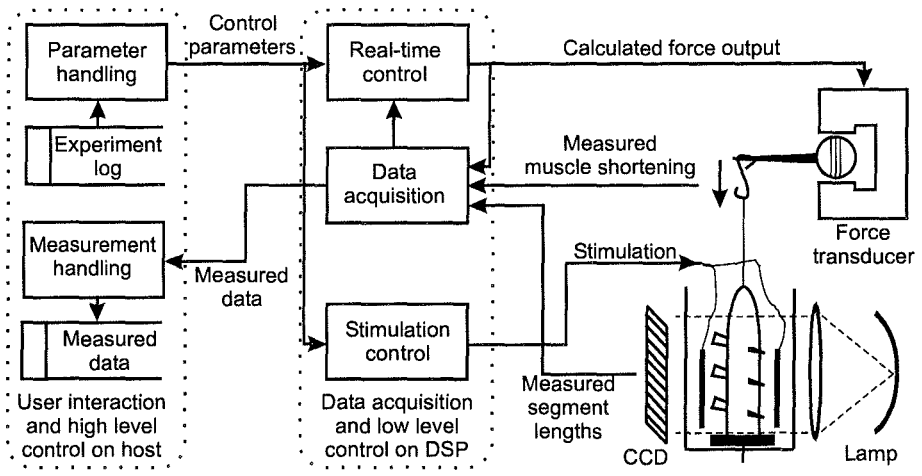

Figure 1: Main components and data flow in the system. An application for real-time control, data acquisition, and stimulation control was running on the DSP board. Total muscle shortening and muscle segment lengths were measured and sent via the DSP-board to the host computer through a measurement channel and optionally stored in a text-file (Measured data). An application for user interaction and high level control was running on the host computer. Control parameters set by the user or read from a text-file (Experiment log) were sent from the host computer to the DSP-board through a parameter channel.

2.3 Dimensionless Expressions of Mechanical Dynamics

To study the mechanical dynamics in twitches including changes in both length and stress, we used two dimensionless expressions, defined as the sum of normalized stress and shortening. We required that the peak value of the expressions in the extreme cases of isotonic and isometric twitches should be normalized (= 1). In the first expression we used only total stress and muscle shortening:

$$M1(t) = \frac{\sigma_t(t) - \sigma_r(l_{max})}{max\{\sigma_{a,im}\}} + \frac{\varepsilon(t)}{max\{\varepsilon_{it}\}} \quad (1)$$

where

$$\sigma_a(t) = \sigma_t(t) - \sigma_r(l(t))$$
$$\varepsilon(t) = 1 - \frac{l(t)}{l_{max}}$$

σ_t and σ_a denote total and active stress, $\sigma_r(l)$ is resting stress at a given muscle length l, $max\{\sigma_{a,im}\}$ is peak isometric active stress, and $max\{\varepsilon_{it}\}$ is peak isotonic shortening.

Total stress in Eq. 1 is the sum of active and passive stress. One possible shortcoming of expression $M1$ (Eq. 1) is that total stress is constant during isotonic shortening, although active and passive stress changes due to the passive stress-length relation (Figure 2).

An alternative to Eq. 1 is therefore to use active stress instead of developed stress ($\sigma_d = \sigma_t - \sigma_r(l_{max})$). Peak active stress in isotonic twitches is equal to passive stress at l_{max} minus passive stress at the shortest length. Therefore, to obtain equal peak values in the resulting traces of isometric and isotonic twitches, we modified Eq. 1:

$$M2(t) = \frac{\sigma_a(t)}{max\{\sigma_{a,im}\}} + \frac{\varepsilon(t)}{max\{\varepsilon_{it}\}} \cdot \left[1 - \frac{max\{\sigma_{a,it}\}}{max\{\sigma_{a,im}\}}\right] \quad (2)$$

2.4 Experiment Protocol

In nine papillary muscles, we measured one series of afterloaded and one series of physiological twitches with increasing afterload from isotonic to isometric, and one series of auxotonic twitches at different loads from isotonic to isometric. Initial length was l_{max} in all these twitches. Eight isotonic stabilization twitches preceded each measured twitch. One additional series of isometric twitches at increasing length was measured to derive passive stress-length relations for each muscle (Figure 2).

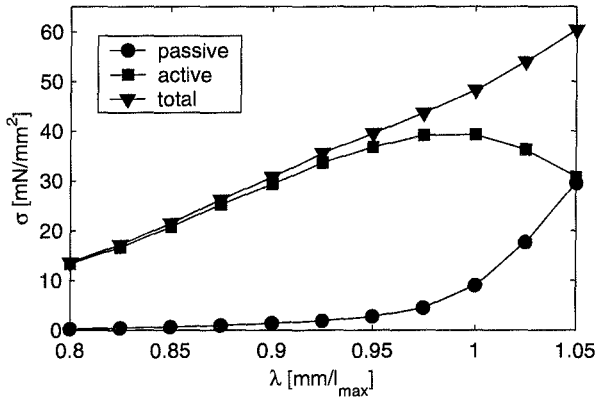

Figure 2: Passive (circles), active (squares), and total (triangles) stress-length relations from a series of isometric twitches at increasing length.

2.5 Data Analysis

We used Eq. 1 and 2 to calculate time traces of dimensionless mechanical dynamics ($M1$ and $M2$) for all muscles and all twitches. The individual passive stress-length relations were used to calculate instantaneous active stress in afterloaded, physiological, and auxotonic twitches. We measured resting diameter of all muscles at l_{max} to calculate cross-sectional area. We have used stress (force per resting cross sectional area) and relative length ($\lambda = l/l_{max}$) in all analyses where nothing else is noticed.

Expression $M1$ was used to estimate peak isometric stress and peak isotonic shortening with two different methods. First, we used linear regression on all the intermediate twitches. In this case, the peak values were calculated according to

$$\alpha = (A^T A)^{-1} A^T y \tag{3}$$

where

$$\begin{aligned} \alpha &= [1/max\{\sigma_{a,im}\} \quad 1/max\{\varepsilon_{it}\}]^T \\ A &= \begin{bmatrix} max\{\sigma_d, tw1\} & max\{\varepsilon, tw1\} \\ \vdots & \vdots \\ max\{\sigma_d, twN\} & max\{\varepsilon, twN\} \end{bmatrix} \\ y &= [1 \cdots 1]^T \quad \text{or} \quad y = [0.94 \cdots 0.94]^T \end{aligned}$$

Second, we calculated peak isometric stress and peak isotonic shortening from all pairs of intermediately loaded twitches. For both methods we used both the peak value of the isometric and isotonic twitches (= 1) and the average peak value of the intermediate twitches (= 0.94, see Results) as the intercept (y in Eq. 3).

The calculation and visualization of $M1$ and $M2$ and the estimation of peak isometric stress and peak isotonic shortening were performed with Matlab (MathWorks Inc.). All statistical analysis were performed with Excel (Microsoft Corp.).

3 Results

3.1 Dimensionless Time Traces of Mechanical Dynamics

Figure 3 presents time traces of total stress (panel A), relative length (panel B), and mechanical dynamics from the two expressions $M1$ (Eq. 1, panel C) and $M2$ (Eq. 2, panel D) from a series of afterloaded twitches with increasing afterload from isotonic to isometric. Figure 4 and 5 demonstrate similar plots of a series of physiological (i.e. isometric-isotonic relaxation sequence) twitches at increasing afterload and a series of auxotonic twitches at increasing auxotonic load from the same muscle. All series of twitches included one isotonic and one isometric reference twitch.

3.1.1 Contraction

An interesting observation about the mechanical dynamics in the contraction phase was that $M1$ and $M2$ varied little at different loading conditions and twitch types. There was a small reduction in the rate of mechanical dynamics after an abrupt change from isometric to isotonic contraction when expression $M1$ was used. In the other expression ($M2$), when active stress was used instead of total stress, there was very little difference between twitches with different loading. The same small variation in mechanical dynamics during contraction was found when we performed a series of twitches with a non-physiological isotonic-isometric contraction sequence (Figure 8).

3.1.2 Relaxation

During relaxation dynamics, however, $M1$ and $M2$ demonstrated considerable differences in mechanical dynamics dependent on the loading conditions. The difference between isotonic and isometric rate of $M1$ and $M2$ during relaxation was clearly demonstrated in the physiological twitches (Figure 4), where we had an isometric-isotonic relaxation sequence. Mechanical dynamics during isotonic relaxation were markedly faster than during isometric relaxation. Time from stimulus did not seem to change the rates of $M1$ and $M2$ markedly. The same may also be true for the afterloaded twitches (Figure 3), although the transition from isotonic to isometric relaxation yielded a very fast initial isometric stress decline.

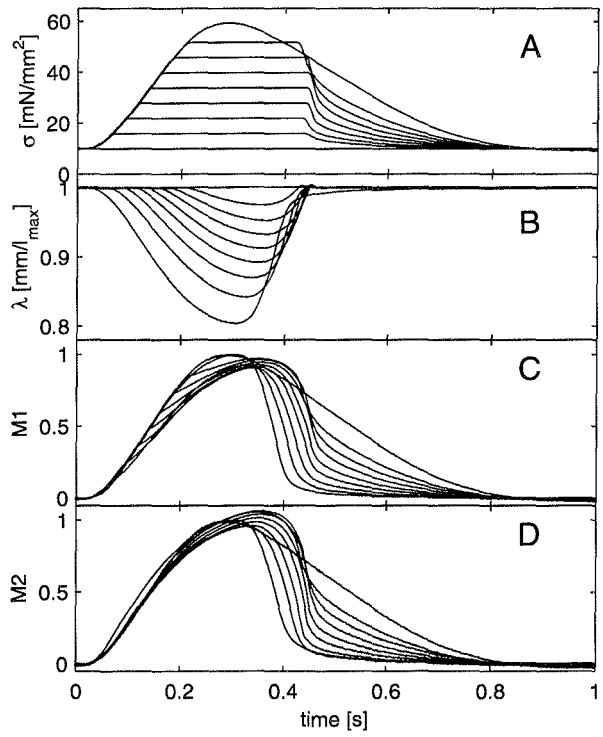

Figure 3: Total stress (A), relative length (B), $M1$ (C), and $M2$ (D) from a series of afterloaded twitches at increasing afterload from isotonic to isometric.

In both the afterloaded and the physiological twitches, there were abrupt changes between isotonic and isometric loading conditions. After these abrupt changes, there seemed to be a small transition time before the mechanical dynamics followed the expected isotonic or isometric patterns. In afterloaded relaxation, the change was from fast (isotonic) to slow (isometric), and therefore the initial stress decline was fast.

So far, we have noticed the fast isotonic and the slow isometric rate of relaxation. The auxotonic twitches were supposed to give a smooth transition from isotonic to isometric loading. The rate of relaxation in the auxotonic twitches (Figure 5), in terms of the two dimensionless expressions defined here, seemed to give a similar smooth transition in the rate of relaxation; from isotonic towards isometric at increasing auxotonic load (k_a). We observed a decreasing rate of relaxation when k_a increased from isotonic towards isometric.

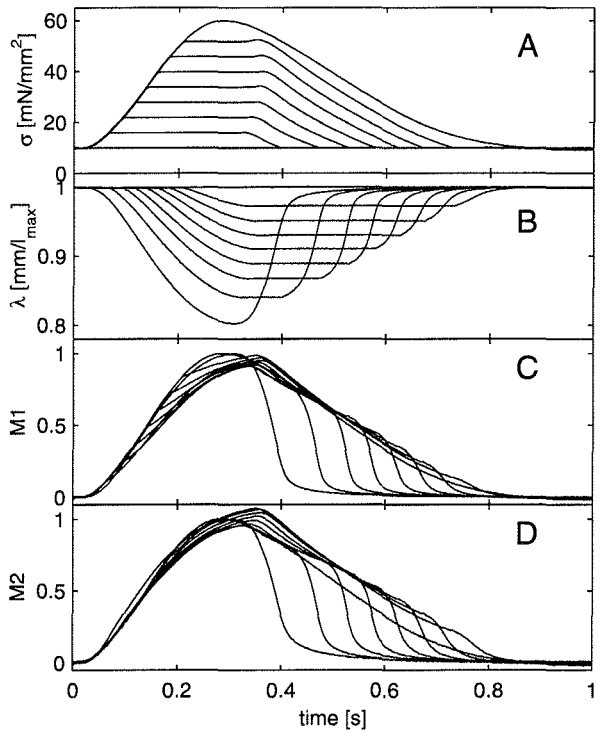

Figure 4: Total stress (A), relative length (B), $M1$ (C), and $M2$ (D) from a series of physiological twitches at increasing afterload from isotonic to isometric.

3.2 Peak Values of Intermediately Loaded Twitches

One requirement for the dimensionless expression of the mechanical dynamics was that the peak value of the time trace should be equal for isotonic and isometric twitches. In the examples in Figure 3 to 5, the peak values of the intermediately loaded twitches were also close to the peak values of the isotonic and isometric twitches ($max\{M1\} = max\{M2\} = 1$).

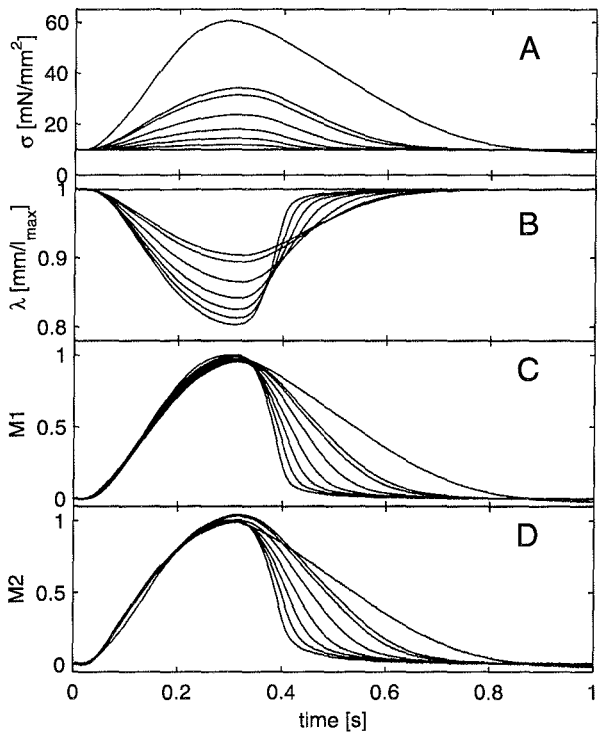

Figure 5: Total stress (A), relative length (B), $M1$ (C), and $M2$ (D) from a series of auxotonic twitches at increasing auxotonic load from isotonic to isometric.

Table 1 presents the average peak values of the intermediate twitches (all twitches except isotonic and isometric) of all twitch types and for both dimensionless expressions ($M1$ and $M2$). For $M1$, the peak values were less than 1, and in general lower for afterloaded and physiological twitches than for auxotonic twitches (paired t-test; $P<0.0001$). This may be related to the discontinuities in the stress and length due to the abrupt change between isometric and isotonic loading conditions [33]. When we used instantaneous active stress in the dimensionless expression ($M2$), we obtained peak values close to one in all twitch types. The more equal peak values of $M2$ in afterloaded and physiological twitches compared to auxotonic twitches, are partly due to the different distribution of twitches between isotonic and isometric and to the non-linear passive stress-length relation (Figure 2).

Table 1: Peak values of $M1$ and $M2$ in all twitches except isotonic and isometric twitches (n=9).

	Afterloaded	Physiological	Auxotonic	All
$max\{M1(t)\}$ (mean ± SD)	0.931 ± 0.031	0.937 ± 0.034	0.961 ± 0.022	0.944 ± 0.032
$max\{M2(t)\}$ (mean ± SD)	1.011 ± 0.035	1.016 ± 0.039	1.011 ± 0.022	1.012 ± 0.032

3.3 Estimation of Peak Isometric Stress and Peak Isotonic Shortening

Based on the fact that the peak values of the intermediately loaded twitches were close to the peak values of the isometric and isotonic twitches, it may be possible to estimate the peak isometric stress and peak isotonic shortening from two or more intermediately loaded twitches. The peak values from the $M2$-expression were closest to one. This expression, however, required that the passive stress-length relation was known from isometric measurements, and therefore estimation of peak isometric stress was not interesting. Expression $M1$ only requires total stress and shortening from at least two differently loaded twitches as input. Therefore, we used this expression to estimate peak isometric stress and peak isotonic shortening. We used two different methods as described in the Methods section. First, we used linear regression on all the intermediate twitches (Eq. 3). Second, we calculated peak isometric stress and peak isotonic shortening from all pairs of intermediately loaded twitches. The resulting estimation errors from the two methods are presented as bar-plots in Figure 6 and 7.

As one would expect from the peak values in Table 1, we got a small underestimation of the peak values with both methods. In auxotonic twitches, the estimation of peak isotonic shortening was better than the estimation of the peak isometric stress. In afterloaded and physiological twitches, the twitches were isometric in the first part of the contraction before they were switched to isotonic. The average estimation error and the variance were a little higher for the second estimation method (all pairs of intermediate twitches).

4 Discussion

This study has presented two possible expressions for the mechanical dynamics of cardiac muscle twitches. Both expressions combine stress and length dynamics. This makes it possible to compare the mechanical dynamics of twitches with different loading conditions from isotonic to isometric. Both expressions demonstrate fundamental differences between the mechanical dynamics in contraction and in relaxation.

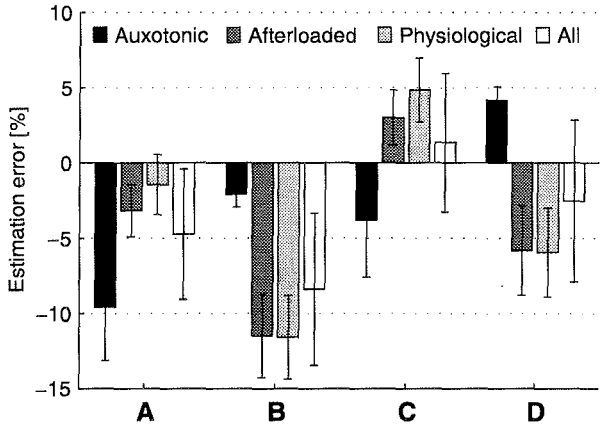

Figure 6: Estimation error (mean ± SD, n= 9) from estimation of peak isometric stress (A and C) and peak isotonic shortening (B and D). Linear regression with one on the intercept in A and B, and linear regression with the average peak value of $M1$ (Table 1) on the intercept in C and D.

4.1 Mechanical Dynamics in Twitches

Mechanical dynamics in the intact heart have traditionally been studied with different measures like positive and negative peak dP/dt, positive and negative peak velocities, and pressure-volume relations. Some of the measures have been normalized in different ways and used as indices on contractility and diastolic function [4, 22]. Similar measures for isolated muscles are peak dF/dt and v_{max}. Such measures may be misleading and not represent the true mechanical dynamics in twitches with sequences of isotonic and isometric phases. For example, in afterloaded twitches (Figure 3) peak dF/dt will increase with increasing afterload level, until the afterload exceeds the force with peak dF/dt in the complete isometric twitch. When normalized to, for instance, peak force, the dependence on the loading condition is even more pronounced [32]. To be able to visualize the qualitative differences in mechanical dynamics in twitches with different loading conditions, we proposed two expressions of the mechanical dynamics as the sum of normalized stress and shortening. Notice, that due to the same series of stabilization twitches before each recorded twitch, the contractile state and metabolic state were the same in all our experiments. Therefore, the differences in the $M1$ and $M2$ traces are all load-dependent differences, and not differences in, for instance, contractility.

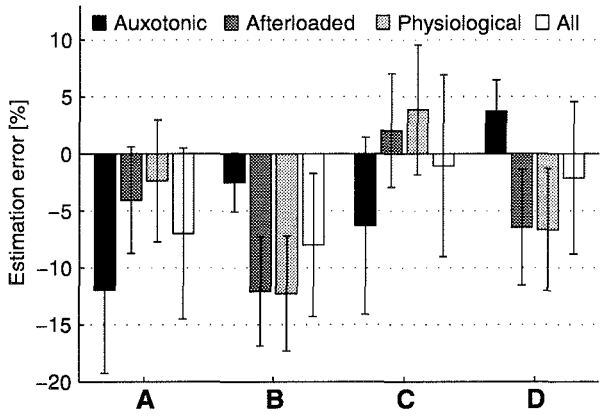

Figure 7: Estimation error (mean ± SD, n= 9) from estimation of peak isometric stress (A and C) and peak isotonic shortening (B and D). Calculated form all pairs of intermediately loaded twitches. Estimates calculated with one on the intercept in A and B, and with the average peak value of $M1$ (Table 1) on the intercept in C and D.

4.2 Mechanical Dynamics during Contraction and Relaxation

When we used the proposed expressions ($M1$ and $M2$) to calculate the mechanical dynamics in twitches with different loading conditions from isotonic to isometric, the most remarkable result was the difference between the contraction and relaxation phases. Even when the contraction phase was separated in one isometric and one isotonic phase, the contraction phase of the $M1$ and $M2$ traces had very similar shape. In relaxation, however, the $M1$ and $M2$ traces were widely separated depending on the loading condition and loading history. The latter demonstrates the concept of load dependence of relaxation [9, 34]. The independence of the amount of shortening and stress development on the contraction phase indicates that the common shape reflects the relative time-course of recruitment of new cross-bridges. In isometric contraction, this only adds force. Araki et al. [2] represent isovolumetric pressure rise with a function of the probability that the inhibitory effect of each single tropomyosin is removed within a given time after stimulation. During shortening, the recruitment of new cross-bridges compensates for the detachment of other cross-bridges and the reduction of the single overlap region in the sarcomere [21].

Activation (contraction) and inactivation (active relaxation) may be balanced by the level of free Ca^{2+} in the cytoplasm. During relaxation, there is a net amount of Ca^{2+} that dissociates from troponin C and enters the cytoplasm, where it is pumped

into the sarcoplasmic reticulum and out of the cell through the cell membrane. It has been reported that force-bearing cross-bridges have a cooperative effect on activation [5, 11, 16, 18, 21, 31]. This may be partly responsible for the difference in rate of relaxation in isotonic and isometric twitches. During isotonic lengthening, the number of cycling cross-bridges must be higher than during isometric force decline at the same force. Given a lower rate of inactivation for sites on the thin filament that are attached to cross-bridges versus sites that are not attached to cross-bridges, the isotonic relaxation will be faster than isometric relaxation.

4.3 Effect of the Transition between Isometric and Isotonic Loading on Mechanical Dynamics

There are four different abrupt changes between the two extreme isotonic and isometric loading conditions in our experiments. These are 1) from isometric to isotonic during contraction (Figure 3 and 4), 2) from isotonic to isometric during contraction (Figure 8), 3) from isotonic to isometric during relaxation (Figure 3), and 4) from isometric to isotonic during relaxation (Figure 4 and 8).

Not only the change in the number of cross-bridges determine the changes in active stress. During shortening and lengthening, some cross-bridges will either be moved from the single overlap region into the double overlap region (shortening) or in the opposite direction (lengthening) [21]. This effect may be observed after abrupt changes from isometric to isotonic or from isotonic to isometric loading. Other factors may also be partly responsible for the observed transition in the dynamics after switches between isometric and isotonic conditions. Viscous effects of muscle fibers and the surrounding tissue may play a role as well as transition from kinetic to potential energy which may be responsible for additional break-down of cross-bridges (in afterloaded twitches). Brutsaert and Sys [9] explain the rapid initial force decline in afterloaded twitches as an inherent property of the preceding lengthening process.

4.4 Estimation of Muscle Performance Parameters

Like in time traces of stress and length, it is possible to extract peak values and timing parameters from the $M1$ and $M2$ traces. In afterloaded and physiological twitches with sequences of isometric and isotonic loading conditions, it is not possible to measure time to half contraction and time to half relaxation from individual stress and length traces. This, however, is possible from the $M1$ and $M2$ traces.

We found that the $M1$ expression could also be used to obtain estimates of the peak isometric stress and peak isotonic shortening from intermediately loaded twitches. In auxotonic twitches, the estimation of peak isotonic shortening was better than the estimation of the peak isometric stress. This may be due to more auxotonic twitches closer to isotonic than to isometric loading. In afterloaded and physiological twitches, the twitches were isometric in the first part of the contraction before they abruptly

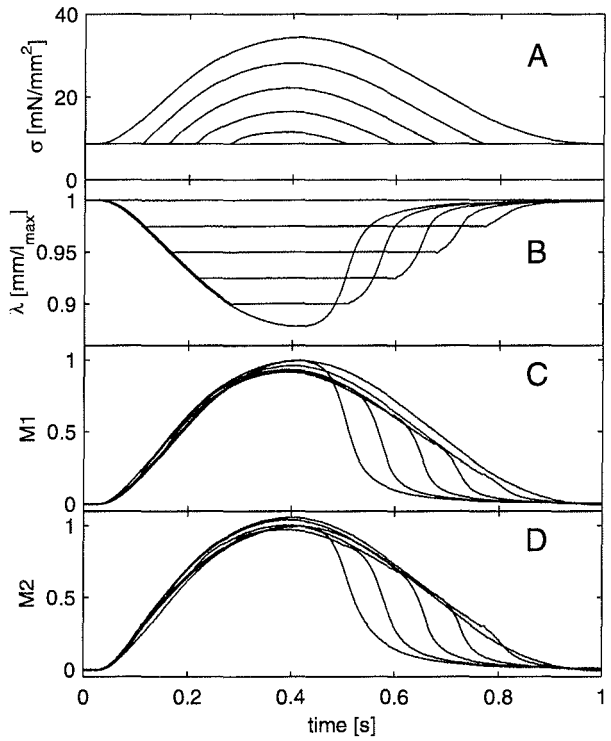

Figure 8: Total stress (A), relative length (B), $M1$ (C), and $M2$ (D) from a series of twitches with isotonic-isometric contraction sequence and isometric-isotonic relaxation sequence at decreasing peak shortening from isotonic to isometric.

changed to isotonic. This may be the reason why these twitches had the best estimates of peak isometric stress.

The average estimation error and the variance were a little higher for the second estimation method (all pairs of intermediate twitches). With this method, some pairs were close to each other and at the same time close to either isotonic or isometric loading. In such cases, the estimation of the other extreme loading may be difficult. We made no attempt to exclude such cases.

4.5 Consequences for Cardiac Muscle Modeling

It is difficult to develop mathematical models of the cardiac muscle that incorporates the differences in load dependence of contraction and relaxation and the many, more or less coupled, underlying processes. Especially if one wants to simulate muscle twitches over a wide range of loading conditions. A number of investigators use a compartment approach in the modeling of the cardiac muscle function [21, 27, 31]. This model approach is especially suitable for modeling the calcium and thin filament activation. This way it may be possible to incorporate cooperativity and length-dependent activation related to calcium sensitivity [1]. One of the fundamental problems with this model-approach is that it is to a high degree based on results from isometric and to some degree calcium-activated experiments. It may, therefore, be a challenge to extrapolate these models also to simulate non-isometric behavior adequately.

In a much more phenomenological approach, Araki and co-workers [2, 22, 25] has fitted the isovolumetric pressure curve and isometric force curve to a combination of two logistic functions. The problem with this approach is that it only represents isometric (and isovolumetric) conditions. The first function, representing the contraction phase, should also fit to the contraction phase of the traces from our dimensionless expressions because these traces are very similar to the isometric force trace. This implies that the logistic function of contraction may also represent non-isometric conditions or sequences of isotonic and isometric conditions. It is also reasonable that it is possible to fit the second function to the relaxation phase of the dimensionless expressions for all the auxotonic twitches from isotonic to isometric. For the afterloaded and physiological twitches, however, there will be a transition between the slopes of two different logistic functions representing the isotonic and isometric relaxation. This is again due to the concept of load dependence of relaxation [9].

The results presented in this paper demonstrate a coupling between changes in stress and changes in length in cardiac muscle twitches at a wide range of loading conditions. Quantitatively, for example as the relation between the peak isometric stress development and peak isotonic shortening and the peak values of the intermediately loaded twitches. Qualitatively, for example as the differences in rate of lengthening and rate of stress decline. Such relations may be used as constraints on cardiac muscle models.

4.6 Clinical Relevance

In a clinical setting, it is very important to distinguish between observations that result from altered muscle properties and observations that result from altered loading conditions [3]. Therefore, it has been focused on how to extract load-independent indices of contractility from different measurements [4]. We have demonstrated that for the whole range of afterloaded and auxotonic loading conditions from isotonic to isometric, the sum of the normalized stress and shortening is nearly load-independent during contraction. But, even though the pattern of the contraction phase is barely

load dependent, the distribution of stress versus shortening has major implications on the patterns of the relaxation phase.

This study shows that more stress development during contraction leads to a prolonged relaxation. Therefore, what may be interpreted as an impaired relaxation due to a prolonged isovolumetric relaxation time (or rate), may in fact be a result of increased systolic stress development due to pressure or volume overload.

4.7 Conclusions

This study has presented two possible expressions for the mechanical dynamics of cardiac muscle twitches. Both expressions combine stress and length dynamics. This makes it possible to compare the mechanical dynamics of twitches with different loading conditions from isotonic to isometric. The $M2$ expression had peak values close to one for all twitch types and loading conditions, and $M2$ may therefore better demonstrate the active dynamics of the muscle. However, with the $M1$ expression it is possible to obtain a rough estimate of peak isometric stress and peak isotonic shortening form measurements of total stress and shortening. Both expressions demonstrate fundamental differences between contraction and relaxation dynamics.

Acknowledgements: This research has been supported in part by the Norwegian Research Council (NFR) grant # 107409/320.

References

1. Allen DG and Kentish JC. The cellular basis of the length-tension relation in cardiac muscle. *J. Mol. Cell. Cardiol.* 17:821–40, 1985.

2. Araki J, Matsubara H, Shimizu J, Mikane T, Mohri S, Mizuno J, Takaki M, Ohe T, Hirakawa M, and Suga H. Weibull distribution function for cardiac contraction: Integrative analysis. *Am. J. Physiol.* 277:H1940–H1945, 1999.

3. Borow KM, Neumann A, Marcus RH, Sareli P, and Lang RM. Effects of simultaneous alterations in preload and afterload on measurements of left ventricular contractility in patients with dilated cardiomyopathy: Comparisons of ejection phase, isovolumetric and end- systolic force-velocity indexes. *J. Am. Coll. Cardiol.* 20:787–95, 1992.

4. Braunwald E. Assessment of cardiac function. In: Braunwald E, ed., *Heart Disease: A Textbook of Cardiovascular Medicine*, volume 1, 419–443. W. B. Saunders Company, Philadelphia, USA, 4th edition, 1992.

5. Bremel RD and Weber A. Cooperation within actin filament in vertebrate skeletal muscle. *Nat. New. Biol.* 238:97–101, 1972.

6. Brutsaert DL and Claes VA. Onset of mechanical activation of mammalian heart muscle in calcium- and strontium-containing solutions. *Circ. Res.* 35:345–57, 1974.

7. Brutsaert DL, Claes VA, Chuck LM, Housmans PR, Sys SU, and DeClerck NM. New technology in studying the origin of non-uniformity in cardiac muscle. In: Kitamura K and Abe H, eds., *New approaches in cardiac mechanics*, 31–45. Gordon and Breach, New York, USA, 1986.

8. Brutsaert DL, Meulemans AL, Sipido KR, and Sys SU. Effects of damaging the endocardial surface on the mechanical performance of isolated cardiac muscle. *Circ. Res.* 62:358–66, 1988.

9. Brutsaert DL and Sys SU. Relaxation and diastole of the heart. *Physiol. Rev.* 69:1228–315, 1989.

10. de Tombe PP and ter Keurs HE. Sarcomere dynamics in cat cardiac trabeculae. *Circ. Res.* 68:588–96, 1991.

11. Fitzsimons DP and Moss RL. Strong binding of myosin modulates length-dependent Ca2+ activation of rat ventricular myocytes. *Circ. Res.* 83:602–7, 1998.

12. Gibbons Kroeker CA, Ter Keurs HE, Knudtson ML, Tyberg JV, and Beyar R. An optical device to measure the dynamics of apex rotation of the left ventricle. *Am. J. Physiol.* 265:H1444–9, 1993.

13. Hancock WO, Martyn DA, and Huntsman LL. Ca2+ and segment length dependence of isometric force kinetics in intact ferret cardiac muscle. *Circ. Res.* 73:603–11, 1993.

14. Hill AV. The heat of shortening and the dynamic constants of muscle. *Proc. R. Soc. Ser. B* 126:136–195, 1938.

15. Hittinger L, Crozatier B, Belot JP, and Pierrot M. Regional ventricular segmental dynamics in normal conscious dogs. *Am. J. Physiol.* 253:H713–9, 1987.

16. Hofmann PA and Fuchs F. Evidence for a force-dependent component of calcium binding to cardiac troponin C. *Am. J. Physiol.* 253:C541–6, 1987.

17. Housmans PR, Chuck LH, Claes VA, and Brutsaert DL. Nonuniformity of contraction and relaxation of mammalian cardiac muscle. *Adv. Exp. Med. Biol.* 170:837–40, 1984.

18. Housmans PR, Lee NK, and Blinks JR. Active shortening retards the decline of the intracellular calcium transient in mammalian heart muscle. *Science* 221:159–61, 1983.

19. Hunter PJ, McCulloch AD, and ter Keurs HE. Modelling the mechanical properties of cardiac muscle. *Prog. Biophys. Mol. Biol.* 69:289–331, 1998.

20. Huxley AF and Simmons RM. Proposed mechanism of force generation in striated muscle. *Nature* 233:533–8, 1971.

21. Landesberg A and Sideman S. Mechanical regulation of cardiac muscle by coupling calcium kinetics with cross-bridge cycling: A dynamic model. *Am. J. Physiol.* 267:H779–95, 1994.

22. Matsubara H, Takaki M, Yasuhara S, Araki J, and Suga H. Logistic time constant of isovolumic relaxation pressure-time curve in the canine left ventricle. Better alternative to exponential time constant. *Circulation* 92:2318–26, 1995.

23. McMahon TA. *Muscles, Reflexes, and Locomotion.* Princeton University Press, Princeton, New Jersey, USA, 1984.

24. Milnor WR. *Hemodynamics.* Williams & Wilkins, Baltimore, USA, 2nd edition, 1989.

25. Mizuno J, Mikane T, Araki J, Hatashima M, Moritan T, Ishikawa T, Komukai K, Kurihara S, Hirakawa M, and Suga H. Hybrid logistic characterization of isometric twitch force curve of isolated ferret right ventricular papillary muscle. *Jpn. J. Physiol.* 49:145–58, 1999.

26. Peterson JN, Hunter WC, and Berman MR. Control of segment length or force in isolated papillary muscle: An adaptive approach. *Am. J. Physiol.* 256:H1726–34, 1989.

27. Peterson JN, Hunter WC, and Berman MR. Estimated time course of Ca2+ bound to troponin C during relaxation in isolated cardiac muscle. *Am. J. Physiol.* 260:H1013–24, 1991.

28. Pinto JG. A constitutive description of contracting papillary muscle and its implications to the dynamics of the intact heart. *J. Biomech. Eng.* 109:181–91, 1987.

29. Rademakers FE, Buchalter MB, Rogers WJ, Zerhouni EA, Weisfeldt ML, Weiss JL, and Shapiro EP. Dissociation between left ventricular untwisting and filling. Accentuation by catecholamines. *Circulation* 85:1572–81, 1992.

30. Rayhill SC, Daughters GT, Castro LJ, Niczyporuk MA, Moon MR, Ingels NBJ, Stadius ML, Derby GC, Bolger AF, and Miller DC. Dynamics of normal and ischemic canine papillary muscles. *Circ. Res.* 74:1179–87, 1994.

31. Rice JJ, Winslow RL, and Hunter WC. Comparison of putative cooperative mechanisms in cardiac muscle: Length dependence and dynamic responses. *Am. J. Physiol.* 276:H1734–54, 1999.

32. Sørhus V, Angelsen BAJ, and Sys SU. Analysis of the controlled auxotonic twitch in isolated cardiac muscle. *Submitted* 2000.

33. Sørhus V, Sys SU, Natås A, Demolder MJ, and Angelsen BAJ. Controlled auxotonic twitch in papillary muscle: A new computer-based control approach. *Submitted* 2000.

34. Sys SU and Brutsaert DL. Determinants of force decline during relaxation in isolated cardiac muscle. *Am. J. Physiol.* 257:H1490–7, 1989.

Paper D

Simulation Model of Auxotonic Contraction and Relaxation

Vidar Sørhus[1], Stanislas U. Sys[2], and Bjørn A. J. Angelsen[1]

[1] Dept. of Physiology and Biomedical Engineering, NTNU, Trondheim, Norway.
[2] Dept. of Human Physiology and Pathophysiology, UIA (RUCA), Antwerp, Belgium.

Abstract

Mathematical models have been used to represent the cardiac muscle function or some of its underlying mechanisms. The models range from simple force-velocity relations to complex models of calcium handling and cross-bridge kinetics. Typically, a model is developed to validate hypotheses that have evolved from some experimental findings. However, mathematical models can also be used to estimate parameters that represent the function of the system. In this study, we wanted to develop a mathematical model of contraction-relaxation sequences of the cardiac muscle under a wide range of loading conditions from isotonic to isometric. Especially, we wanted to incorporate auxotonic loading conditions. Furthermore, in order to strengthen the relation between the measured stress and length and the model parameters, we wanted to develop a model with minimal complexity. The model simulations of auxotonic twitches corresponded well with the experimental results. There was a trade-off between model complexity and a good representation of all features of isometric and afterloaded twitches. A moderate increase in the model complexity allowed more realistic simulation of the timing of isometric twitches at increasing length and the initial rapid stress decline after an abrupt change from isotonic to isometric relaxation in afterloaded twitches.

Keywords: cardiac muscle function; papillary muscle; activation; inactivation

1 Introduction

1.1 Background

Mathematical modeling of the cardiac muscle function is based on a long history of experiments on skeletal and cardiac muscles from the whole organ [18] to the interaction between single myosin and actin molecules [67].

The work by Hill [24] on the energetics of skeletal muscle led to the force-velocity relation which is still important in modeling of both cardiac and skeletal muscle. Hill [24] studied the energy liberation of shortening after quick release of tetanized (maximally activated) frog skeletal muscle. From quick release experiments and passive and tetanized force-length relations, a three-component model structure has evolved [49]. This three-component structure consists of one series elastic element, one parallel elastic element, and one contractile element. Abbott and Mommaerts [1] were the first to study the force-velocity relation for cardiac muscle under sub-maximal activation, i.e. at different time during contraction.

The discovery of the thick (mainly myosin) and thin (actin, tropomyosin, and troponin complex) filaments and the sliding of the filaments [33, 36] led to better understanding of the contractile element and establishment of the sliding filament or cross-bridge theory [32, 35]. A number of kinetic models have been proposed that are based on the cross-bridge interactions between the thick and thin filaments [13, 25, 32]. Such models are often called cross-bridge models or biophysical models, because they describe the cross-bridge cycle with a finite number of states with rate-constants that determine the transitions between the different states. In the simplest case, the cross-bridge can be in one of two states, i.e. attached and detached. Often, the attached cross-bridge is divided into weak and strong conformations.

In a model of the mechanics of the cardiac muscle, Wong [75, 76] used a cross-bridge model as the contractile element in the three-component model structure. Panerai [55] used a similar approach, but included Ca^{2+}-troponin C (TnC) interaction and a plateau in the activation function. One problem with the original cross-bridge model is that the displacement (x) of the actin site relative to the equilibrium position of the myosin head is a variable in the model. Therefore, a description of the population of the displacement of all actin sites is needed for each time step to be able to simulate the developed force. Because of the interaction with the series elastic element, this leads to a large number of coupled equations [55]. To make the complex biophysical models simpler, several researchers have proposed constitutive equations (without the population of displacements), which are based on the cross-bridge theory, for skeletal [73, 77, 78] and for cardiac muscle [21, 74].

The major difference between skeletal and cardiac muscle function is the activation. The fact that the cardiac muscle works under sub-maximal activation has made it difficult to apply the same models on skeletal and cardiac muscles. Cardiac muscles undergo a contraction - relaxation sequence (twitch) in each heart cycle. Numerous attempts have been made to include the time-course of activation in the models [21, 55,

74, 75, 76]. The importance of the activation [16] in cardiac muscle twitches has resulted in a shift from models that are very focused on the cross-bridge kinetics towards so-called compartment models. Such models are used to describe the binding of calcium to TnC and the activation of the thin filament in addition to the cross-bridge kinetics [9, 31, 42, 57, 59]. Typical variables of the compartment models are concentrations of intracellular Ca^{2+}, bound Ca^{2+} to TnC, and different binding conformations of actin and myosin. Active force is then proportional to the relative concentration of cross-bridges in the strong conformation.

The importance of the activation on cardiac muscle performance and the importance of calcium on activation have also led to models that include the whole or parts of the excitation-contraction coupling, i.e. the sequence of processes that couples the excitation of the muscle cell from the action potential to the contractile machinery [42, 44]. The main processes are: 1) the calcium release through the cell membrane (sarcolemma), 2) subsequent release of calcium from the internal calcium storage (sarcoplasmic reticulum), 3) binding of calcium to calmodulin, two high-affinity sites and one low-affinity regulatory site on TnC, 4) calcium re-uptake to sarcoplasmic reticulum, and 5) calcium fluxes out of the sarcoplasm through the sarcolemma. This, however, includes a number of new parameters and little is known about the values of these parameters under varying loading conditions in the intact muscle.

It is well known that isometric tetanized stress is length dependent [20] with maximal stress at the length corresponding to maximal overlap between the thick and thin filaments. In cardiac muscles, the length dependence of isometric peak stress is more pronounced, and also dependent on the level of Ca^{2+} [14]. The latter has led to the concept of length-dependent activation which is reviewed by Allen and Kentish [3]. The relation between the Ca^{2+} level and force in skinned preparations is highly non-linear, and is dependent on the sarcomere length [39]. This length-dependent calcium sensitivity may be explained both as length-dependent properties of the cardiac TnC isoform [2, 22] or as change in the lateral distance between the thick and thin filament [19, 48]. A cooperative effect on activation by strong-binding cross-bridges may give additional length dependence of the calcium sensitivity [15, 28].

In addition to the already mentioned length-dependent activation, two more properties of the cardiac muscle are connected to the activation process and the inactivation process, i.e. the processes responsible for relaxation. These are the concept of shortening deactivation or cooperativity and the concept of load-dependent relaxation. The first concept is based on the observation that peak developed force in an isometric twitch exceeds peak force in a twitch that includes shortening to the length of the isometric twitch. This may be due to enhanced inactivation caused by shortening (shortening deactivation) [8, 12, 43] or enhanced activation caused by cross-bridges (cooperative effect) [6, 28, 37, 42, 59].

The second concept is related to relaxation, where the intracellular calcium transient is reduced towards its resting level. Brutsaert and Sys [8, 69] have introduced the concept of load-dependent relaxation. By using phase-plots of F (force) versus dF/dt, they found that isometric relaxation at a given length, but with different loading history and at different time from stimulus, was only dependent on the actual load. In a recent study, we have found that force is the main determinant of force decline also in auxotonic twitches with simultaneous changes in force and length [64].

The mathematical models of the cardiac function are based on observations in experiments on isolated muscles, muscle fibers, and single cells. In addition to special experimental settings like quick release, load clamps, sinusoidal perturbations, and calcium activation, the normal twitches range from isotonic (constant force) to isometric (constant length). Between these two extremes, afterloaded twitches (Figure 9, panel A) are isometric until the force reaches a given afterload. At this load, the muscle shortens and re-lengthens isotonically. Finally, the force declines isometrically. Furthermore, to mimic the ventricular pump, a twitch with physiological (isometric-isotonic) relaxation sequence has been used [8](Figure 10, panel A). All these twitches contain sequences of isometric and isotonic loading. In the intact heart, however, the loading of the muscle fiber is more complex. There are simultaneous and coupled changes in both stress and length in all phases of the cardiac cycle. This is caused by factors like stress development and decline, shortening and lengthening, torsion, changes in the ventricular shape and geometry, and non-uniformity in excitation and performance [7, 26, 70].

To be able to study the behavior of the cardiac muscle under a controlled condition of simultaneous changes in stress and length, we included a controlled auxotonic twitch in a recently developed PC-based measurement and control system for isolated papillary muscle experiments [66]. In the controlled auxotonic twitch, there are proportional changes in developed stress and shortening as if the muscle is acting against an ideal spring. The auxotonic twitches do not include discontinuities in length, velocity, force, or dF/dt. Such auxotonic twitches demonstrated a load-independent timing of contraction and a load-dependent timing of relaxation [64](Figure 6, panel A).

1.2 Purpose

Based on the features of the auxotonic twitches, the main goal of this project has been to develop a simple model structure of the cardiac muscle including: 1) separation of active and passive stress, 2) length-dependent activation, 3) a lumped model representing muscle activity including calcium-troponin kinetics, activation of the thin filament, and cross-bridge kinetics.

In this paper, we want to present the mathematical model. Furthermore, we want to present an evaluation of the ability of the model to reproduce auxotonic twitches from isotonic to isometric loading and also to simulate other conventional twitch types. We will investigate different approaches to separate activation and inactivation. Finally, we want to discuss the possibility of the model to reproduce specific experimental

observations in different twitch types and pros and cons of the different separation approaches.

The model development section begins with a presentation of some important experimental observations from cardiac muscle experiments that we want to include as features of the model. A presentation of what we believe is the main components of the complete cardiac muscle model will then follow before we present our model structure with the lumped model of activity. The simulation section contains simulations of auxotonic, isometric, afterloaded, and physiological twitches using the three model alternatives with different separation of activation and inactivation. The discussion section includes evaluation of the ability of the model to reproduce measured features.

2 Methods

2.1 Muscle Experiments

This paper includes some examples from isolated cardiac muscle experiments. All examples are from papillary muscles isolated from rabbit right ventricle. The experimental setup is described in Sørhus et al. [66]. The examples are taken from the set of experiments that are presented in Sørhus et al. [64] which also includes descriptions of the muscle preparation and the experiment protocol.

2.2 Abbreviations

ATP	adenosine triphosphate
ODE	ordinary differential equation
SR	sarcoplasmic reticulum
THC	time to half contraction
THR	time to half relaxation
TnC	troponin C
TPC	time to peak contraction

2.3 Nomenclature

$A(t)$	activity	
$A_{max}(t)$	maximal potential activity	
$A_c(t)$	activation	
$A_r(t)$	inactivation	
a	scaling parameter in passive stress-length relation	
a_0	isometric activation time constant	$[s^{-1}]$
a_1	isometric inactivation time constant	$[s^{-1}]$
b	shape parameter in passive stress-length relation	
$\alpha(\lambda)$	relative length of the single overlap region	
$Ca_i(t)$	intracellular Ca^{2+} concentration	$[\mu M]$
Ca_{i0}	resting level of intracellular Ca^{2+} concentration	$[\mu M]$
$Ca_{i,max}$	peak value of intracellular Ca^{2+} transient	$[\mu M]$
$Ca_{i,tr}$	threshold level of calcium sensitivity function	$[\mu M]$
$F(t)$	force	$[mN]$
$f(t,\dots)$	weight function of activation	
$g(t,\dots)$	weight function of inactivation	
$\gamma(\lambda)$	lateral distance between thick and thin filaments	
k_a	spring constant or auxotonic load	$[mN/mm]$
k_f	force-bearing fraction of the cross-bridge cycle	
$l(t)$	muscle length	$[mm]$
l_{max}	length with maximal isometric active stress	$[mm]$
$\lambda(t)$	relative length	$[mm/l_{max}]$
λ_{ref}	λ in reference configuration	$[mm/l_{max}]$
n	slope of calcium sensitivity function	
n_r	exponentiation of inactivation	
$\sigma(t)$	stress	$[mN/mm^2]$
$\sigma_t(t)$	total stress	$[mN/mm^2]$
$\sigma_a(t)$	active stress	$[mN/mm^2]$
$\sigma_p(\lambda)$	passive stress	$[mN/mm^2]$
σ_{max}	scaling parameter	
T_{int}	transition time interval	$[s]$
t_p	transition time between activation and inactivation	$[s]$
τ_{Cai}	time constant of intracellular Ca^{2+} transient	$[s^{-1}]$
$v_{max,c}$	scaling parameter of velocity dependence in activation function	$[s^{-1}]$
$v_{max,r}$	scaling parameter of velocity dependence in inactivation function	$[s^{-1}]$
$w_c(t)$	weight function	

3 Model Development

3.1 Cardiac Muscle Properties

In the following paragraphs, we will present some experimentally observed properties of the cardiac muscle that are important for the development of a model of cardiac muscle twitches.

3.1.1 Filament Overlap and Distance

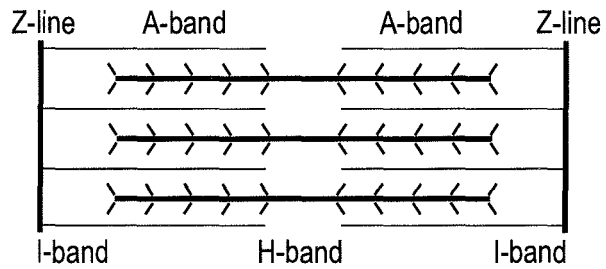

Figure 1: Schematic view of the organization of thick and thin filaments in the sarcomere.

The sarcomere geometry may influence the active stress development in two different ways. First, the thick and thin filaments are organized so that they form regions with different overlap in the sarcomere length direction. One end of the $1\mu m$ long thin filaments are originated at the z-lines (the end surface of the sarcomere) (Figure 1). The 1.6–1.7 μm long thick filaments are centered in the sarcomere length direction. When the sarcomere is longer than the thick filament, there is a region near the z-line with only thin filaments, which is called the I-band. When the sarcomere is longer than 2 μm, there is a region in the center of the sarcomere with only thick filaments, which is called the H-band. The I-band and the H-band may together be called the non-overlap region. When the sarcomere is shorter than 2 μm, there is a region in the center of the sarcomere with both thick filaments and thin filaments from both directions, which may be called the double overlap region. The region with both thick and thin filaments is called the A-band. The region with thick filaments and thin filaments from only one direction may be called the single overlap region. Although there may be cross-bridges in the double-overlap region, only cross-bridges in the single overlap region are assumed to contribute to the net force generation [42]. Therefore, the active stress will not only be dependent on the density of cross-bridges, but also on the length of the single overlap region.

Second, the volume of the sarcomere is considered constant also during active shortening [50]. Therefore, the lateral distance between the thick and thin filaments will

change proportionally with the change in length. This may have several implications on the active stress development. The probability of cross-bridge attachment, the rate of cross-bridge detachment, the unitary force, and the step size may all be altered with changed filament distance. The individual factors will be described below. Together with a cooperative effect, this may be responsible for the length-dependent calcium sensitivity of force generation [15, 19, 48].

3.1.2 Passive Stress-Length Relation

Figure 2, panel A gives an example of the passive stress-length relation. It is not possible to measure negative force (restoring force) with our experimental setup (the muscle is mounted vertically), therefore the relation is only valid for lengths longer than slack length, i.e. the length of the muscle when no force is applied, $\approx 0.85 \cdot l_{max}$, where l_{max} is the muscle length with maximal isometric active stress. The passive properties of intact myocardium, isolated cardiac muscle, and single myocytes have been extensively studied [23, 31, 51, 54, 58, 61]. A network of connective tissue (mainly collagen) surrounding the muscle fibers, proteins in the sarcomeres (e.g. titin), and other contents of the myocardial cell (e.g. cell membrane, t-tubules, and mitochondria) are assumed to be responsible for the measured passive properties. The passive properties are non-linear and visco-elastic [58], but often modeled as non-linear elastic. The passive stress increases exponentially when the muscle is stretched above slack length [51].

The slope of the passive stress-length relation just above slack length continues at shorter lengths (below slack length), but there are uncertainties about the slope at shorter sarcomere lengths than the length of the thick filament. This is because the thick filament may buckle at rest, but not in an actively shortening muscle [23]. One may expect a very steep increase in the restoring force at shorter lengths than the length of the thick filament [31, 68]. In the intact heart the restoring forces that are developed during contraction are believed to enhance the filling of the ventricle in early diastole. This is called suction or elastic recoil [45, 61].

3.1.3 Length-Dependent Activation

One important factor in muscle modeling is the relation between length and developed stress. Gordon et al. [20] presented a length-tension diagram based on experiments on tetanized skeletal muscle. Their length-tension diagram has been connected to the geometry of the sarcomere. They found that maximal tension was developed at sarcomere lengths between 2 and 2.2 μm which corresponds to the maximal overlap of the thick and thin filaments. This sarcomere length has therefore been related to l_{max} on the muscle level, assuming that the average sarcomere has maximal overlap.

Figure 2, panel A shows an example of passive, active and total stress-length relations obtained from isometric twitches at different lengths in an isolated papillary muscle. The single overlap region between the thick and thin filaments is reduced at lengths below l_{max}. Due to a simple sliding of the thin filament, yielding a double over-

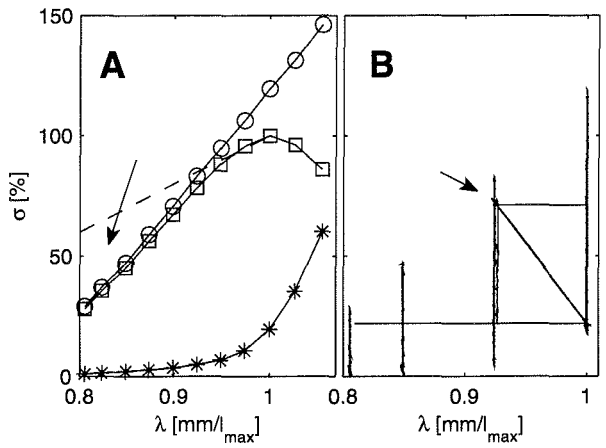

Figure 2: *Panel A*: Passive (stars), peak active (squares), and peak total (circles) stress versus relative isometric length. Dashed line show relative reduction of single overlap region versus muscle length. *Panel B*: Total stress of four isometric twitches at different length together with one preloaded isotonic, one physiological, and one auxotonic twitch from the same muscle versus relative length.

lap region where the net generated force is zero [42], a 10% reduction in length gives 20% reduction of the single overlap region. This relation is included as a dashed line in Figure 2, panel A. From the figure, we can see (arrow) that the relative reduction in peak stress is more than what is expected from the reduction in the single overlap region.

The ascending part of the stress-length relation of cardiac muscle is known to be steeper than that of skeletal muscle [14]. In addition, the slope is dependent on the level of intracellular Ca^{2+} [3, 41, 72]. The relation between available calcium and force has been studied in skinned cardiac muscles, resulting in a s-shaped $F - pCa$ relation ($pCa = -log_{10}Ca^{2+}$). Kentish et al. [39] found this relation at different sarcomere lengths (their Figure 7) and demonstrated that both the level of maximally activated force and the slope of the relation depend on sarcomere length.

The basic explanation of the length-dependent calcium sensitivity has been under debate [3]. Some investigators have found that TnC has length-dependent affinity of calcium [2, 22]. They have replaced skeletal with cardiac TnC and vice versa and found that the length dependence of calcium sensitivity is reduced with skeletal TnC. Other investigators have tried to do similar experiments, but failed to show the same difference [47, 53]. As an alternative explanation the distance between the thick and thin filament is proposed to give the length-dependent calcium sensitivity [19, 48]. The sarcomere volume is considered constant [50], and therefore the filament distance

will increase at shorter lengths. Fitzsimons and Moss [15], however, proposed that the cooperative effect (see below) of an increased number of strong-binding cross-bridges at longer lengths is an additional explanation of the length-dependent calcium sensitivity.

3.1.4 Shortening Deactivation/Cooperativity

Panel B in Figure 2 demonstrates one additional effect on the stress-length relation. The arrow shows that twitches that shorten to the length of an isometric twitch do not reach the peak stress in the isometric twitch. This seems to be true both in afterloaded and physiological twitches where we have separated phases of stress development and shortening (isometric-isotonic), and in auxotonic twitches where we have simultaneous changes in stress and length (auxotonic). Notice that, according to the length-dependent activation described above, the isometric twitch has initially lower activation than the two other because they start at a longer length (length-dependent activation). This implies that the activation in cardiac muscle depends on the loading history. This phenomenon is known as shortening deactivation or cooperativity [6, 8, 30, 42, 43, 59]. The concept of cooperativity is based on the observations that a cross-bridge in the strong conformation has a positive effect on the activation of neighboring actin sites and on the affinity of TnC for Ca^{2+} [6]. Therefore, in an isometric twitch, the higher force further increases the recruitment of new cross-bridges.

3.1.5 Load-Dependent Activation

When analyzing the properties of cardiac muscle twitches, the relation between loading conditions and timing is important. The duration of isometric twitches is much longer than the duration of the isotonic twitches [8]. However, the difference is mainly related to differences in the duration of relaxation. It is also found that time to peak contraction (TPC) in afterloaded twitches are prolonged at increasing afterload. We have found that TPC was constant in auxotonic twitches with different auxotonic load [64]. The little variation in TPC despite large variations in load demonstrates the load dependence of activation. It is not known what are the underlying mechanisms for the difference between TPC in afterloaded and auxotonic twitches. Both kinds of twitches start at the same initial values and have similar peak shortening – peak developed stress relations. The difference in timing must therefore be related to the differences in the loading history. One possible mechanism for the prolonged TPC in afterloaded twitches is the influence of length changes on the intracellular calcium transient, which is described below. But there are no similar measurements of intracellular calcium from auxotonic twitches and, therefore, we cannot conclude that this is the reason for the difference between afterloaded and auxotonic twitches.

3.1.6 Load-Dependent Inactivation

Inactivation can be defined as the integrative effect of all processes that are bringing the muscle back to the resting state after it has been activated by the excitation-contraction coupling. The concept of load-dependent relaxation is reviewed by Brutsaert and Sys [8]. The fact that TPC in differently loaded contractions varies much less than the duration of relaxation implies that the load dependence of relaxation is different from the load dependence of contraction. Sys and Brutsaert [69] found that during isometric relaxation at a given length the rate of force decline (dF/dt) was only dependent on the force and independent on the time from stimulus. The $dF/dt - F$ relation was slightly altered at different lengths. We also found that in auxotonic twitches with different auxotonic load the force decline in the last half of relaxation was force dependent [64].

Both the isovolumetric pressure decline in the intact heart and the isometric force decline in the isolated muscle have been modeled as a mono-exponential fall [42, 46, 57]. It has been demonstrated, however, both at the ventricular and muscular level that the pressure or force decline are not mono-exponential, but rather s-shaped [5, 46, 52, 69]. Therefore, to be able to obtain realistic force decline in isometric twitches, this property of inactivation must be included in the model.

3.2 Underlying Processes of Muscle Activity

The cardiac muscle properties described above are results of a number of underlying mechanisms. Based on hypotheses and observations from isolated experiments, a general understanding of the underlying processes responsible for the activity in the cardiac muscle has been established. But still there are discrepancies and questions about the extrapolation of the results from low-level experiments (e.g. assays on isolated proteins). In the following, we will describe briefly three major underlying processes; the intracellular Ca^{2+} transient, the Ca^{2+}-TnC kinetics, and the cross-bridge kinetics.

3.2.1 Intracellular Ca^{2+} Transient

It is well established that the contractile machinery is controlled by Ca^{2+} which has to bind to TnC in order to remove the inhibitory effect of tropomyosin on the actin-myosin interaction. How much Ca^{2+} that is bound to TnC is therefore an important determinant of the potential of cross-bridge binding. It is not possible to measure the level of bound Ca^{2+} to TnC in the intact muscle. What is possible to measure, however, is the level of free Ca^{2+} in the sarcoplasm [4, 71]. The resulting time trace of free Ca^{2+} is known as the intracellular Ca^{2+} transient. This transient represents the residual of the summation of Ca^{2+}-fluxes into the sarcoplasm through calcium channels in the cell membrane and from internal Ca^{2+}-stores (sarcoplasmic reticulum), Ca^{2+}-fluxes out of the sarcoplasm through pumps and exchangers, and binding and unbinding of Ca^{2+} to intracellular proteins like calmodulin and TnC.

The intracellular Ca^{2+} transient has been studied under different loading conditions [4, 30, 40]. Both Housmans et al. [30] and Lab et al. [40] found that although an isotonic twitch is shorter than an isometric twitch, the calcium transient is prolonged in the isotonic twitch. Both groups argue that different unbinding rates from TnC under isotonic and isometric conditions is the most likely reason for the differences in the intracellular Ca^{2+} transient. An increased release of calcium from TnC will increase the level of free calcium as well. Housmans et al. [30] demonstrated how this prolonged calcium transient during shortening is consistent with the concept of cooperativity. If force-bearing cross-bridges either increase the affinity of TnC for calcium or keep the calcium bound to TnC and if the number of force-bearing cross-bridges is inversely proportional to the speed of shortening, then the concepts of shortening deactivation and cooperativity may result from the same underlying mechanism.

3.2.2 Ca^{2+}-TnC Kinetics

Very little is known about the effects of length, velocity, and stress on the binding and unbinding of Ca^{2+} to TnC in the intact cardiac muscle. However, because of the regulatory effect of calcium on contraction, these effects are important if we want to model the muscle function from the level of Ca^{2+}-TnC kinetics. This is done in so-called compartment models [42, 57]. In such models, the binding and unbinding rates are taken from steady-state Ca^{2+}-binding data [60] and modified to achieve cooperative effects, e.g. as decreased off-rate at increasing number of cross-bridges in the strong conformation.

Hunter et al. [31] included a cooperative effect similar to Landesberg and Sideman [42] in the equation for binding of Ca^{2+} to TnC. In both cases, stress (or number of cross-bridges) modified the dissociation rate. In Hunter et al. [31] and Peterson et al. [57] the bound Ca^{2+} diminished well before the stress trace. This difference is explained by the hypothesis that cross-bridges can be responsible for activation of the thin filament [28] and in this way obtain activation with less bound calcium.

3.2.3 Cross-Bridge Kinetics

When Ca^{2+} binds to TnC, troponin I dissociates from actin. This leads to a structural movement of tropomyosin away from a position where it blocks actin-myosin interaction, which represents the activation of the actin sites. There are indices that cross-bridges in the strong conformation are able to keep the thin filament in this activated state also after Ca^{2+} has unbound from TnC [6, 28].

Cross-bridge kinetics have been studied in different settings. In a fully activated muscle (tetanized), perturbations in length as quick releases and quick stretches, load clamps, and oscillations in length or load are assumed to give explicit information about the cross-bridge dynamics [31]. The problem, however, is that in such experiments the activation of the thin filament is constant, which is not the case in normal cardiac muscle twitches where the activation of the thin filament is changing. Another

problem, e.g. in quick release experiments, is that cooperative effects may result in special shortening conditions that neither represent cross-bridge interaction nor represent unloaded shortening velocity. The well-known force-velocity relation and its representation in the Hill equation [24] has evolved from such studies. Quick release experiments give a hyperbolic relation between force and velocity. Hunter et al. [31] included a "fading memory" of velocity in their model of cross-bridge kinetics. This was done to represent the force recovery after the initial drop in force after a length step [34].

Another rather new approach to study cross-bridge kinetics is based on experiments on single or a few actin and myosin molecules [see 67, for review]. In such experiments, it has been possible to measure the step size related to the hydrolysis of one ATP molecule and the force generated by one myosin molecule, called the unitary force. The force is generated in a pulse-like fashion with a force generating state only as a fraction of the ATPase cycle time. The force-velocity relation at this level was found to be hyperbolic, but the curvature changed direction in the middle range of the load. Sugiura [67] proposed that the ratio between the time interval that actin and myosin is attached and the ATP hydrolysis cycle time (duty ratio) increases with increasing load. An alternative explanation is that more than one cross-bridge cycle can take place during one ATP hydrolysis cycle at low loads (loose coupling concept).

3.3 The Complete Muscle Model

The complete model of the cardiac muscle should include all the observed details about excitation, intracellular calcium transient [4, 10, 30, 40, 44], the role of sarcoplasmic reticulum [62], effect of length [4, 30, 40], velocity, and force [27, 28] on calcium binding kinetics [57, 60], activation of the thin filament [29, 59], actin-myosin interaction [13, 32, 35, 67], and passive properties [23, 51]. Shortening deactivation or cooperativity should also be incorporated [12, 28, 43, 59].

Such a complete model would include a large number of model parameters and state variables. Many of these model parameters can only be extracted from chemical determinations in vitro or assays on isolated proteins, e.g. calcium binding rates and single actin-myosin interactions. In intact muscles, the only variables that we are able to measure directly are length and force. Free Ca^{2+} can be measured indirectly by different markers [4, 71]. But variables like bound Ca^{2+} to TnC, number of activated actin sites, number of cross-bridges in different states, and force per cross-bridge cannot be measured directly in the intact muscle. The knowledge of these variables under varying loading conditions is limited.

3.4 A Lumped Model of Activity

Our goal has been to develop a model with minimal complexity that can reproduce length and stress traces under different loading conditions. According to the many open questions about the kinetics of the underlying processes under different loading

conditions, we wanted to incorporate the calcium binding kinetics, the activation of the thin filament, and the cross-bridge kinetics in one variable, called activity. The activity variable will depend on length and load according to the above descriptions of the cardiac muscle properties.

Special attention has been directed towards the following aspects of the model; 1) timing of auxotonic twitches, 2) separation between activation and inactivation, 3) load-dependent activation and inactivation.

Based on the descriptions of cardiac muscle properties and our definition of the activity variable, the model assumptions can be summarized as follows:

- total stress is a summation of active stress and passive stress
- the passive stress-length relation is non-linear elastic
- a cross-bridge is force-bearing a fraction k_f of the cross-bridge cycle; k_f is dependent on the sliding velocity, and is one at zero velocity (isometric)
- the average force from one cross-bridge cycle is the unitary force times k_f
- active stress is given by 1) the relative length of the single overlap region, 2) the sum of the average force from each active cross-bridge cycle, and 3) a scaling parameter
- the cross-bridges in the double overlap region do not contribute to the active stress
- the volume of the sarcomere is constant, consequently the filament spacing depends on the sarcomere length

3.4.1 Total Stress

The total stress in this model is defined as the sum of active stress (σ_a) and passive stress (σ_p):

$$\sigma_t = \sigma_a + \sigma_p(\lambda) \tag{1}$$

where $\lambda = l/l_{max}$, l is length, and l_{max} is the length with maximal isometric active stress.

3.4.2 Passive Stress

The passive stress-length relation is taken from Sys [68] and incorporates both the exponential increase in stress at lengths above l_{max} and the restoring force which increases at decreasing lengths.

$$\sigma_p(\lambda) = a \cdot \frac{tan(b \cdot (\lambda - 0.85))}{tan(b \cdot (1 - 0.85))} \tag{2}$$

Simulated passive stress-length relations with different parameter values are presented in Figure 3.

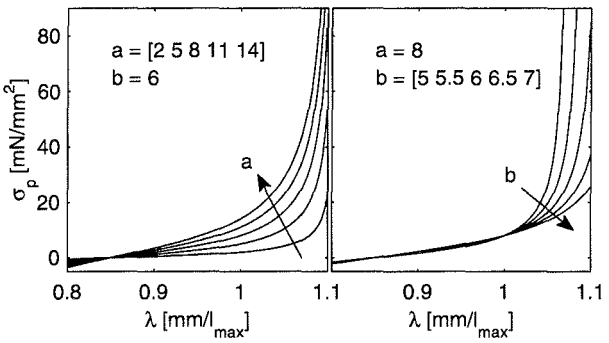

Figure 3: Passive stress-length relations from Eq. 2 with different values of parameters a (left panel) and b (right panel). Arrows represent increasing parameter values.

3.4.3 Active Stress

Active stress is modeled as:

$$\sigma_a = \sigma_{max} \cdot A \cdot \alpha(\lambda) \tag{3}$$

$$\alpha(\lambda) = 1 - 2|\lambda - 1| \tag{4}$$

where σ_{max} is a scaling parameter, A is activity (see below), and $\alpha(\lambda)$ represents the length of the single overlap region relative to l_{max}. From Eq. 3 we have that the time derivative of instantaneous active stress must be:

$$\frac{d\sigma_a}{dt} = \sigma_{max}\left[\frac{dA}{dt} \cdot \alpha(\lambda) + A \cdot \frac{d\alpha(\lambda)}{d\lambda} \cdot \frac{d\lambda}{dt}\right] \tag{5}$$

Depending on the loading condition, the time derivative of instantaneous active stress can also be found as

$$\begin{aligned} \sigma_t &= \sigma_a + \sigma_p(\lambda) = k_a(1-\lambda) + \sigma_p(\lambda_{ref}) \\ \frac{d\sigma_a}{dt} &= -k_a \cdot \frac{d\lambda}{dt} - \frac{d\sigma_p(\lambda)}{d\lambda} \cdot \frac{d\lambda}{dt} \end{aligned} \tag{6}$$

where k_a represents the auxotonic load and λ_{ref} is the reference length, resulting in the following expression of velocity in isotonic ($k_a = 0$), auxotonic ($k_a = < 0, \infty >$), and isometric ($k_a \to \infty$) loading conditions:

$$\frac{d\lambda}{dt} = -\frac{\sigma_{max} \cdot \dot{A} \cdot \alpha(\lambda)}{\sigma_{max} \cdot A \cdot \alpha'(\lambda) + \sigma_p'(\lambda) + k_a} \tag{7}$$

Figure 4 demonstrates a typical pattern of instantaneous active stress. During contraction, the active stress development was very dependent on loading conditions. But as we have seen previously for all different twitches, the sum of normalized stress and shortening was almost identical at different loads [65]. During relaxation, the slope of the active stress decline was very similar under isometric and auxotonic loading conditions. Because the length is changing only in the auxotonic twitches, this means that the first term on the right hand side of Eq. 5 must be reduced when the last term increases due to increased lengthening velocity.

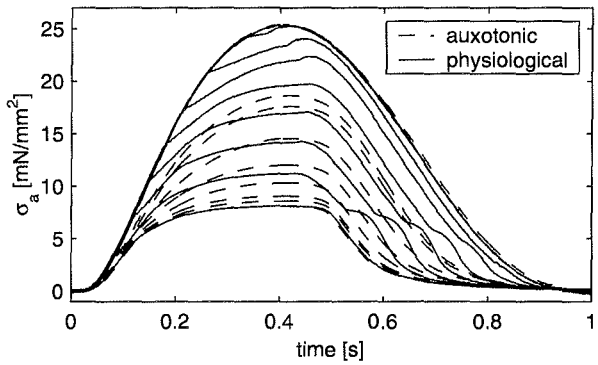

Figure 4: Instantaneous active stress in physiological (solid) and auxotonic (dashed) twitches. Instantaneous active stress is calculated from total stress and passive stress-length relations.

3.4.4 Activity

Activity (A) is defined as the length density of cycling cross-bridges times the average unitary force [67] times the average fraction of the cross-bridge cycle that the cross-bridge is in the force generating conformation. As described above, this activity incorporates at least three dynamic processes; the Ca^{2+}-TnC kinetics, activation of the thin filament, and cross-bridge kinetics. The reason we wanted to incorporate all these processes in one activity variable, is that the dynamics of the individual processes were difficult to separate from the length and stress dynamics of the muscle twitch.

The average number of force-bearing cross-bridges depends on the number of cycling cross-bridges, i.e. active actin-sites and myosin heads in all phases of the cross-bridge cycle, and the shortening and lengthening velocity. For fully activated (tetanized) muscle this is described by the Hill equation. In cardiac muscle twitches, it is difficult to separate activation of the thin filament and cross-bridge kinetics because the muscle is operating in a non-steady state. The activation of the thin filament is again related to the Ca^{2+}-TnC kinetics.

3.4.5 Transition between Activation and Inactivation

In order to satisfy two observations from auxotonic and afterloaded twitches, we decided to separate the model of activity into two models of activation and inactivation. The two observations are related to the load dependence of activation and inactivation.

First, we have observed that TPC in auxotonic twitches varied very little at different auxotonic load. The difference between TPC in isotonic and isometric twitches was also small. In afterloaded twitches, however, TPC was prolonged at mid-range afterloads, i.e. 20-80% of isometric peak stress (Figure 9, panel A). As already noticed, the intracellular calcium transient was also altered in the afterloaded twitches. This means that the loading conditions have major impact on the stress development versus shortening, but little influence on the duration of the contraction phase.

The second observation is that the load dependence of relaxation was different from the load dependence of contraction. The duration of relaxation (THR-TPC) in auxotonic twitches was highly correlated with peak stress which again was dependent on the auxotonic load (Figure 6, panel A). From the first observation we know that the duration of contraction (TPC) was independent of the auxotonic load.

Based on these two observations, it is clear that the activation and inactivation models must be separated to make it possible to simulate auxotonic twitches with a wide range of loads with almost no range in TPC. With this model structure we have modeled the integrative effect of all the underlying processes. The general equations for the activity are given by:

$$\gamma(\lambda) = 0.5(1-\lambda)+1 \tag{8}$$

$$A_{max} = \alpha(\lambda) - \int_0^t |\dot{\lambda}(\tau)| d\tau \tag{9}$$

$$\frac{dA_c}{dt} = \left[a_0 \cdot \gamma(\lambda) - \frac{|\dot{\lambda}|}{v_{max,c}} \right] \cdot (A_{max} - A) \tag{10}$$

$$\frac{dA_r}{dt} = -\left[a_1 \cdot \gamma(\lambda) + \frac{|\dot{\lambda}|}{v_{max,r}} \right] \cdot A^{n_r} \tag{11}$$

$$\frac{dA}{dt} = f \cdot \frac{dA_c}{dt} + g \cdot \frac{dA_r}{dt} \tag{12}$$

where γ represents the influence of the filament spacing. A_{max} is the maximal potential activity, and incorporates the concepts of length-dependent activation and shortening deactivation/cooperativity. f and g are the weight functions of activation and inactivation, respectively. a_0 and a_1 are the time constants of isometric stress development and decline at l_{max}. $v_{max,c}$ and $v_{max,r}$ are scaling parameters for the velocity dependence of the activation and inactivation functions.

We used A^{n_r} in the inactivation model (Eq. 11) to obtain a more realistic isometric force decline than a pure mono-exponential decline. $n_r < 1$ enhances inactivation when activity is low.

In this study, we have included three different approaches to separate the activation and inactivation models, yielding different f and g functions:

Model 1: Activation Weighted with Intracellular Ca^{2+} Transient

Activation is weighted with an intracellular calcium transient in the first approach. In contrast to the calcium bound to TnC, the intracellular calcium transient has been measured so that a normal pattern can be assumed. The problem with most expressions representing this transient is that they have an exponential decay which means that the activation may contribute too much during early relaxation and too little during late contraction. This way they may not separate the contraction and relaxation phases sharply enough. This may be solved by a s-shaped relation between the level of intracellular calcium and the weight of activation (Figure 5).

The observed intracellular Ca^{2+} transient is the residual Ca^{2+} after influx from extra-cellular space and sarcoplasmic reticulum (SR) through Ca^{2+} channels, efflux to extra-cellular space through Na-Ca^{2+} exchanger, efflux to SR through Ca^{2+} pumps, and binding to calmodulin and TnC (high and low affinity sites). Because this involves many different processes with a large number of unknown parameters (especially under non-isometric conditions) [56], we modeled the intracellular Ca^{2+} transient as a simple function of time. We chose the same function as Hunter et al. [31].

$$Ca_i = Ca_{i0} + (Ca_{i,max} - Ca_{i0}) \frac{t}{\tau_{Cai}} e^{1-\frac{t}{\tau_{Cai}}} \tag{13}$$

where Ca_{i0} and $Ca_{i,max}$ are the resting level and peak value of the intracellular Ca^{2+} concentration, respectively. τ_{Cai} is the time constant of the intracellular Ca^{2+} transient.

In addition to the general equations (Eq. 1 - 12) and the intracellular calcium transient (Eq. 13), the following f and g functions were used for the simulation of model 1:

$$\begin{aligned} f &= 1 - \frac{1}{1 + (\frac{Ca_i}{Ca_{i,tr}})^n} \\ g &= 1 \end{aligned} \tag{14}$$

where $Ca_{i,tr}$ and n are the threshold level and the slope of the calcium sensitivity function, respectively. The s-shaped relation between f and Ca_i with different parameter values is presented in Figure 5.

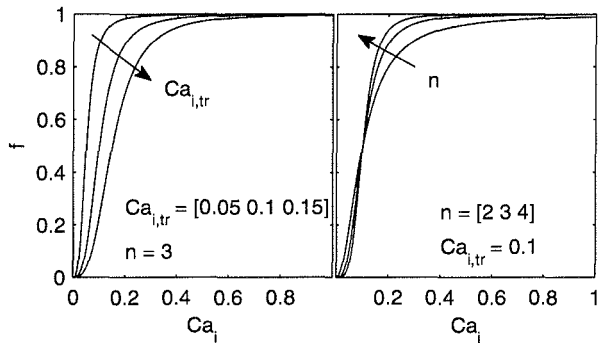

Figure 5: The relation between the weight function of activation and the level of intracellular Ca^{2+} from Eq. 14 with different values of parameters $Ca_{i,tr}$ (left panel) and n (right panel). Arrows represent increasing parameter values.

Model 2: Transition Defined by Maximal Potential Activity

In the second approach, we divided the twitch into three phases; one contraction phase and one relaxation phase separated by a transition phase. In the contraction phase, the activity is given by the activation model. In the relaxation phase, the activity is given by the inactivation model. The transition phase yields a smooth transition from activation to inactivation. The transition phase starts when the difference between the level of activity and the maximal potential activity (A_{max}) approaches zero.

For the simulation of model 2 we used the general equations (Eq. 1 - 12). The simulation scheme included a transition from contraction, where $f = 1$ and $g = 0$ yields $\dot{A} = \dot{A}_c$, to relaxation, where $f = 0$ and $g = 1$ yields $\dot{A} = \dot{A}_r$. The onset of transition was determined by the relative difference between A_{max} and A. During the transition interval (here: $100ms$) the activation and inactivation functions were weighted symmetrically.

Model 3: Activation and Inactivation as Two Weighted Local Models

In the third approach, two local models of activation and inactivation are weighted with symmetric sine-functions in a region around a specific transition time, i.e. when activation and inactivation are equally weighted. The transition time (t_p) and the transition interval (T_{int}) are then the only timing parameters in the model.

For simulation of model 3 we used the general equations (Eq. 1 - 12). Activation $\dot{A}_c$ and inactivation $\dot{A}_r$ were weighted (Eq. 12) with the following weight function:

$$
\begin{aligned}
w_c &= \begin{cases} 1 & , \quad t < t_p - 0.5 \cdot T_{int} \\ 0.5 \cdot (1 - sin(\pi \cdot \frac{t - t_p}{T_{int}})) & , \quad t_p - 0.5 \cdot T_{int} \leq t \leq t_p + 0.5 \cdot T_{int} \\ 0 & , \quad t > t_p + 0.5 \cdot T_{int} \end{cases} \\
f &= w_c \\
g &= 1 - w_c
\end{aligned}
$$

where t_p and T_{int} are the transition time and the transition interval, respectively.

Table 1: Parameter values for model 1 simulations

Parameter	Value
Ca_{i0}	0
$Ca_{i,max}$	1 μM
τ_{Cai}	0.06 s^{-1}
$Ca_{i,tr}$	0.1 μM
n	3
a_0	4
$v_{max,c}$	0.7 s^{-1}
a_1	2
$v_{max,r}$	0.5 s^{-1}
n_r	0.5
σ_{max}	80 mN/mm^2
a	8
b	6
k_a	[0 50 100 200 500 1000 ∞]

4 Simulations

In this section, we will present simulations by using the three models representing the three different approaches to separate activation and inactivation. First, for comparison, we will present an example of measured auxotonic, isometric, afterloaded, and physiological twitches from isolated papillary muscles. Second, we will present model simulations of auxotonic, isometric, afterloaded, and physiological twitches with each of the three models. Finally, because the three models in their simplest form fail to represent all details in the measured twitches, we will present a few possible model extensions in order to incorporate these effects.

Table 2: Parameter values for model 2 simulations

Parameter	Value
a_0	10
$v_{max,c}$	0.12 s^{-1}
a_1	3
$v_{max,r}$	0.4 s^{-1}
n_r	0.5
σ_{max}	50 mN/mm^2
a	8
b	6
k_a	[0 20 50 100 200 500 1000 ∞]

Table 3: Parameter values for model 3 simulations

Parameter	Value
t_p	0.3 s
T_{int}	0.3 s
a_0	4
$v_{max,c}$	0.3 s^{-1}
a_1	2.5
$v_{max,r}$	0.5 s^{-1}
n_r	0.5
σ_{max}	80 mN/mm^2
a	8
b	6
k_a	[0 50 100 200 500 1000 ∞]

4.1 Examples of Measured Twitches

A series of measured auxotonic twitches from isotonic to isometric is presented in Figure 6, panel A. In addition to total stress and relative length, normalized developed stress is also plotted in the lower panel to demonstrate some of the special features of the auxotonic twitch. TPC was almost constant in all twitches, and so was the contraction trajectory of the normalized developed stress. The relative rate of relaxation, however, decreased with increasing auxotonic load from isotonic to isometric. The series of normalized developed stress demonstrated the difference in load dependence between contraction and relaxation.

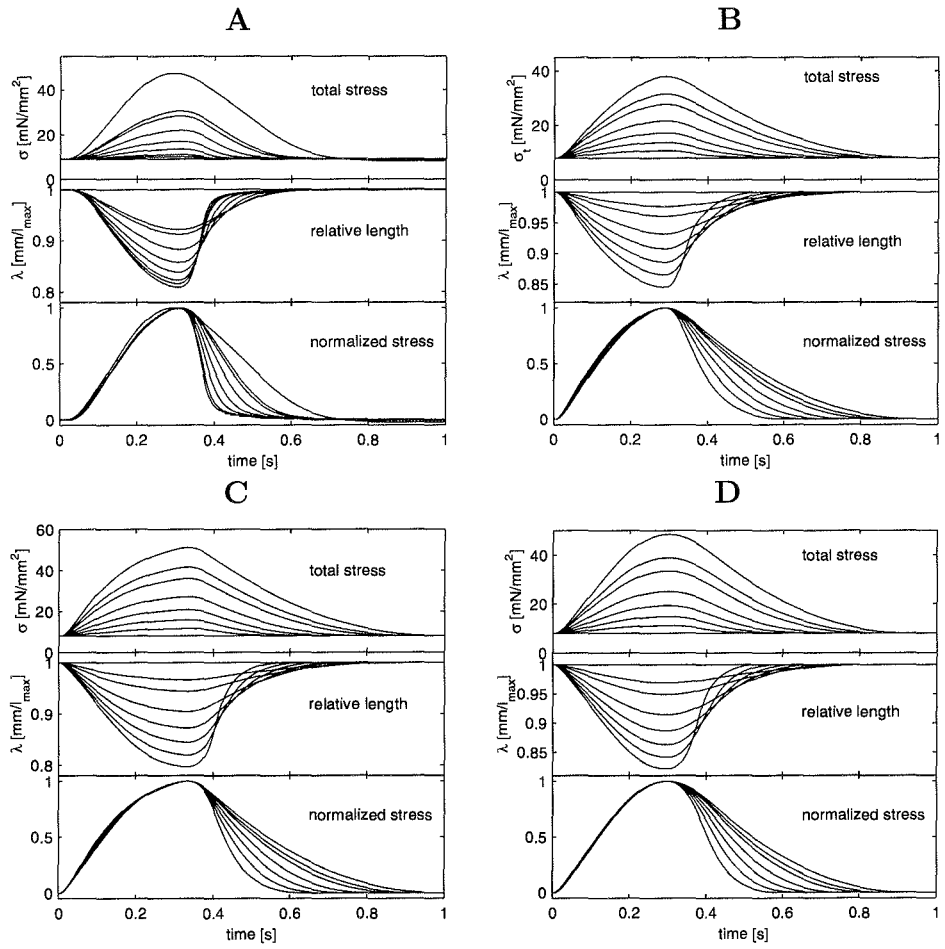

Figure 6: *Panel A*: Measured auxotonic twitches with increasing auxotonic load from experiment on isolated papillary muscle. Total stress (upper), relative length (middle), and normalized developed stress (lower). The other panels show simulations of similar series of auxotonic twitches from model 1 (B), model 2 (C), and model 3 (D).

Figure 8, panel A shows a series of isometric twitches at increasing length from $\lambda = 0.8$ to $\lambda = 1.05$. Both TPC and THR minus TPC increased at increasing length up to l_{max} ($\lambda = 1$).

Afterloaded twitches with conventional (isotonic-isometric) and physiological (isometric-isotonic) relaxation sequences are plotted in Figure 9, panel A and Figure 10, panel A, respectively. Both twitch types had similar isometric-isotonic contractions, and therefore similar prolongation of TPC at increasing afterload up to a given afterload. A special feature of the afterloaded twitches was the very fast initial stress decline after the switch from isotonic to isometric relaxation (Figure 9, panel A). Notice the parallelism of the isometric stress decline and isotonic lengthening in the physiological twitches (Figure 10, panel A).

4.2 Simulation of Auxotonic Twitches

Figure 6, panel B demonstrates stress (upper panel) and relative length (middle panel) in auxotonic twitches at increasing auxotonic load from isotonic to isometric, simulated with model 1. We calculated normalized developed stress which is presented in the lower panel. The parameters used in the simulations of all twitch types with model 1 are given in Table 1. The simulated auxotonic twitches demonstrated qualitatively similar patters as the measured auxotonic twitches (Figure 6, panel A). TPC was almost constant at different auxotonic loads. The normalized developed stress demonstrated the typical difference between contraction and relaxation. The model simulations had a slower late relaxation phase than the presented example of measured auxotonic twitches (panel A).

Figure 6, panel C demonstrates similar simulations of auxotonic twitches with model 2. The parameters used in the simulations of all twitch types with model 2 are given in Table 2. The simulations with model 2 were qualitatively similar to those with model 1 (panel B), although the shape of the time traces were slightly different in the two models.

A series of auxotonic twitches simulated with model 3 with the parameters given in Table 3 is presented in Figure 6, panel D. Because of the weight function, model 3 has a smoother transition between contraction and relaxation than the other model approaches. Therefore, the auxotonic twitch simulations were smoother than the two previous models. As for the previous models, the normalized developed stress (lower panel) demonstrated the same features as the measured auxotonic twitches (Figure 6, panel A).

The different separation approaches gave different activity A in the three models. This is demonstrated for isotonic, auxotonic ($k_a = 200\ mN/mm$), and isometric twitches in Figure 7.

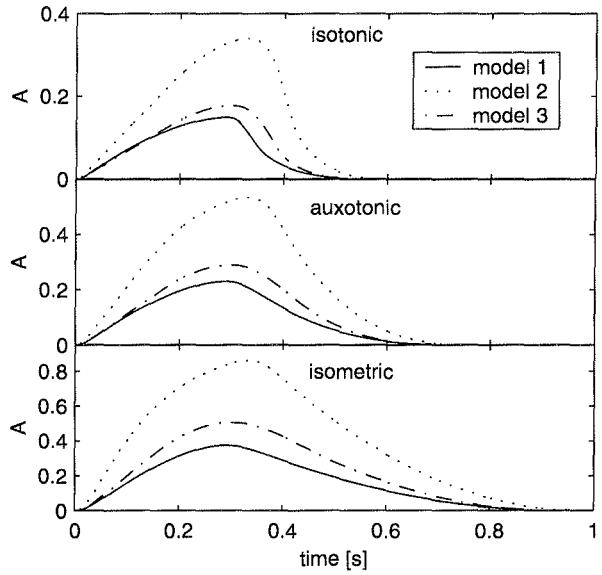

Figure 7: Activity A in corresponding twitches from model 1, model 2, and model 3. Isotonic twitches in the upper panel, auxotonic twitches with $k_a = 200$ mN/mm in the middle panel, and isometric twitches in the lower panel. Notice that the scaling of the y-axis is different in the different panels.

4.3 Simulation of Isometric Twitches

Figure 8, panel B demonstrates model 1 simulations of stress (upper panel) in isometric twitches at increasing lengths (see arrow), equally distributed between $\lambda = 0.8$ and $\lambda = 1.05$. Normalized developed stress is presented in the lower panel. The relative peak values of active stress at different lengths were in accordance with measured values (Figure 2 versus Figure 11), but the measured isometric twitches had larger variations in TPC and THR.

Figure 8, panel C demonstrates similar simulations with model 2. The relative peak values of active stress were, like for model 1, in accordance with measured values. Although, still less than in measured isometric twitches, the differences in TPC and THR were larger with this model approach than in model 1. This follows from the differences in separation between activation and inactivation in the two models.

Although, a little smoother, the isometric twitches at increasing length simulated with model 3 (Figure 8, panel D) were very similar to the isometric twitches from model 1 (panel B). Especially model 1 and model 3, both with separation between activation and inactivation given as a function of time, showed little variation in TPC.

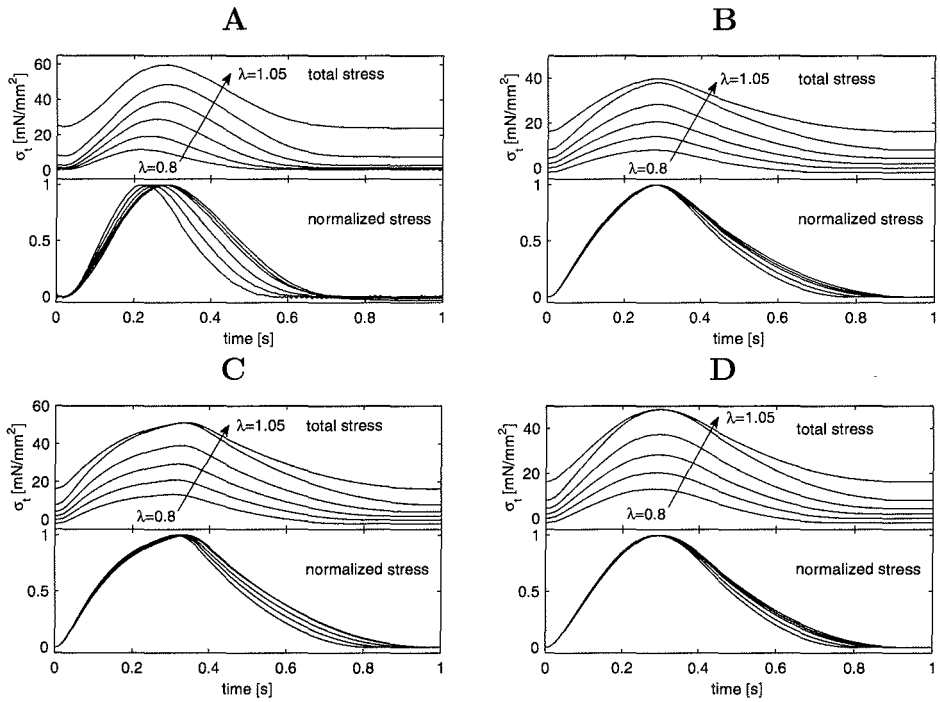

Figure 8: *Panel A*: Measured isometric twitches with increasing length from experiment on isolated papillary muscle. Total stress (upper) and normalized developed stress (lower). The other panels show simulations of similar series of isometric twitches from model 1 (B), model 2 (C), and model 3 (D).

4.4 Simulation of Afterloaded and Physiological Twitches

Figure 9, panel B and Figure 10, panel B demonstrate model 1 simulations of stress (upper panels) and relative length (lower panels) in afterloaded and physiological twitches with increasing afterload from isotonic to isometric. Compared with measured data from similar twitches (panel A in both figures) the simulations failed to reproduce the prolonged TPC with increasing afterload, demonstrating the main drawback of the sharp separation as a given function of time. The sharp separation between activation and inactivation yielded a very similar TPC in all twitch types. The model also failed to represent the rapid stress decline after the abrupt switch from isotonic lengthening to isometric stress decline during relaxation (Figure 9, panel B). The physiological relaxation is better represented by the model (Figure 10, panel B).

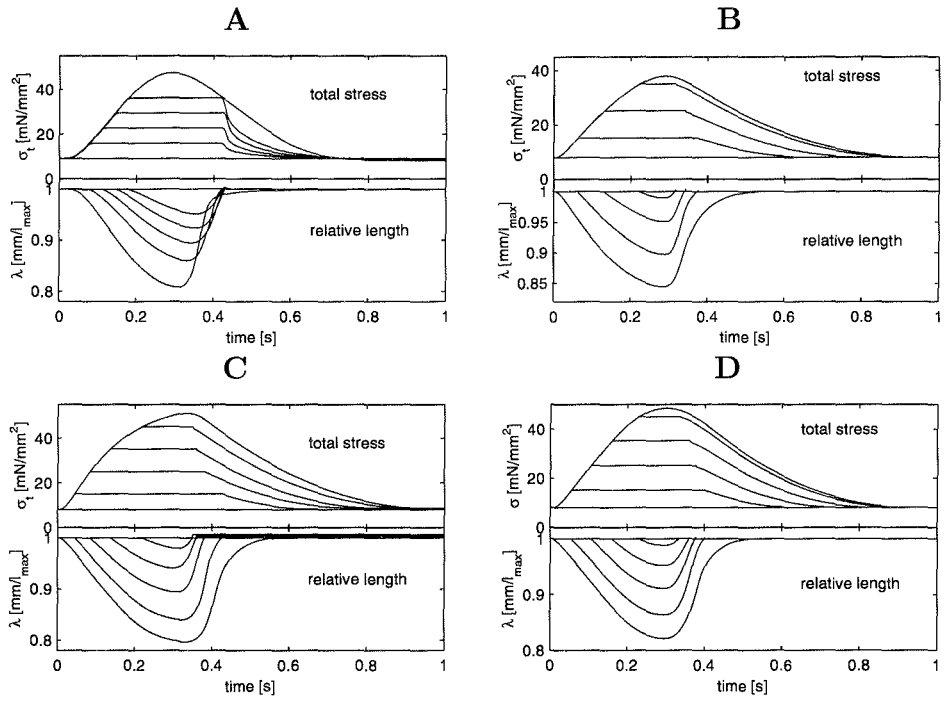

Figure 9: *Panel A:* Measured afterloaded twitches with increasing afterload from isotonic to isometric from experiment on isolated papillary muscle. Total stress (upper) and relative length (lower). The other panels show simulations of similar series of afterloaded twitches from model 1 (B), model 2 (C), and model 3 (D).

In model 2, it was difficult to obtain the differences in TPC between auxotonic and afterloaded twitches. Figure 9, panel C and 10, panel C demonstrate model 2 simulations of stress (upper panels) and relative length (lower panels) in afterloaded and physiological twitches with increasing afterload from isotonic to isometric. In these simulations we used the same parameter values as in the simulation of auxotonic twitches. With load-independent TPC in the auxotonic twitches, we obtained abbreviated TPC at increasing afterload in the afterloaded and physiological twitches, which is in contradiction to what is measured (panel A in Figure 9 and 10). To obtain reasonable timing of afterloaded twitches with this model, we needed to extend the complexity of the model. This is presented below.

The separation of activation and inactivation in model 1 and 3 differs from the separation in model 2, because in model 2 the onset of transition is based on the level of activity, while in model 1 and 3 the separation is based on time from onset of mechanical contraction. In model 1 we used the same representation of the intracellu-

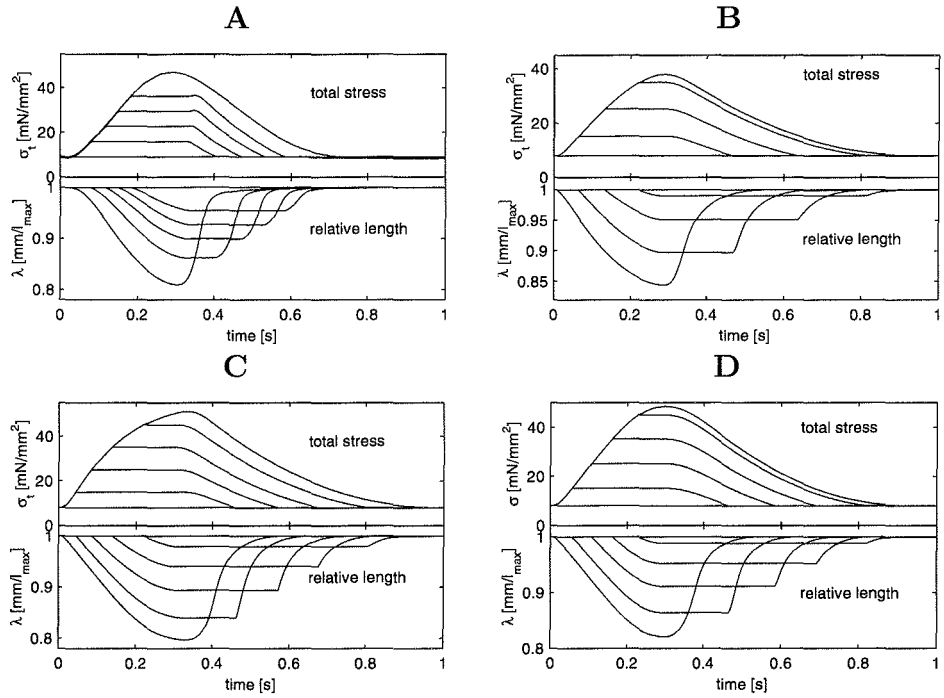

Figure 10: *Panel A*: Measured physiological twitches with increasing afterload from isotonic to isometric from experiment on isolated papillary muscle. Total stress (upper) and relative length (lower). The other panels show simulations of similar series of physiological twitches from model 1 (B), model 2 (C), and model 3 (D).

lar calcium transient in the weight function of activation in all twitches. In model 3 we used a weight function with predefined transition time and transition interval between activation and inactivation. Therefore, the TPC in afterloaded and physiological twitches from model 3 (Figure 9, panel D and 10, panel D) varied little with increasing afterload, like in model 1.

4.5 Stress-Length Loops

Figure 11 presents stress-length loops of the simulated twitches from all three model approaches. From this figure, we can see that all three models represented the relative peak values of stress and shortening in accordance with the measured twitches in Figure 2, panel B. The different peak values between the models are due to the different separation approaches and different parameter values.

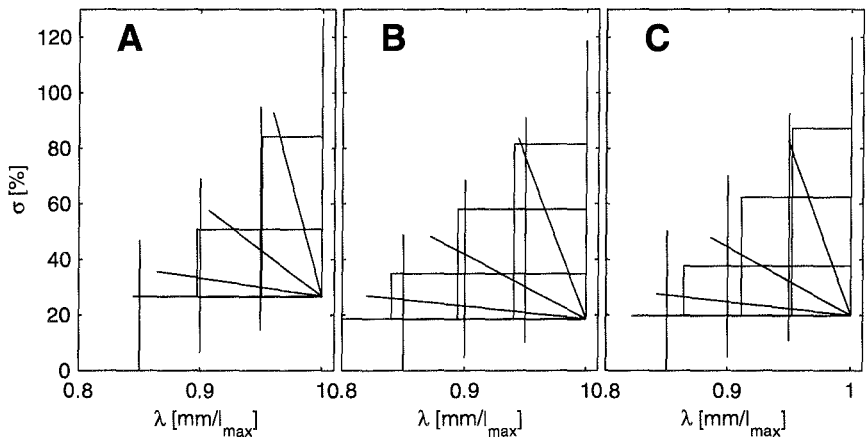

Figure 11: Simulated stress-length loops from isometric, auxotonic, and physiological twitches from Model 1 (panel A), Model 2 (panel B), and Model 3 (panel C). Total stress is normalized to peak active stress in isometric twitches at l_{max}. Simulated twitches are the same as are presented in the previous figures.

4.6 Timing of Isometric Contraction and Relaxation

As already noticed, the separation of activation and inactivation yielded a reasonable TPC in simulated auxotonic twitches for all three model approaches. However, the separation also gave little variation of TPC in isometric and afterloaded twitches (Figure 12). In the general model structure, we included a length dependence γ of the rate of activation and inactivation that only represented the relative change in the lateral distance between the thick and thin filaments. This was due to the observed differences in the rate of stress development and decline in isometric twitches at different lengths. Since we do not know the details about this relation, we cannot exclude the possibility that the length dependence is a function of the lateral distance and that the length dependence is different for activation and inactivation. In Figure 13, panel B, we have plotted the results of model 3 simulations of isometric twitches at increasing lengths with enhanced length dependence of inactivation and the same length dependence of

activation. This yielded differences in twitch duration which were more in accordance with the measured differences (Figure 12, panel C).

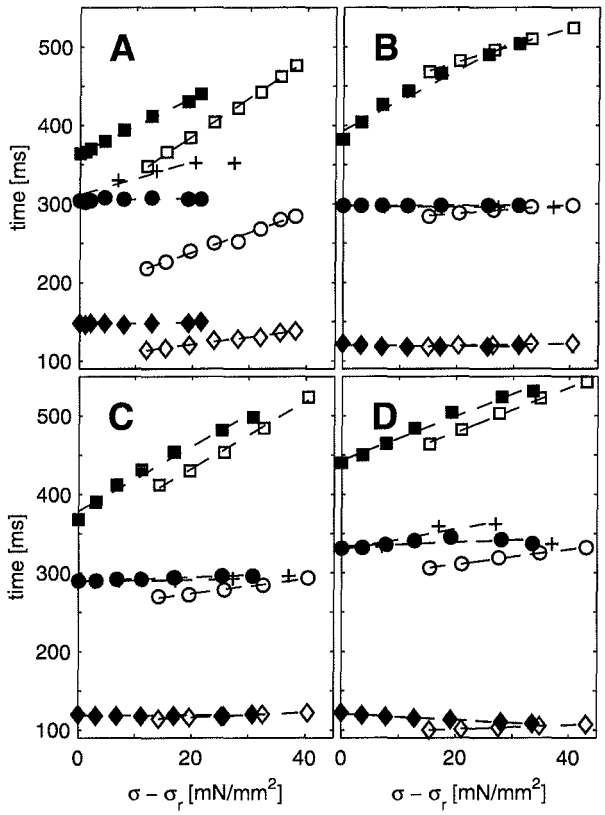

Figure 12: Timing of contraction and relaxation versus peak developed stress in measured (panel A) and simulated twitches (panel B, C, and D). THC (diamonds), TPC (circles), and THR (squares) in isometric twitches (open symbols) at increasing muscle length (from left to right) and auxotonic twitches (closed symbols) at increasing k_a, in addition to TPC of afterloaded twitches (crosses) at increasing afterload, are plotted in each panel. Regression lines are included. *Panel A*: Timing parameters obtained from measured twitches presented in Figure 6, 8, and 9. *Panel B*: Timing parameters from model 3 simulations presented in Figure 6, 8, and 9. *Panel C*: Timing parameters from model 3 simulations presented in Figure 13. *Panel D*: Timing parameters from model 2 simulations presented in Figure 16 and 17.

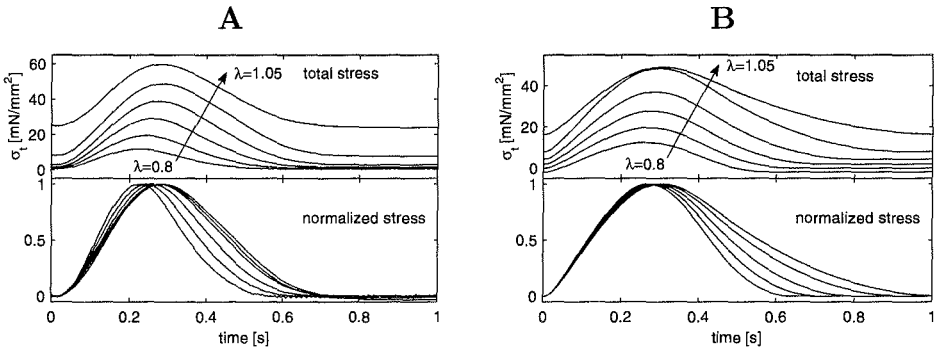

Figure 13: *Panel A*: Measured isometric twitches with increasing length from experiment on isolated papillary muscle. Total stress (upper), relative length (middle), and normalized developed stress (lower). *Panel B*: Model 3 simulations of isometric twitches with different length dependence of rate of activation and rate of inactivation.

4.7 Abrupt Shift between Isotonic and Isometric Loading Conditions

The afterloaded and physiological twitches represent sequences of isometric and isotonic phases. From muscle experiments one can observe some special features just after a switch between the isometric and isotonic states (Figure 14, panel A and 15, panel A). Especially during relaxation it seems to be a transition from one state to the other, which is not instant. In afterloaded twitches, there is a rapid stress decline during the first few milliseconds after the switch from isotonic to isometric. This follows a rapid lengthening at high load just prior to the switch. In physiological twitches, there is a rather slow initial lengthening after the switch from isometric stress decline to isotonic lengthening. This follows a slow stress decline prior to the switch. There may be several underlying mechanisms that are causing these features. But in terms of our modeling approach the features during relaxation may be related to some sort of memory of velocity (viscosity/kinetic energy breakdown). One possible extension of the model is therefore to include a low-pass filter on the velocity dependence of inactivation.

Figure 14, panel B shows a series of afterloaded twitches from model 3 where we included a $50ms$ moving average filter on the velocity input to the inactivation model. This yielded a faster initial stress decline after a switch from isotonic lengthening to isometric stress decline which is more similar to the measured afterloaded twitches (Figure 14, panel A).

Similar results were obtained for physiological twitches when the same settings were chosen for model 3 simulation (Figure 15).

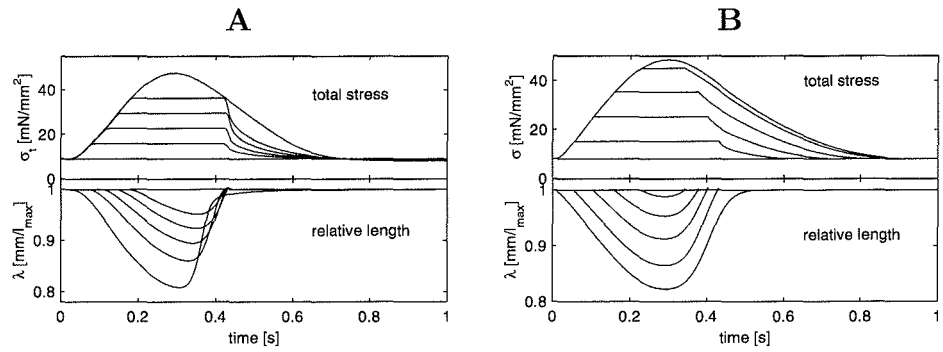

Figure 14: *Panel A*: Measured afterloaded twitches with increasing afterload from isotonic to isometric from experiment on isolated papillary muscle. Total stress (upper) and relative length (lower). *Panel B*: Model 3 simulations of afterloaded twitches, simulated with a memory of velocity in the inactivation function.

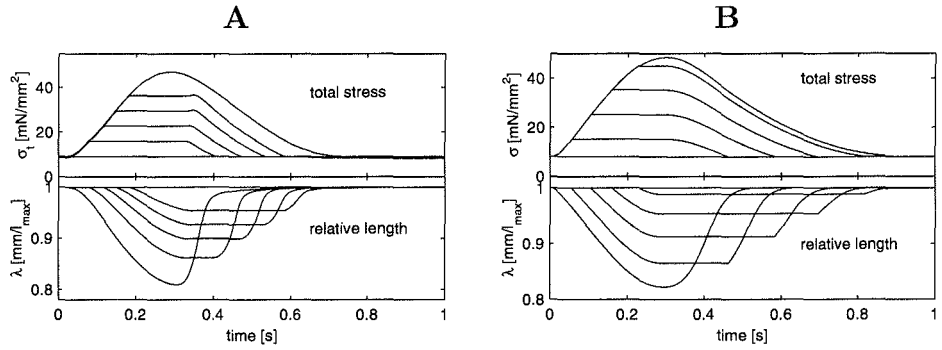

Figure 15: *Panel A*: Measured physiological twitches with increasing afterload from isotonic to isometric from experiment on isolated papillary muscle. Total stress (upper) and relative length (lower). *Panel B*: Model 3 simulations of physiological twitches, simulated with a memory of velocity in the inactivation function.

4.8 Timing of Afterloaded Contraction

From the stress-length loops of auxotonic and afterloaded twitches (Figure 2) we have observed that the afterloaded twitches almost reach the same peak shortening as auxotonic twitches with similar peak stress. Because the initial conditions and the preceding stabilization twitches are the same for both twitch types, the different loading history during contraction must be responsible for the different TPC. Although there are observed alterations in the intracellular calcium transient following the load-clamp in

afterloaded twitches, the underlying cause for the differences in timing is unclear.

One mechanical difference between afterloaded and auxotonic twitches is that in afterloaded twitches the power must be higher to obtain the same shortening under higher loads. In our modeling approach, one phenomenological way to incorporate the difference in TPC between auxotonic and afterloaded twitches, is to make the development of activity non-linearly dependent on power. We did this in two different ways for model 2. First, we reduced the rate of activation ($\dot{A}_c$) at high power, and second, we increased the potential for the activity (A_{max}) at high power.

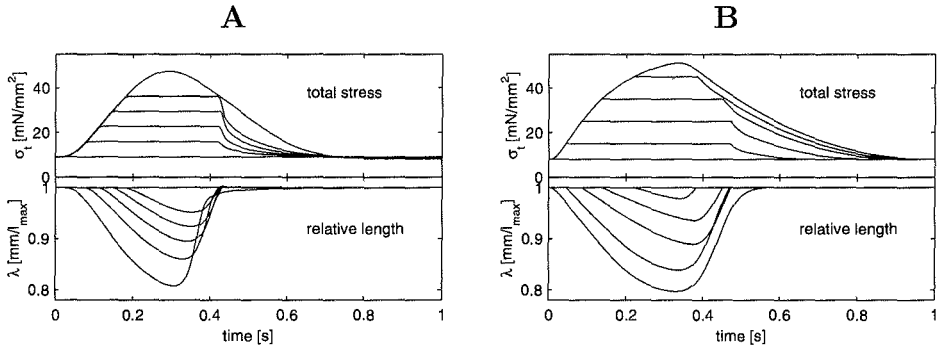

Figure 16: *Panel A*: Measured afterloaded twitches with increasing afterload from isotonic to isometric from experiment on isolated papillary muscle. Total stress (upper) and relative length (lower). *Panel B*: Model 2 simulations of afterloaded twitches when dependence on power was included in calculation of A_{max} and A. A memory of velocity was included in the inactivation function.

Figure 16, panel B presents a series of afterloaded twitches which include the dependence on power of A and A_{max}. This simulation also included the filtered velocity as input to the inactivation model as in Figure 14, panel B for model 3. Compared with the measured afterloaded twitches (Figure 16, panel A), this simulation resulted in more realistic TPC and initial isometric stress decline (Figure 12, panel D).

Figure 17, panel B shows a series of auxotonic twitches simulated with the same settings as the previous afterloaded twitches. TPC was slightly altered compared to Figure 6, panel C, but much less than the change in TPC for the afterloaded twitches. This is because we used a non-linear dependence on power.

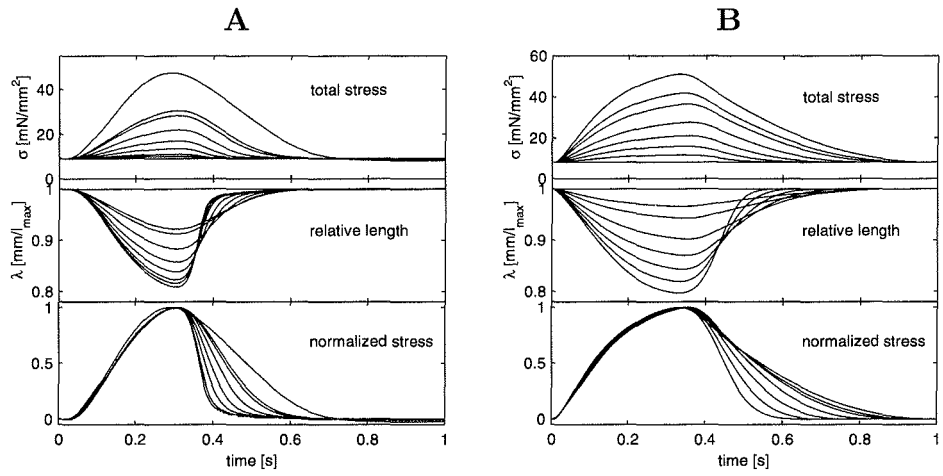

Figure 17: *Panel A*: Measured auxotonic twitches with increasing auxotonic load from experiment on isolated papillary muscle. Total stress (upper), relative length (middle), and normalized developed stress (lower). *Panel B*: Model 2 simulations of auxotonic twitches when dependence on power was included in calculation of A_{max} and A.

5 Discussion

We have developed a mathematical model for simulation of auxotonic twitches of the cardiac muscle based on experiments on isolated papillary muscles. The general model structure included models of load-dependent activation, load-dependent inactivation, and passive stress. We investigated three different approaches to separate activation and inactivation according to observed timing of contraction in auxotonic twitches. We simulated auxotonic twitches at increasing auxotonic load from isotonic to isometric, isometric twitches at increasing length, and afterloaded and physiological twitches at increasing afterload with all three separation approaches and the same general structure. We have also demonstrated how specific measured features may be incorporated by increasing the complexity of the model.

In this discussion section, we will initially discuss the general structure and the separation between activation and inactivation in our model. Furthermore, we will discuss the ability of the model to represent the time traces of different twitches under different loading conditions. Finally, we will discuss some limitations and possible improvements of the model.

5.1 The General Model Structure

The aim of this study was to develop a model on the level of stress and length, based on experimental observations in cardiac muscle twitches. From recent experiments on controlled auxotonic twitches [63, 65], we know that timing of contraction is independent of the auxotonic load, which is not the case when the contraction phase consists of a sequence of isometric and isotonic states. This means that during contraction the auxotonic load only influences the stress development versus shortening and not the time to peak contraction. From the same experiments it is also clear that the load dependence of relaxation is different. The duration of relaxation is mainly dependent on the peak stress, and the (peak) rate of stress decline is mainly dependent on the stress itself, like in isometric relaxation [69]. These observations together with the concepts of shortening deactivation and cooperative activity [8, 30, 42, 43, 59] formed the basis for the development of the activation and inactivation models.

There are two main reasons why we chose one activity variable separated into one activation model and one inactivation model instead of modeling the different components underlying our activity variable, namely the Ca^{2+}-TnC kinetics, activation of the thin filament, and the cross-bridge kinetics. First, we wanted a model with a limited number of parameters. A minimal number of model parameters and state variables enables the possibility to estimate model parameters from measurements of stress and length. Second, we wanted a strong relation between the measured variables and the state variables of the model. Therefore, we have modeled the integrative effect of all the underlying components, yielding the net contribution of the underlying processes to activation and inactivation.

5.2 Separation of Activation and Inactivation

Like the cardiac cycle, the muscle twitch has been divided into different phases in many ways, and the different phases have been given many names [8]. According to our model strategy with minimal model complexity, we found that the best way to obtain the different load dependence of contraction and relaxation was to implement the load dependence in two different models; one representing contraction (activation) and one representing relaxation (inactivation). This, however, required a reasonable way of separating the two models. In measured auxotonic twitches, TPC is almost constant at different auxotonic loads [64]. This implies that even though the activation and inactivation may be represented during the whole contraction-relaxation sequence, the balance between them occurs at the same time at all loads.

Based on this, we wanted to study three different approaches to separate the activation and inactivation. The first approach (model 1) was to use a general time trace of intracellular calcium as input. This is also used by other investigators [31, 57]. The problem with the intracellular calcium transient is that it falls exponentially from an early peak. This means that near TPC, the level of free calcium changes very slowly, which implies that TPC will be sensitive to load, because the level of activity will

depend on the load. One possible explanation why a slow decline of free calcium can be consistent with a constant TPC is the observation of a s-shaped $F - pCa$ relation [39]. We included a similar sensitivity of calcium in our model with the expected result. The main advantage with this approach is the well known fact that calcium is the most important regulator of activation. The major disadvantage is that we cannot measure the true intracellular calcium transient in vivo, although we know that it may be different at different loading conditions [4, 30, 40].

In the second approach (model 2), we based the separation on the load dependence of peak activation. TPC is supposed to occur when the activity reaches its maximal potential. This maximal potential, called A_{max} in our model, is defined by the stress-length relation, incorporating the concept of length-dependent activation and the concept of shortening deactivation/cooperativity. A_{max} was also used in the other approaches, but only in model 2 as the determinator of the onset of transition from contraction to relaxation. One advantage with this approach is that it relates the transition between contraction and relaxation to the peak values of the measurable variables stress and length. In addition, the σ_{max} parameter will be more closely related to the contractile state of the muscle. The use of stress and length to determine the onset of transition from contraction to relaxation may also be a pitfall in some pathological states where the stress-length relations are different.

The third approach (model 3) is inspired by the concept of local models in dynamic system theory [17, 38]. This concept has also been used in modeling of skeletal muscles with irregular stimulation [11]. The idea is that a complex non-linear system can be decomposed to a set of simpler models describing different working regimes. This way it is possible to combine a priori knowledge about the physical process with heuristic knowledge. Here we use only two local models of activation and inactivation that are weighted in time from stimulus. This concept allows smooth transition between models with completely different properties when one or more variables change (here: time). The main advantage is that we reduce model complexity by including heuristic knowledge. Compared to the first model approach, this approach uses only two timing parameters as input instead of a complete time trace of intracellular calcium.

One problem with our separation of activation and inactivation in order to obtain reasonable timing of auxotonic twitches, is that we also limit the variation of TPC in other twitch types, like isometric twitches at different lengths and afterloaded twitches at different afterload.

5.3 Simulation of Auxotonic Twitches

Simulations of auxotonic twitches with all three model approaches (Figure 6, panel B–D) gave qualitatively the same load dependence of contraction and relaxation as in the measured auxotonic twitches (Figure 6, panel A). This implies that the general model structure incorporated these features well, and that the separation of activation and inactivation yielded a simple implementation of the load dependence of contraction and relaxation.

Beside the load dependence of contraction and relaxation, we were especially interested in the timing of the auxotonic twitches. By the separation of activation and inactivation, we obtain very small variations in TPC with all three separation methods, as in the measured twitches.

This study does not include an estimation of model parameters to fit the model output to a given set of measured data. Therefore, there are quantitative differences between the models and between individual models and the measured twitches. Other parameter values will alter the peak values, the timing, and the exponential decay during relaxation of the auxotonic twitches.

5.4 Timing of Isometric and Afterloaded Twitches

As we have demonstrated for the auxotonic twitches, the separation of activation and inactivation has made it possible to obtain reasonable load dependence in both contraction and relaxation with a very simple model structure. The main problem of this modeling philosophy is that the separation will also imply small variations in TPC in other twitch types, although, variations in TPC have been measured in these twitch types. This is the case in isometric twitches at different length and afterloaded and physiological twitches at different afterload (Figure 12). The problem is therefore how to obtain reasonable timing in all kinds of twitches.

When we simulated isometric twitches with the same settings as for the auxotonic twitches, TPC varied less than in the measured case. In calcium activated muscle experiments, it is found that the $F - pCa$ relation is length dependent [3], yielding a higher calcium sensitivity at longer lengths. If we assume no or little changes in the intracellular calcium transient in isometric twitches at different length, an altered calcium sensitivity may influence the balance between activation and inactivation. A possible modification of model 1 would therefore be to make the threshold level in the calcium sensitivity ($Ca_{i,tr}$) dependent on length. The problem with this is that it will also influence the timing of auxotonic twitches if we use the same intracellular calcium transient in all twitches. We know that the intracellular calcium is different in isometric and afterloaded (also preloaded isotonic) twitches [4, 30, 40], but we do not know what is the effect of auxotonic twitches on the intracellular calcium transient. With a smooth transition in the auxotonic intracellular calcium transient from isotonic to isometric, a combination of this difference and the length-dependent calcium sensitivity may yield realistic TPC in both auxotonic and isometric twitches. Information about the intracellular calcium in auxotonic twitches is needed before it can be incorporated in the model. Another, more empirical way of varying the TPC in isometric twitches is to alter the balance between activation and inactivation. We did this for the third separation method where we have a given transition interval. By using a more pronounced length dependence of inactivation than of activation (Figure 13, panel B), we obtained both a variation in TPC and a wider separation of THR in accordance with the measured THR of isometric twitches.

TPC in afterloaded twitches is different from both auxotonic twitches and isomet-

ric twitches. TPC increases with increasing afterload until the afterload exceeds a given level ($\approx$ 80% of isometric peak stress), and then it decreases again towards the isometric TPC. As already noticed, the intracellular calcium transient is prolonged in afterloaded twitches [4, 30, 40]. In the light of our first separation approach, this may delay the balance between activation and inactivation. Landesberg and Sideman [42] demonstrated qualitatively the same changes in the intracellular calcium transient of their model as in the measurements. However, this requires a complex model of the calcium transient together with a model of the calcium-troponin kinetics.

On the level of stress and shortening, the difference between auxotonic and afterloaded contractions is the loading history. Both twitch types have the same initial values and almost similar peak values. While the auxotonic twitches shorten against an increasing load, the afterloaded twitches shorten against a constant (higher) load. For the intermediately loaded twitches, the afterloaded twitches perform more work (i.e. shortens at higher power) than the auxotonic twitches with similar peak values. We included a non-linear dependence of activation on power in model 2. This model had a small abbreviation of TPC at increasing afterload (Figure 9, panel C) when we used the initial model with the same settings as in the simulation of auxotonic twitches (Figure 6, panel C). With the power dependence included in the model, we obtained much more realistic TPC values in the afterloaded twitches (Figure 16), and still little variation in TPC in auxotonic twitches (Figure 17, panel B).

5.5 Abrupt Changes in Load between Isotonic and Isometric

Another specific feature of afterloaded and physiological twitches compared with auxotonic twitches is the abrupt changes in load when the control system switches from isometric to isotonic or from isotonic to isometric. This is most pronounced in afterloaded relaxation. Normally, isometric relaxation is slow compared to isotonic relaxation, but just after a switch from isotonic lengthening to isometric stress decline the stress decline is much faster than we would expect during isometric stress decline. The underlying mechanisms for this is not fully known [8], but it must be caused by the sudden stop in lengthening velocity.

Therefore, we implemented a low-pass filter on the velocity which was used to calculate the instantaneous velocity dependence of the inactivation model. Again, in the lack of reliable knowledge we did not model the underlying mechanisms, but tried to adapt the velocity dependence according to the measured observations on the stress and length level. Figure 14 and 15 present simulations of afterloaded and physiological twitches with the third model approach including filtered velocity dependence. This modification of the velocity dependence had negligible influence on the simulation of auxotonic twitches.

5.6 Limitations

We have demonstrated a simple model for simulation of auxotonic twitches. The focus has been on the load dependence of contraction and relaxation and the timing of auxotonic twitches. The simplicity of the model is obtained by separating the activity into one model of activation and one model of inactivation. As we have shown, the drawback of this modeling philosophy is that specific features in other twitch-types are difficult to reproduce. We have seen that some of these features, e.g. timing in isometric twitches, timing in afterloaded twitches, and effects of abrupt changes in load, to some degree can be included by increasing the model complexity.

5.7 Conclusions

In this paper, we have presented a mathematical model of contraction-relaxation sequences of cardiac muscle based on experiments on isolated papillary muscles. The general model structure was divided into models of load-dependent activation, load-dependent inactivation, and passive stress. We investigated three different approaches to separate activation and inactivation according to observed timing of contraction in auxotonic twitches. We simulated auxotonic twitches at increasing auxotonic load from isotonic to isometric in agreement with the experimental results. By increasing the complexity of the model we were also able to reproduce more realistic timing of isometric twitches at increasing length and more realistic relaxation sequences in afterloaded twitches.

Acknowledgements: Special thanks to Stein Inge Rabben for fruitful discussions and suggestions. This research has been supported in part by the Norwegian Research Council (NFR) grant # 107409/320.

References

1. Abbott BC and Mommaerts WFHM. A study of inotropic mechanisms in the papillary muscle preparation. *J. Gen. Physiol.* 42:533–551, 1959.

2. Akella AB, Su H, Sonnenblick EH, Rao VG, and Gulati J. The cardiac troponin C isoform and the length dependence of Ca2+ sensitivity of tension in myocardium. *J. Mol. Cell. Cardiol.* 29:381–9, 1997.

3. Allen DG and Kentish JC. The cellular basis of the length-tension relation in cardiac muscle. *J. Mol. Cell. Cardiol.* 17:821–40, 1985.

4. Allen DG and Kurihara S. The effects of muscle length on intracellular calcium transients in mammalian cardiac muscle. *J. Physiol.* 327:79–94, 1982.

5. Araki J, Matsubara H, Shimizu J, Mikane T, Mohri S, Mizuno J, Takaki M, Ohe T, Hirakawa M, and Suga H. Weibull distribution function for cardiac contraction: Integrative analysis. *Am. J. Physiol.* 277:H1940–H1945, 1999.

6. Bremel RD and Weber A. Cooperation within actin filament in vertebrate skeletal muscle. *Nat. New. Biol.* 238:97–101, 1972.

7. Brutsaert DL. Nonuniformity: A physiologic modulator of contraction and relaxation of the normal heart. *J. Am. Coll. Cardiol.* 9:341–8, 1987.

8. Brutsaert DL and Sys SU. Relaxation and diastole of the heart. *Physiol. Rev.* 69:1228–315, 1989.

9. Burkhoff D. Explaining load dependence of ventricular contractile properties with a model of excitation-contraction coupling. *J. Mol. Cell. Cardiol.* 26:959–78, 1994.

10. Cannell MB and Allen DG. Model of calcium movements during activation in the sarcomere of frog skeletal muscle. *Biophys. J.* 45:913–25, 1984.

11. Donaldson NN, Gollee H, Hunt KJ, Jarvis JC, and Kwende MK. A radial basis function model of muscle stimulated with irregular inter- pulse intervals. *Med. Eng. Phys.* 17:431–41, 1995.

12. Edman KA. Mechanical deactivation induced by active shortening in isolated muscle fibres of the frog. *J. Physiol.* 246:255–75, 1975.

13. Eisenberg E and Hill TL. Muscle contraction and free energy transduction in biological systems. *Science* 227:999–1006, 1985.

14. Fabiato A and Fabiato F. Dependence of the contractile activation of skinned cardiac cells on the sarcomere length. *Nature* 256:54–6, 1975.

15. Fitzsimons DP and Moss RL. Strong binding of myosin modulates length-dependent Ca2+ activation of rat ventricular myocytes. *Circ. Res.* 83:602–7, 1998.

16. Ford LE. Mechanical manifestations of activation in cardiac muscle. *Circ. Res.* 68:621–37, 1991.

17. Foss BA and Johansen TA. Local modeling as a tool for semi- empirical and semi-mechanistic process modeling. In: Bulsari AB, ed., *Neural Networks for Chemical Engineers*, 297–334. Elsevier, Amsterdam, 1995.

18. Frank O, Translated by Chapman CB, and Wasserman E. On the dynamics of cardiac muscle (Zur dynamik des herzmuskels). *Am. Heart. J.* 58:282–317, 1959.

19. Fuchs F and Wang YP. Sarcomere length versus interfilament spacing as determinants of cardiac myofilament Ca2+ sensitivity and Ca2+ binding. *J. Mol. Cell. Cardiol.* 28:1375–83, 1996.

20. Gordon AM, Huxley AF, and Julian FJ. The variation in isometric tension with sarcomere length in vertebrate muscle fibres. *J. Physiol.* 184:170–92, 1966.

21. Guccione JM, Motabarzadeh I, and Zahalak GI. A distribution-moment model of deactivation in cardiac muscle. *J. Biomech.* 31:1069–73, 1998.

22. Gulati J. Molecular biology of the length-tension relation in cardiac muscle. *Adv. Exp. Med. Biol.* 332:593–602, 1993.

23. Helmes M, Trombitas K, and Granzier H. Titin develops restoring force in rat cardiac myocytes. *Circ. Res.* 79:619–26, 1996.

24. Hill AV. The heat of shortening and the dynamic constants of muscle. *Proc. R. Soc. Ser. B* 126:136–195, 1938.

25. Hill TL, Eisenberg E, Chen YD, and Podolsky RJ. Some self-consistent two-state sliding filament models of muscle contraction. *Biophys. J.* 15:335–72, 1975.

26. Hittinger L, Crozatier B, Belot JP, and Pierrot M. Regional ventricular segmental dynamics in normal conscious dogs. *Am. J. Physiol.* 253:H713–9, 1987.

27. Hofmann PA and Fuchs F. Effect of length and cross-bridge attachment on Ca2+ binding to cardiac troponin C. *Am. J. Physiol.* 253:C90–6, 1987.

28. Hofmann PA and Fuchs F. Evidence for a force-dependent component of calcium binding to cardiac troponin C. *Am. J. Physiol.* 253:C541–6, 1987.

29. Holmes KC. The actomyosin interaction and its control by tropomyosin. *Biophys. J.* 68:2S–7S, 1995.

30. Housmans PR, Lee NK, and Blinks JR. Active shortening retards the decline of the intracellular calcium transient in mammalian heart muscle. *Science* 221:159–61, 1983.

31. Hunter PJ, McCulloch AD, and ter Keurs HE. Modelling the mechanical properties of cardiac muscle. *Prog. Biophys. Mol. Biol.* 69:289–331, 1998.

32. Huxley AF. Muscle structure and theories of contraction. *Prog. Biophys. Mol. Biol.* 7:255–318, 1957.

33. Huxley AF and Niedergerke R. Structural changes in muscle during contraction. *Nature* 173:971–973, 1954.

34. Huxley AF and Simmons RM. Proposed mechanism of force generation in striated muscle. *Nature* 233:533–8, 1971.

35. Huxley H. The double array of filaments in cross-striated muscle. *J. Biophysic. Biochem. Cytol.* 3:631–47, 1957.

36. Huxley H and Hanson J. Changes in the cross-striations of muscle during contraction and stretch and their structural interpretation. *Nature* 173:973–976, 1954.

37. Izakov VY, Katsnelson LB, Blyakhman FA, Markhasin VS, and Shklyar TF. Cooperative effects due to calcium binding by troponin and their consequences for contraction and relaxation of cardiac muscle under various conditions of mechanical loading. *Circ. Res.* 69:1171–84, 1991.

38. Johansen TA and Foss BA. Constructing NARMAX models using ARMAX models. *Int. J. Control* 58:1125–1153, 1993.

39. Kentish JC, ter Keurs HEDJ, Ricciardi L, Bucx JJJ, and Noble KIM. Comparison between the sarcomere length-force relations of intact and skinned trabeculae from rat right ventricle. *Circ. Res.* 58:755–768, 1986.

40. Lab MJ, Allen DG, and Orchard CH. The effects of shortening on myoplasmic calcium concentration and on the action potential in mammalian ventricular muscle. *Circ. Res.* 55:825–9, 1984.

41. Lakatta EG and Jewell BR. Length-dependent activation: Its effect on the length-tension relation in cat ventricular muscle. *Circ. Res.* 40:251–7, 1977.

42. Landesberg A and Sideman S. Mechanical regulation of cardiac muscle by coupling calcium kinetics with cross-bridge cycling: A dynamic model. *Am. J. Physiol.* 267:H779–95, 1994.

43. Leach JK, Brady AJ, Skipper BJ, and Millis DL. Effects of active shortening on tension development of rabbit papillary muscle. *Am. J. Physiol.* 238:H8–13, 1980.

44. Lee JA and Allen DG. EMD 53998 sensitizes the contractile proteins to calcium in intact ferret ventricular muscle. *Circ. Res.* 69:927–36, 1991.

45. LeWinter MM, Fabian J, and Bell SP. Left ventricular restoring forces: Modulation by heart rate and contractility. *Basic. Res. Cardiol.* 93 Suppl 1:143–7, 1998.

46. Matsubara H, Takaki M, Yasuhara S, Araki J, and Suga H. Logistic time constant of isovolumic relaxation pressure-time curve in the canine left ventricle. Better alternative to exponential time constant. *Circulation* 92:2318–26, 1995.

47. McDonald KS, Field LJ, Parmacek MS, Soonpaa M, Leiden JM, and Moss RL. Length dependence of Ca2+ sensitivity of tension in mouse cardiac myocytes expressing skeletal troponin C. *J. Physiol.* 483:131–9, 1995.

48. McDonald KS and Moss RL. Osmotic compression of single cardiac myocytes eliminates the reduction in Ca2+ sensitivity of tension at short sarcomere length. *Circ. Res.* 77:199–205, 1995.

49. McMahon TA. *Muscles, Reflexes, and Locomotion.* Princeton University Press, Princeton, New Jersey, USA, 1984.

50. Millman BM. The filament lattice of striated muscle. *Physiol. Rev.* 78:359–91, 1998.

51. Mirsky I and Parmley WW. Assessment of passive elastic stiffness for isolated heart muscle and the intact heart. *Circ. Res.* 33:233–43, 1973.

52. Mizuno J, Mikane T, Araki J, Hatashima M, Moritan T, Ishikawa T, Komukai K, Kurihara S, Hirakawa M, and Suga H. Hybrid logistic characterization of isometric twitch force curve of isolated ferret right ventricular papillary muscle. *Jpn. J. Physiol.* 49:145–58, 1999.

53. Moss RL, Nwoye LO, and Greaser ML. Substitution of cardiac troponin C into rabbit muscle does not alter the length dependence of Ca2+ sensitivity of tension. *J. Physiol.* 440:273–89, 1991.

54. Niggli E and Lederer WJ. Restoring forces in cardiac myocytes. Insight from relaxations induced by photolysis of caged ATP. *Biophys. J.* 59:1123–35, 1991.

55. Panerai RB. A model of cardiac muscle mechanics and energetics. *J. Biomech.* 13:929–40, 1980.

56. Peskoff A and Langer GA. Calcium concentration and movement in the ventricular cardiac cell during an excitation-contraction cycle. *Biophys. J.* 74:153–74, 1998.

57. Peterson JN, Hunter WC, and Berman MR. Estimated time course of Ca2+ bound to troponin C during relaxation in isolated cardiac muscle. *Am. J. Physiol.* 260:H1013–24, 1991.

58. Pinto JG and Fung YC. Mechanical properties of the stimulated papillary muscle in quick- release experiments. *J. Biomech.* 6:617–30, 1973.

59. Rice JJ, Winslow RL, and Hunter WC. Comparison of putative cooperative mechanisms in cardiac muscle: Length dependence and dynamic responses. *Am. J. Physiol.* 276:H1734–54, 1999.

60. Robertson SP, Johnson JD, and Potter JD. The time-course of Ca2+ exchange with calmodulin, troponin, parvalbumin, and myosin in response to transient increases in Ca2+. *Biophys. J.* 34:559–69, 1981.

61. Robinson TF, Factor SM, and Sonnenblick EH. The heart as a suction pump. *Sci. Am.* 254:84–91, 1986.

62. Schouten VJ, van Deen JK, de Tombe P, and Verveen AA. Force-interval relationship in heart muscle of mammals. A calcium compartment model. *Biophys. J.* 51:13–26, 1987.

63. Sørhus V, Angelsen BAJ, and Sys SU. Length and load dependence of controlled auxotonic twitch durationin isolated papillary muscle. In: *Proc of the European Medical and Biological Engineering Conference, 1999, Vienna, Austria*, volume 37 Suppl 2 of *Med Biol Eng Comput*, 290–291. 1999.

64. Sørhus V, Angelsen BAJ, and Sys SU. Analysis of the controlled auxotonic twitch in isolated cardiac muscle. *Submitted* 2000.

65. Sørhus V, Demolder M, Angelsen BAJ, and Sys SU. Dimensionless time traces of mechanical dynamics from stress and shortening in isolated papillary muscle. In: *Proc of the European Medical and Biological Engineering Conference, 1999, Vienna, Austria*, volume 37 Suppl 2 of *Med Biol Eng Comput*, 1184–1185. 1999.

66. Sørhus V, Sys SU, Natås A, Demolder MJ, and Angelsen BAJ. Controlled auxotonic twitch in papillary muscle: A new computer-based control approach. *Submitted* 2000.

67. Sugiura S. Actin-myosin interaction. *Cardiovasc. Res.* 44:266–273, 1999.

68. Sys SU. *Physiologic control of mechanics of isolated cardiac muscle.*. Ph.D. thesis, University of Antwerp, Antwerp, Belgium, 1992.

69. Sys SU and Brutsaert DL. Determinants of force decline during relaxation in isolated cardiac muscle. *Am. J. Physiol.* 257:H1490–7, 1989.

70. Taber LA, Yang M, and Podszus WW. Mechanics of ventricular torsion. *J. Biomech.* 29:745–52, 1996.

71. Takahashi A, Camacho P, Lechleiter JD, and Herman B. Measurement of intracellular calcium. *Physiol. Rev.* 79:1089–1125, 1999.

72. ter Keurs HEDJ, Rijnsburger WH, van Heuningen R, and Nagelsmit MJ. Tension development and sarcomere length in rat cardiac trabeculae. *Circ. Res.* 46:703–714, 1980.

73. Tözeren A. Constitutive equations of skeletal muscle based on cross-bridge mechanism. *Biophys. J.* 47:225–36, 1985.

74. Tözeren A. Continuum rheology of muscle contraction and its application to cardiac contractility. *Biophys. J.* 47:303–9, 1985.

75. Wong AY. Mechanics of cardiac muscle, based on Huxley's model: Mathematical stimulation of isometric contraction. *J. Biomech.* 4:529–40, 1971.

76. Wong AY. Mechanics of cardiac muscle, based on Huxley's model: Simulation of active state and force-velocity relation. *J. Biomech.* 5:107–17, 1972.

77. Zahalak GI and Ma SP. Muscle activation and contraction: Constitutive relations based directly on cross-bridge kinetics. *J. Biomech. Eng.* 112:52–62, 1990.

78. Zahalak GI and Motabarzadeh I. A re-examination of calcium activation in the Huxley cross-bridge model. *J. Biomech. Eng.* 119:20–9, 1997.